SYNTHESIS AND CATALYTIC STUDY OF SHELL-SHELL, CORE-SHELL HOLLOW GOLD NANOCATALYSTS

A Dissertation
Presented to
The Academic Faculty

by

Batyr Garlyyev

In Partial Fulfillment
of the Requirements for the Degree
Doctor of Philosophy in the
School of Chemistry and Biochemistry

Georgia Institute of Technology
May 2016

SYNTHESIS AND CATALYTIC STUDY OF SHELL-SHELL, CORE-SHELL HOLLOW GOLD NANOCATALYSTS

Approved by:

Dr. M. El-Sayed, Advisor
School of Chemistry and Biochemistry
Georgia Institute of Technology

Dr. L. Bottomley,
School of Chemistry and Biochemistry
Georgia Institute of Technology

Dr. J. Sadighi,
School of Chemistry and Biochemistry
Georgia Institute of Technology

Dr. J. Carson Meredith,
School of Chemical and Biomolecular Engineering
Georgia Institute of Technology

Dr. J. Zhang,
School of Chemistry and Biochemistry
Georgia Institute of Technology

Date Approved: March 22, 2016

“Sell your cleverness and buy bewilderment”
Rumi

To my loved ones.

ACKNOWLEDGEMENTS

Professionally, I would like to acknowledge my advisor, Prof. Dr. Mostafa El-Sayed, for his guidance and support during my five years at Georgia Tech. I also would like to thank my undergraduate advisor Prof. Dr. Ramazan Ozturk for his guidance and helping me. I would like to thank the LDL group, especially Dr. Mahmoud A. Mahmoud, Dr. Paul Szymanski, Dr. Steven Hira, Dr. Nasrin Hooshmand, Dr. Sajanlal R. Panikkanvalappil, Justin Bordley, Daniel O'Neil, Mena Aioub, Jane, Chrystal, Mostafa Ali, and Leslie Dionne White for the academic assistance. Also I would like to thank my committee members Prof. Dr. Lawrence Bottomley, Prof. Dr. Joseph Sadighi, Prof. Dr. John Zhang, and Prof. Dr. Carson Meredith for their time and academic assistance during my PhD studies.

Personally, I would like to thank my parents and sisters (Sona and Sulgun), all my friends and Annika Orth for their support and patience during my five years in U.S.

TABLE OF CONTENTS

LIST OF TABLES

Page

LIST OF FIGURES

Page

LIST OF ABBREVIATIONS

LSPR	localized surface plasmon resonance
SERS	surface enhanced Raman spectroscopy
4-NTP	4-nitrothiophenol
BH	sodium borohydride
AuHNS	hollow gold nanosphere
Pt	platinum
Au	gold
Ag	silver
Pd	palladium
AuNS	gold nanosphere
DDA	discrete dipole approximation
AuPtNRT	gold platinum nanorattle
PVP	polyvinylpyrrolidone
DI	deionized water
AgNS	silver nanosphere
EG	ethylene glycol
AuNC	gold nanocage
AgNC	silver nanocage
SEM	scanning electron microscope
TEM	transmission electron microscope
OD	optical density
LB	Langmuir-Blodgett technique

HR-TEM	high resolution transmission electron microscopy
ICP-MS	inductively coupled plasma mass spectrometry
4-NP	4-nitrophenol
UV	ultraviolet spectroscopy
BET	Brunauer–Emmett–Teller theory
FTIR	Fourier transform infrared spectroscopy
MOF	metal-organic framework
EDS	energy-dispersive X-ray spectroscopy
4ATP	4-aminothiophenol
AuPdNC	gold-palladium double shell nanoparticles
AuPtNC	gold platinum nanocages
AuPdNC	gold palladium nanocages
NIR	near infrared
N_A	Avogadro's number
ε	molar extinction coefficient
AgNPT	Silver nanoplates

SUMMARY

Use of metal nanoparticles in catalysis is a rapidly growing field that has gone an explosive growth during the past two decades. Metal nanoparticles have a large surface area to volume ratio compared to their bulk counterparts, which makes them attractive to use as catalysts. Atoms on the surface of metal nanoparticles are very active due to their high surface energy, which comes from their unsatisfied valency. High activity of surface atoms raises the possibility that the metal nanoparticles can replace bulk materials use in catalysis. First recent advances in metal nanoparticle colloidal synthetic techniques and characterization methods were discussed in detail. Synthesis of gold nanoparticles with different shapes and bimetallic structure are explored. Solution catalysis with metallic nanoparticles can either take place on the surface of the nanoparticle (heterogeneous mechanism) or in solution by atoms or ions leached from the nanoparticle surface (homogeneous mechanism). Experimental method which could distinguish between the two mechanisms by using hollow plasmonic gold nanocatalyst was developed.

Nanocage catalysts made of a single metal such as gold, platinum, and palladium or two metals, such as double shell structures of gold-platinum, gold-palladium, and platinum-palladium have presented high catalytic efficiency due to the cage effect. The electron-transfer reactions on the surface of gold nanoshells were discussed, where the reaction mechanism was changed by adding an inner platinum or palladium nanoshell.

Controlling the selectivity of the catalyst is an important goal of catalysis research. This can be accomplished by designing the catalyst to include different surface facets with different atomic density and surface energy. In the last chapter selectivity of

the plasmonic nanocatalyst with multiple plasmon modes were explored, where selectivity can be controlled by changing the wavelength of the exciting light.

CHAPTER 1

INTRODUCTION TO NANOCATALYSIS

Summary

This chapter will discuss basic characteristics of metal nanoparticles and their application in catalysis. Nanoparticles have been explored since some centuries but only recently scientists began to understand properties of metal nanoparticles. Firstly, the high surface area to volume ratio of nanoparticles is key characteristics in their catalytic applications will be discussed. Another property of metal nanoparticles is their coupling interaction with light of certain wavelength where maximum amount of coupling happens at surface plasmon resonance which will be defined in this chapter. Also current literature of how catalytic properties of metal nanoparticles depends on the shape and structure will be discussed. Finally outline and main focus of dissertation will be presented briefly.

Beginning of Nanomaterials

Scientists were and are always in search of new materials which will make our lives easier. As it was stones in Stone Age and bronze in Bronze Age then with industrial revolution steel, polymers and many other materials were invented. Malleability and durability of new materials are some of the most important characteristics and we have come long way in improving them. Nowadays we live in an information age where we utilize use of semiconductors, conductive polymers, nanomaterials and fiber optic internet with a lightning speed. One of the important fields where nanomaterials are utilized is in catalysis which is also called as Nanocatalysis – using nanoparticles to catalyze chemical reactions, has been one of the hot topics for research in the past three decades. For more efficient and faster synthesis, catalysts are used in production of over 90% percent of materials in industry and it accounts for a yearly turnover of about 900 billion.[1] Due to easily tunable properties, interest in metal nanoparticles and their use in nanocatalysis is rapidly increasing and has shown promising results in numerous fields, including chemical production, sustainable energy, and materials chemistry.

Metal nanoparticles have been known for a quite long time and have been extensively used in art. One of the examples dating to the 4th century, the Lycurgus Cup, incorporates gold nanoparticles into the glass to give the cup a dichroic property, shown in figure 1.1. When the cup is under illumination of normal daylight, cup appears green due to the fact that bluish-green light is scattered by the particles. But when the cup is illuminated from inside, the particles inside the glass absorb the green light and the remaining colors of the white light appear reddish-orange so the cup appears ruby red.

Figure 1.1. This Roman cup is made of ruby glass and gold nanoparticles. If the cup is viewed in reflected light, it appears green (left image). However, when the light is illuminated from inside and transmitted through the glass, it appears ruby-red (right image). (British Museum - The Lycurgus Cup)

Another application of metal nanoparticles were the stain glass windows of the cathedrals where gold or silver nanoparticles were incorporated into the glass to give the panes various hues. Back in the days nanoparticles were used for purely artistic purposes and amazing colors of cup and stain glass windows are still preserved. What excites scientists nowadays about metal nanoparticles is their tunable characteristics, simply changing shape, size or environment can vary their electromagnetic, electronic and chemical properties.

Characteristics of Metal Nanoparticles

Nanocatalysis has undergone an exponential growth during the past two decades, both in homogeneous and heterogeneous catalysis. One of the main advantages of using metal nanoparticles as catalysts over their bulk counterparts is their high surface to volume ratio. Imagine that mathematically 1 kg of cubic particles with 1 mm edge length has the same surface area as 1 mg of particles of 1 nm edge length which results in tremendous increase of surface area to material ratio.

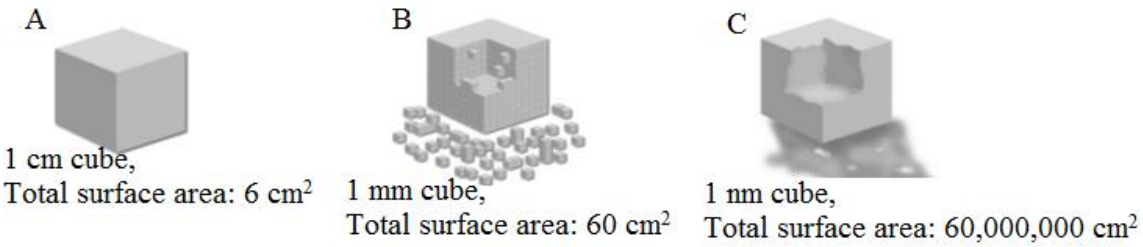

Figure 1.2. Schematic representation for comparing surface area. Solids with 1 cm edge length with the surface area of 6 cm^2 (A). Solids with 1 mm edge length with the surface area of 60 cm^2 (B), and Nanocubes with 1 nm edge length with surface area of 6 x 10^7 cm^2 (C).

The effective catalytic properties of the metallic nanoparticles are based on their high surface area to volume ratio[2], the surface potential of the nanocatalyst facets which depends on their atomic density[3], the number of valency unsaturated surface atoms [4,5], the capping material surface density of the nanocatalyst, and the energy of the Fermi level in redox reactions[6]. In general atoms on the surface of the particles are covalently unsaturated and more active which results in higher catalytic activity compared to atoms inside the particle.

In addition to the catalytic properties of the plasmonic metal nanocatalysts, they are characterized by the presence of localized surface plasmon resonance (LSPR) spectrum.[7] The LSPR is a coherent, collective spatial oscillation of the conduction electrons in a metallic nanoparticle, which is excited by light of specific wavelength. The LSPR involves generation of a strong plasmon field which decays by enhanced

absorption and scattering processes.[8] The scattered photons have been used in plasmon imaging[9], enhanced Raman scattering[10], plasmonic nanolensing[11]. The absorbed photons have been used to induce photochemical reactions such as energy transfer in hydrogen production[12] or initiating photodimerization of aromatic nitro compounds into *azo* dimers[13,14]. The photons absorbed by the nanoparticles can also decay generating heat as in case of the photothermal therapy[9] and photothermal enhanced catalytic reactions[15].

According to the electromagnetic mechanism of surface enhanced Raman spectroscopy (SERS)[10], the plasmon field of the plasmonic nanoparticles enhances the exciting light and the Raman signal of any analyte located in its domain. The SERS enhancement factor[16] can approach the value of 10^{10}, which improves the sensitivity of SERS as an analytical technique[13,17]. Previously, in order to improve the detection by SERS, the plasmon field intensity has been maximized[18,19] and the scattering spectrum of the nanoparticles has been enhanced[20]. Gold and silver nanoparticles of different shapes[21,22], sizes[23,24], and structure[25,26] have been prepared and examined in SERS[27-30]. Asymmetric nanoparticles have proven to provide stronger and more concentrated plasmon field intensity compared to highly symmetric shapes.[20,31] The asymmetric nanoparticles have more than one plasmon mode[32,33] which made it possible to use different laser excitations.[34]

Catalysis by Metal Nanoparticles

As I mentioned earlier Nanocatalysis is using nanoparticles to catalyze chemical reactions. Introducing sharp corners and edges to the shape of the nanocatalysts further increases their catalytic efficiency.[4] As the activity of the nanocatalyst depends on the number of high energy active centers,[35] atoms located at the sharp tips are thermodynamically and catalytically active because they are unsatisfied in valency.[2] Although the nanocatalysts with sharp tips present well-enhancement of the catalytic efficiency, their sharp ends become rounded after the catalytic reaction, which causes a

remarkable decrease in the catalytic efficiency.[36] The shape change of the nanocatalyst could be due to leaching or rearrangement of the atoms located on its sharp ends.[36] Confinement of the reacting materials within the nanocatalysts has been found to improve their catalytic efficiency.[37-44] This confinement is acquired either by designing the nanocatalyst to have a cavity, or by fixing the catalyst on the surface of the inside wall of an inert support of containing voids. Nanocage catalysts made of a single metal such as gold, platinum, and palladium or two metals, such as double shell structures of gold-platinum, gold-palladium, and platinum-palladium have presented high catalytic efficiency due to the cage effect.[37-40] The idea of cage catalysis was supported by comparing the catalytic efficiency of gold nanocages with that of the solid nanocatalyst of similar shape, and the gold nanocages were found to have a higher catalytic efficiency than the solid nanocatalyst.[45,46] The cage effect was also observed for palladium nanotubes, which showed a high catalytic efficiency for the Suzuki reaction.[41]

There are couple of ways to implement metal nanoparticles in catalysis, one of them is to use colloidal metal nanoparticle solutions in direct solution catalysis. Solution catalysis with metallic nanoparticles can either take place on the surface of the nanoparticle (heterogeneous mechanism) or in solution by atoms or ions leached from the nanoparticle surface (homogeneous mechanism).[47] It has been difficult to determine which mechanism is dominant in colloidal solution nanocatalysis.[48-50] It is easy to examine the dependence of the rate of the reaction on the available surface area of the nanoparticle. This can be done by partially poisoning the surface of metal nanoparticles with different amounts of compound which will bind to the surface of particles such as 4-nitrothiophenol (4-NTP) and studying the effect on the efficiency of the nanocatalyst.

Dissertation Outline and Focus

Use of metal nanoparticles in catalysis is a rapidly growing field that has gone an explosive growth during the past two decades. Metal nanoparticles have a large surface area to volume ratio compared to their bulk counterparts, which makes them attractive to use as catalysts. Atoms on the surface of metal nanoparticles are very active due to their high surface energy, which comes from their unsatisfied valency. High activity of surface atoms raises the possibility that the metal nanoparticles can replace bulk materials use in catalysis. However, more research needs to be done on how to manipulate activity and selectivity of metal nanoparticles by synthesizing different shapes and by alloying different metals into one nanoparticle. This kind of examination is necessary in order to truly examine the usefulness of nanoparticles as catalysts.

Chapter 2 discusses recent advances in metal nanoparticle colloidal synthetic techniques and characterization methods. Synthesis of gold nanoparticles with different shapes and bimetallic structure are explored in detail. Also the analytical techniques used to image the nanoparticles spectroscopically and using electron microscopy are discussed.

Solution catalysis with metallic nanoparticles can either take place on the surface of the nanoparticle (heterogeneous mechanism) or in solution by atoms or ions leached from the nanoparticle surface (homogeneous mechanism).[47] It has been difficult to determine which mechanism is dominant in colloidal solution nanocatalysis.[48-50] **Chapter 3** discusses experimental method which could distinguish between the two mechanisms by using hollow plasmonic gold nanocatalyst. We have addressed this problem using the model reaction of the reduction of 4-nitrophenol (4-NP) by sodium borohydride (BH) in aqueous solution by metallic nanoparticles. We studied the reaction yield as a function of the free surface area of the nanoparticle after partial poisoning by 4-nitrothiophenol (4-NTP). Due to the fact both mechanisms will be dependent on the available active surface,

we made use of the plasmonic properties of gold nanoparticles. For surface catalysis, if the products or intermediates have different dielectric value from that of the reactants, the surface plasmon extinction band would shift in the course of the reaction if solid or hollow plasmonic nanoparticles are used for the catalysis. This is observed for the reaction being examined in which hydrogen gas is produced causing a blue shift of the surface plasmon band of the hollow gold nanospheres (AuHNSs) used as a catalyst. Hollow nanoparticles can also be used to test for the involvement of the atomic surface leach mechanism. They have two plasmonic surfaces, the coupling between their surface fields increases by decreasing the wall thickness of the hollow nanoparticle if surface atom leaching takes place. This leads to a red shift of the nanocatalyst plasmon band. In the present study, AuHNSs did not show any red shift of the LSPR during or after the 4-NP-BH reduction. This agrees with a surface heterogeneous type mechanism not involving leached atoms in solution.

Confinement of the reacting materials within the nanocatalysts has been found to improve their catalytic efficiency.[37-44] This confinement is acquired either by designing the nanocatalyst to have a cavity, or by fixing the catalyst on the surface of the inside wall of an inert support of containing voids. Nanocage catalysts made of a single metal such as gold, platinum, and palladium or two metals, such as double shell structures of gold-platinum, gold-palladium, and platinum-palladium have presented high catalytic efficiency due to the cage effect.[37-40] **Chapter 4** discusses the electron-transfer reactions on the surface of gold nanoshells. Where the reaction mechanism was changed by adding an inner platinum or palladium nanoshell in the double shells nanocatalysts. The reduction of 4-nitrothiophenol (4NTP) by borohydride was studied as model reaction when bound to the hollow gold nanocatalysts in the presence and absence of inner platinum and palladium nano shells . To confirm the heterogeneous catalytic mechanism, the nanocatalysts were assembled into a monolayer on the surface of a quartz substrate using the Langmuir-Blodgett technique, and the 4NTP is allowed to bind to the surface of

gold through a strong thiol bond. The stages of the reduction reaction of 4NTP on the surface of gold were successfully followed in real time by time-resolved surface-enhanced Raman spectroscopy (SERS). Although the double shell nanocatalysts have two different catalytically active surfaces, the SERS measurement is able to probe the changes on the gold surface where the plasmon field is strongly focused.

Controlling the selectivity of the catalyst is an important goal of catalysis research.[51-54] This can be accomplished by designing the catalyst to include different surface facets with different atomic density and surface energy. The hydrogenation of benzene on the surface of Pt (111) produces cyclohexane and cyclohexene, while only cyclohexene was obtained on the surface of Pt (100).[55] **Chapter 5** discusses how selectivity of the plasmonic nanocatalyst with multiple plasmon modes can be controlled by changing the wavelength of the exciting light. Gold nanospheres (AuNSs) located inside of gold-platinum double shell nanoparticles in a rattle structure were prepared with different sizes and showed two plasmon spectral modes. The high energy plasmon mode corresponds to the photo-excitation of the small nanosphere, while the low energy plasmonic mode is related to both the gold-platinum double shell plasmon and the inside nanosphere, as assigned by calculation using the discrete dipole approximation (DDA) simulation technique. Photodimerization of 4-nitrothiophenol (4NTP) adsorbed on the surface of gold platinum nanorattles (AuPtNRTs) was studied using the surface-enhanced Raman spectroscopy technique.

Study and development of the new electrocatalysts for oxygen reduction reaction (ORR) is of a great importance for fuel cell applications. In **Appendix A** silver nanoplates of different sizes were synthesized and surface structure sensitivity of ORR was studied. Silver nanoplates were characterized by electron microscopy techniques and have shown to have mainly (111) surface structure on top and bottom and mixture between (100) and (111) structures on the edge surface. Activity of two silver surfaces

towards oxygen reduction reaction was measured via cyclic voltammetry and (111) surface structure was found to be more active compared to (100) surface structure.

Work on this dissertation has been published in various chemistry journals; Chapter 3 from: MA Mahmoud, B. Garlyyev, MA El-Sayed, "Determining the Mechanism of Solution Metallic Nanocatalysis with Solid and Hollow Nanoparticles: Homogeneous or Heterogeneous" The Journal of Physical Chemistry C 117 (42), 21886-21893, 2013. Chapter 4 from: MA Mahmoud, B. Garlyyev, MA El-Sayed, "Controlling the Catalytic Efficiency on the Surface of Hollow Gold Nanoparticles by Introducing an Inner Thin Layer of Platinum or Palladium" The Journal of Physical Chemistry Letters 5 (23), 4088-4094, 2014. Chapter 5 from: MA. Mahmoud, B. Garlyyev, and Mostafa A. El-Sayed, "Wavelength Selective Photocatalysis Using Gold-Platinum Nano-Rattles". The Journal of Physical Chemistry C, 2015, 119 (32), pp 18618–18626.

REFERENCES

1. R&D Magazine, 2005.

2. Burda, C., et al., *Chemistry and properties of nanocrystals of different shapes.* Chemical Reviews, 2005. **105**(4): p. 1025-1102.

3. Bratlie, K.M., et al., *Platinum nanoparticle shape effects on benzene hydrogenation selectivity.* Nano Letters, 2007. **7**(10): p. 3097-3101.

4. Narayanan, R. and M.A. El-Sayed, *Shape-dependent catalytic activity of platinum nanoparticles in colloidal solution.* Nano Letters, 2004. **4**(7): p. 1343-1348.

5. Mahmoud, M.A., et al., *A new catalytically active colloidal platinum nanocatalyst: The multiarmed nanostar single crystal.* Journal of the American Chemical Society, 2008. **130**(14): p. 4590-4591.

6. Bukhtiyarov, V.I. and M.G. Slin'ko, *Metallic nanosystems in catalysis.* Uspekhi Khimii, 2001. **70**(2): p. 167-181.

7. Mahmoud, M. and M. El-Sayed, *Time dependence and signs of the shift of the surface plasmon resonance frequency in nanocages elucidate the nanocatalysis mechanism in hollow nanoparticles.* Nano letters, 2011. **11**(3): p. 946-953.

8. Lee, K.S. and M.A. El-Sayed, *Dependence of the enhanced optical scattering efficiency relative to that of absorption for gold metal nanorods on aspect ratio, size, end-cap shape, and medium refractive index.* Journal of Physical Chemistry B, 2005. **109**(43): p. 20331-20338.

9. Huang, X., et al., *Cancer Cell Imaging and Photothermal Therapy in the Near-Infrared Region by Using Gold Nanorods.* Journal of the American Chemical Society, 2006. **128**(6): p. 2115-2120.

10. Jeanmaire, D.L. and R.P. Van duyne, *Surface Raman Spectroelectrochemistry .1. Heterocyclic, Aromatic, and Aliphatic-Amines Adsorbed on Anodized Silver Electrode.* Journal of Electroanalytical Chemistry, 1977. **84**(1): p. 1-20.

11. Mahmoud, M.A., et al., *Plasmonic Field Enhancement of the Exciton− Exciton Annihilation Process in a Poly (p-phenyleneethynylene) Fluorescent Polymer by Ag Nanocubes.* Journal of the American Chemical Society, 2010. **132**(8): p. 2633-2641.

12. Mubeen, S., et al., *An autonomous photosynthetic device in which all charge carriers derive from surface plasmons.* Nat Nano, 2013. **8**(4): p. 247-251.

13. Li, J.F., et al., *Shell-isolated nanoparticle-enhanced Raman spectroscopy.* Nature, 2010. **464**(7287): p. 392-395.

14. Zhao, L.-B., et al., *A DFT study on photoinduced surface catalytic coupling reactions on nanostructured silver: selective formation of azobenzene derivatives from para-substituted nitrobenzene and aniline.* Physical Chemistry Chemical Physics, 2012. **14**(37): p. 12919-12929.

15. Mahmoud, M.A. and M.A. El-Sayed, *Enhancing Catalytic Efficiency of Hollow Palladium Nanoparticles by Photothermal Heating of Gold Nanoparticles Added to the Cavity: Palladium–Gold Nanorattles.* ChemCatChem, 2014. **6**(12): p. 3540-3546.

16. Xu, H., et al., *Spectroscopy of Single Hemoglobin Molecules by Surface Enhanced Raman Scattering.* Physical Review Letters, 1999. **83**(21): p. 4357-4360.

17. Rodríguez-Lorenzo, L., et al., *Zeptomol Detection Through Controlled Ultrasensitive Surface-Enhanced Raman Scattering.* Journal of the American Chemical Society, 2009. **131**(13): p. 4616-4618.

18. Mahmoud, M.A., B. Snyder, and M.A. El-Sayed, *Surface Plasmon Fields and Coupling in the Hollow Gold Nanoparticles and Surface-Enhanced Raman Spectroscopy. Theory and Experiment†.* The Journal of Physical Chemistry C, 2010. **114**(16): p. 7436-7443.

19. McFarland, A.D. and R.P. Van Duyne, *Single silver nanoparticles as real-time optical sensors with zeptomole sensitivity.* Nano Letters, 2003. **3**(8): p. 1057-1062.

20. Mahmoud, M.A. and M.A. El-Sayed, *Different plasmon sensing behavior of silver and gold nanorods.* The Journal of Physical Chemistry Letters, 2013.

21. Sun, Y.G. and Y.N. Xia, *Shape-controlled synthesis of gold and silver nanoparticles.* Science, 2002. **298**(5601): p. 2176-2179.

22. Sun, Y., B. Mayers, and Y. Xia, *Metal Nanostructures with Hollow Interiors.* Advanced Materials, 2003. **15**(7-8): p. 641-646.

23. Sisco, P.N. and C.J. Murphy, *Surface-Coverage Dependence of Surface-Enhanced Raman Scattering from Gold Nanocubes on Self-Assembled Monolayers of Analyte†.* The Journal of Physical Chemistry A, 2009. **113**(16): p. 3973-3978.

24. Grzelczak, M., et al., *Shape control in gold nanoparticle synthesis.* Chemical Society Reviews, 2008. **37**(9): p. 1783-1791.

25. Xia, Y., et al., *Shape-Controlled Synthesis of Metal Nanocrystals: Simple Chemistry Meets Complex Physics?* Angewandte Chemie International Edition, 2009. **48**(1): p. 60-103.

26. Wilcoxon, J.P. and B.L. Abrams, *Synthesis, structure and properties of metal nanoclusters.* Chemical Society Reviews, 2006. **35**(11): p. 1162-1194.

27. Sajanlal, P.R., et al., *Electric field enhancement and concomitant Raman spectral effects at the edges of a nanometre-thin gold mesotriangle.* Journal of Materials Chemistry, 2010. **20**(11): p. 2108-2113.

28. Camden, J.P., et al., *Probing the Structure of Single-Molecule Surface-Enhanced Raman Scattering Hot Spots.* Journal of the American Chemical Society, 2008. **130**(38): p. 12616-12617.

29. Braun, G., et al., *Chemically Patterned Microspheres for Controlled Nanoparticle Assembly in the Construction of SERS Hot Spots.* Journal of the American Chemical Society, 2007. **129**(25): p. 7760-7761.

30. Hastings, S.P., et al., *Quadrupole-Enhanced Raman Scattering.* ACS Nano, 2014. **8**(9): p. 9025-9034.

31. Kelly, K.L., et al., *The Optical Properties of Metal Nanoparticles: The Influence of Size, Shape, and Dielectric Environment.* J. Phys. Chem. B, 2003. **107**: p. 668-677.

32. Jana, N.R., L. Gearheart, and C.J. Murphy, *Wet chemical synthesis of high aspect ratio cylindrical gold nanorods.* Journal of Physical Chemistry B, 2001. **105**(19): p. 4065-4067.

33. Pastoriza-Santos, I. and L.M. Liz-Marzan, *Colloidal silver nanoplates. State of the art and future challenges.* Journal of Materials Chemistry, 2008. **18**(15): p. 1724-1737.

34. Orendorff, C.J., et al., *Aspect ratio dependence on surface enhanced Raman scattering using silver and gold nanorod substrates.* Physical Chemistry Chemical Physics, 2006. **8**(1): p. 165-170.

35. Abbet, S., et al., *Pd1/MgO(1 0 0): a model system in nanocatalysis.* Surface Science, 2002. **514**(1–3): p. 249-255.

36. Narayanan, R. and M.A. El-Sayed, *Changing Catalytic Activity during Colloidal Platinum Nanocatalysis Due to Shape Changes: Electron-Transfer Reaction.* Journal of the American Chemical Society, 2004. **126**(23): p. 7194-7195.

37. Mahmoud, M.A., F. Saira, and M.A. El-Sayed, *Experimental Evidence For The Nanocage Effect In Catalysis With Hollow Nanoparticles.* Nano Letters, 2010. **10**(9): p. 3764-3769.

38. Mahmoud, M.A. and M.A. El-Sayed, *Time Dependence and Signs of the Shift of the Surface Plasmon Resonance Frequency in Nanocages Elucidate the Nanocatalysis Mechanism in Hollow Nanoparticles.* Nano Letters, 2011. **11**(3): p. 946-953.

39. Mahmoud, M.A., R. Narayanan, and M.A. El-Sayed, *Enhancing colloidal metallic nanocatalysis: sharp edges and corners for solid nanoparticles and cage effect for hollow ones.* Accounts of chemical research, 2013. **46**(8): p. 1795-1805.

40. Mahmoud, M.A., *Surface-Enhanced Raman Spectroscopy of Double-Shell Hollow Nanoparticles: Electromagnetic and Chemical Enhancements.* Langmuir, 2013. **29**(21): p. 6253-6261.

41. Sun, Y.G., B. Mayers, and Y.N. Xia, *Metal nanostructures with hollow interiors.* Advanced Materials, 2003. **15**(7-8): p. 641-646.

42. Yadav, M., et al., *Strong metal-molecular support interaction (SMMSI): Amine-functionalized gold nanoparticles encapsulated in silica nanospheres highly active for catalytic decomposition of formic acid.* Journal of Materials Chemistry, 2012. **22**(25): p. 12582-12586.

43. Park, J.C., et al., *Ni@SiO2 yolk-shell nanoreactor catalysts: High temperature stability and recyclability.* Journal of Materials Chemistry, 2010. **20**(7): p. 1239-1246.

44. Chen, C., et al., *Highly Crystalline Multimetallic Nanoframes with Three-Dimensional Electrocatalytic Surfaces.* Science, 2014. **343**(6177): p. 1339-1343.

45. Zeng, J., et al., *A Comparison Study of the Catalytic Properties of Au-Based Nanocages, Nanoboxes, and Nanoparticles.* Nano Letters, 2010. **10**(1): p. 30-35.

46. Weng, G., M.A. Mahmoud, and M.A. El-Sayed, *Nanocatalysts Can Change the Number of Electrons Involved in Oxidation–Reduction Reaction with the Nanocages Being the Most Efficient.* The Journal of Physical Chemistry C, 2012. **116**(45): p. 24171-24176.

47. Narayanan, R., C. Tabor, and M.A. El-Sayed, *Can the observed changes in the size or shape of a colloidal nanocatalyst reveal the nanocatalysis mechanism type: Homogeneous or heterogeneous?* Topics in Catalysis, 2008. **48**(1-4): p. 60-74.

48. Mahmoud, M.A., *Proposed molecular mechanism for the colloidal nanocatalysis of the hexacyanoferrate III-thiosulfate electron transfer reaction: On the involvement of a Prussian blue analogue complex intermediate.* Journal of Catalysis, 2010. **274**(2): p. 215-220.

49. Landman, U., et al., *Factors in gold nanocatalysis: oxidation of CO in the non-scalable size regime.* Topics in Catalysis, 2007. **44**(1-2): p. 145-158.

50. Wunder, S., et al., *Catalytic Activity of Faceted Gold Nanoparticles Studied by a Model Reaction: Evidence for Substrate-Induced Surface Restructuring.* Acs Catalysis, 2011. **1**(8): p. 908-916.

51. Zaera, F., *Shape-Controlled Nanostructures in Heterogeneous Catalysis.* ChemSusChem, 2013. **6**(10): p. 1797-1820.

52. Somorjai, G.A., et al., *Dynamics of Surface Catalyzed Reactions; the Roles of Surface Defects, Surface Diffusion, and Hot Electrons†.* The Journal of Physical Chemistry B, 2006. **110**(40): p. 20014-20022.

53. Lee, I., et al., *Tuning selectivity in catalysis by controlling particle shape.* Nat Mater, 2009. **8**(2): p. 132-138.

54. An, K. and G.A. Somorjai, *Size and Shape Control of Metal Nanoparticles for Reaction Selectivity in Catalysis.* ChemCatChem, 2012. **4**(10): p. 1512-1524.

55. Bratlie, K.M., et al., *Platinum Nanoparticle Shape Effects on Benzene Hydrogenation Selectivity.* Nano Letters, 2007. **7**(10): p. 3097-3101.

CHAPTER 2

SYNTHESIS AND CHARACTERIZATION OF METAL NANOPARTICLES

Summary

Nanomaterials have been a one of the very intriguing areas in scientific research over the previous few decades. Synthesis of nanoparticles has been widely explored; two main approaches have been used in synthesize of nanoparticles. First one being bottom up method where nanoparticles are constructed atom-by-atom and often in solution phase to produce a colloidal suspension. Second method is known as top down, where one starts with a bulk material and systematically removes material till the desired nanoparticle is left and is typically done by lithography. In this chapter, colloidal synthesis (bottom-up) method is discussed. Specific details of the synthetic routes and monolayer fabrication technique are explained. Lastly instrumentation that was used in characterization of metal nanoparticles in this dissertation are elucidated.

Common Synthetic Methods of Colloidal Metal Nanoparticles.

Colloidal synthetic method of metal nanoparticles can be generalized by simple steps: First, a metallic salt is dissolved in solution. Then the metal salt is reduced using a reducing agent, resulting in ground state metal atoms in solution that begin to bond and form a solid particle. Third step is where the particle grows in size as time progresses until a capping agent restricts the growth at a specific size and or shape. Figure 2.1 shows very basic depiction of the colloidal metal nanoparticle synthesis.

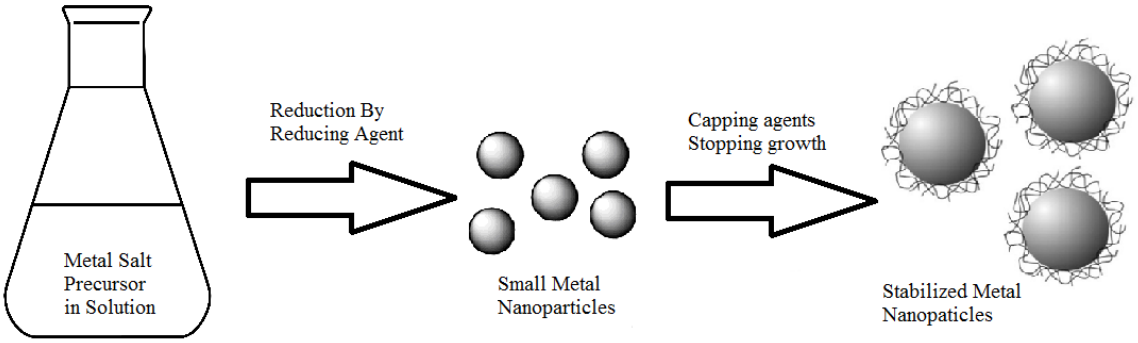

Figure 2.1 Schematic representation of colloidal metal nanoparticle synthesis.

While these steps are generally used for most colloidal syntheses, there are many varieties that can be implemented to produce a variety of shapes and sizes. Main control over shape and size of metal nanoparticles are done by changing capping agent, reducing agent, solvent and temperature. For instance, the reducing agent and capping agent can be same compound sodium citrate, or separate reducing agent and capping material can be implemented.

Gold Nanoparticles Synthesized in Dissertation

Gold nanospheres

Gold nanospheres (AuNSs) were prepared as reported earlier, by the reduction of $HAuCl_4.3H_2O$ using PVP (MW≈10,000).[1,2] Briefly, in a 150 mL flask, 100 mL of 0.085 mM gold salt solution in deionized water (DI) was heated until boiling. Under 500 rpm stirring, 0.5 g PVP was added. The reaction was allowed to proceed until the solution turned to red color and the LSPR peak became narrow.

Gold hollow nanospheres

Gold hollow nanospheres (AuHNSs) were prepared by the galvanic replacement of silver atoms in silver nanosphere (AgNS) template with gold ions. Briefly, AgNSs were prepared by heating of 50 mL of ethylene glycol (EG) in a 100 mL round bottom glass flask at 145 ^oC for 20 minutes. 0.4 g of PVP (MW~55,000) was then added to the hot EG solution. Then, 0.2 g of $AgNO_3$ dissolved in 5 mL EG was added at once at stirring speed of 500 rpm. After heating and stirring for 5 minutes, the reaction was stopped by quenching the solution with ice water. In order to separate the AgNSs from the by-product, 20 mL of AgNSs solution was diluted with 20 mL DI water and centrifuged at 14,000 rpm for 25 minutes. The precipitated AgNSs were dispersed in a solution of 0.01 g of PVP (MW~55,000) dissolved in 100 mL DI water. In order to prepare gold hollow nanospheres (AuHNSs), AgNSs solutions in water were heated and brought to boiling, then $HAuCl_4$ solution (0.01 g/L) was injected slowly into the hot silver solutions until the LSPR peak of the solution shifted to ~ 650 nm. The solution was cooled and cleaned by 10,000 rpm centrifugation as reported earlier.[3] Cleaned nanoparticle solutions were re-dispersed in DI water and the final optical densities were equilibrated to 1.25 for AuNSs and 1.1 for AuHNSs and AuNCs. These stock solutions of nanoparticles were used throughout the study. The cubical gold nanocages (AuNCs) of different sizes were prepared by the galvanic replacement technique.

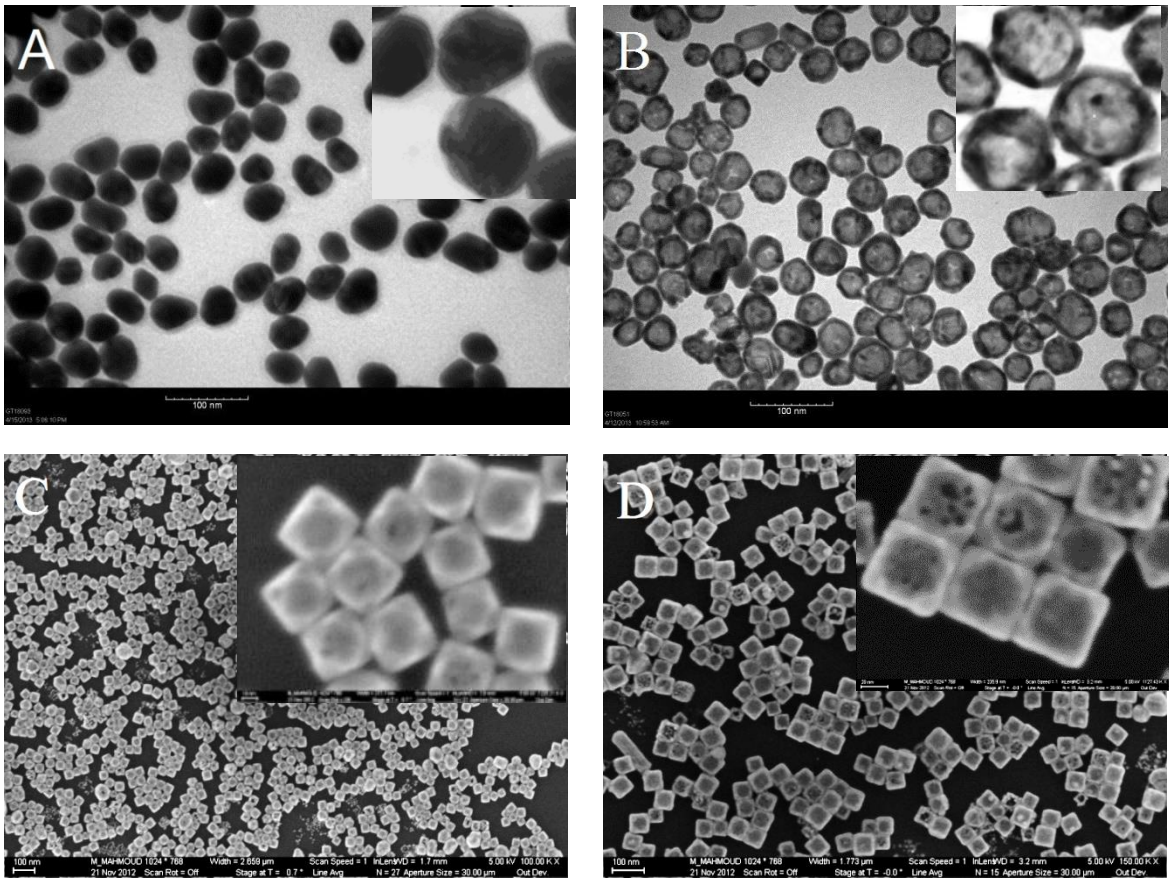

Figure 2.2. TEM images of some of the gold nanoparticles used in this dissertation: A) Solid Gold nanospheres B) Hollow Gold nanospheres. C) And D) are SEM images of Gold nanocages

Gold nanocages

Gold nanocage, gold-platinum double-shell, and gold-palladium double-shell nanocatalysts were prepared from silver nanocubes template by the galvanic replacement technique, as previously reported.[4] Briefly the synthesis of silver nanocubes, in a 100 mL round-bottomed flask, 35 mL of anhydrous ethylene glycol (Sigma Aldrich) was stirred at 400 rpm and heated at 140 °C for 1 h in an oil bath. After 1 h heating 0.35 g polyvinyl pyrrolidone (PVP) (molecular weight of ~55 000 g) dissolved in 5 mL ethylene glycol was added at once to the reaction mixture. The temperature of the reaction mixture was then raised gradually until it reached 155 °C. At this temperature, 0.4 mL of a 3 mM

solution of sodium sulfide in ethylene glycol was added after 5 min from the addition of PVP. 2 ml of $AgNO_3$ solution (0.48 g $AgNO_3$ dissolved in 10 mL ethylene glycol) was added. The solution was stirred briefly under constant heating until the solution turned a yellow/auburn color, at which point the single crystal silver seeds are produced. Growth of these particles into large cubes was achieved through careful monitoring of both the stir speed and temperature until a turbid yellow/greenish solution is produced. The silver nanocubes were cleaned of excess polymer and solvent by dilution to three times its original volume with an acetone-water mixture and centrifugation at 14,000 rpm for 5 minutes. The precipitated particles were then re-dispersed and stored in deionized (DI) water. For gold nanocages 10 mL from the 20 mL cleaned silver nanocubes was diluted to 200 mL with DI water and brought to boiling and stirred with stirring rate of 300 rpm. $HAuCl_4$ solution (0.1 g/L) was injected slowly into the hot silver nanocube solution until the LSPR peak of the solution shifted to 600 nm. The gold nanocages solutions were then continuously refluxed until their absorption spectrum became stable. Then the solution was cooled down to room temperature and left for 2 days to allow the AgCl byproduct to settle down and precipitate. The AgCl precipitate was removed by decantation of the gold nanocages solution. In order to clean the gold nanocages cavity from the AgCl salt, if any are left, the solution of gold nanocages was sonicated for 30 min, and then left for a day until all of the AgCl precipitates settled to the bottom of the solution. The solution was centrifuged at 10 000 rpm for 10 min. and the gold nanocages were dispersed in DI water.

Gold-Platinum hybrid nanocages

In order to synthesize Au−Pt shell−shell nanocages solution of K_2PtCl_4 (0.05 g/10 mL) was added to the gold nanocages solution, after cleaning as shown above. The LSPR peak of gold nanocages shifted to red as the amount of K_2PtCl_4 increased due to the replacement of the remaining silver inside the gold nanocages with formation of Pt inner shell. The LSPR peak position was measured as a function of the volume added from the

salt solution. Solution was left until the LSPR peak position became constant and was not shifting any more.

Gold-Platinum nanorattles

AuPtNRTs were synthesized by preparing AuNSs by the citrate reduction approach.[5] 500 mL of 1% hydrogentertrachloroaurate trihydrate aqueous solution was brought to boiling. Under gentle stirring and heating, 5 mL of 4% trisodium citrate trihydrate was added; the heating and stirring were continued until the color of the solution turned to red wine color. After cooling, the AuNSs were cleaned by centrifugation at 12000 rpm for 10 min and re-dispersed in 100 mL deionized (DI) water. The second step in the synthesis of AuPtNRTs was the synthesis of silver gold core-shell nanoparticles (Ag-AuNSs), and this was carried out by depositing a silver layer of different thicknesses on the surface of AuNSs.[6] Briefly, 400 mL solution of the cleaned AuNSs of OD=0.35 was brought to boiling, and 4 mL of trisodium citrate trihydrate (2%) was added followed by 1.2 mL silver nitrate (0.2 M). The solution was boiled and stirred for 4 min until color turned to yellow. The resulting particles were coated with a thin shell of silver. The thickness of the silver nanoshell was increased by the following steps. After the solution of Ag-AuNSs cooled down, its OD was adjusted to be 0.44. The Ag-AuNSs (OD=0.44) solution of volume of 200, 150, 100, and 75 mL was diluted with 0, 50, 100, 125 mL DI water, respectively. 0.05 g of polyvinyl pyrrolidone (MW = 55 000) dissolved in 10 mL was added to the resulting diluted Ag-AuNSs solution. Under slow stirring, 0.1 M $AgNO_3$ solution and 0.078 M L-Ascorbic acid solution of volume of 0.5, 1, 1.5, and 2 mL was added to the Ag-AuNSs solutions resulting from the dilution of concentrated Ag-AuNSs with volumes of 200, 150, 100, and 75 mL, respectively. The stirring was continued for 5 minutes. The resulting Ag-AuNSs with silver shells of different thicknesses were cleaned by centrifugation at 9,000 rpm for 5 minutes and redispersed in 100 mL DI water. Finally, the AuPtNRTs were prepared by galvanic

replacement technique.[7,8] The silver nanoshell surrounding the surface of AuNSs converted into a gold-platinum double shell by a procedure similar to the early reported technique.[9] 0.05 g of PVP dissolved in 5 mL DI water was added to the cleaned solutions of Ag-AuNSs, and the solution was heated until the temperature reached 80 ^{o}C. Under stirring, an aqueous solution of $HAuCl_4.3H_2O$ (0.001g/10 ml) was added dropwise until the LSPR peak shifted to 600 nm. After 24 hours, the resulting nanoparticles were decanted from the precipitated AgCl. In order to add an internal platinum nanoshell to the gold nanorattle, 10 mL of ammonium tetrachloroplatinate (II) (0.05g/10 mL) was added dropwise to the solution of nanoparticles resulting from the final step. After each drop added from the platinum salt solution, the solution of the nanoparticles was vigorously shaken. The AuPtNRTs solution was kept for 24 hours and decanted from the AgCl precipitate, and then centrifuged at 6,000 rpm for 10 minutes and the residue was re-dispersed in 20 mL DI water. The gold nanorattles were prepared as reported.[6]

Lamgmuir-Blodget Technique for Monolayer Fabrication

Langmuir-Blodgett (LB) technique was first developed by Irving Langmuir and Katherine Blodgett in the late 1920s. Briefly in LB technique monolayers are made by transferring organic molecule from the surface of a water bath to a solid substrate via dipping the substrate into water phase. Figure 2.3 shows a picture of the Langmuir-Blodgett trough used in this work.

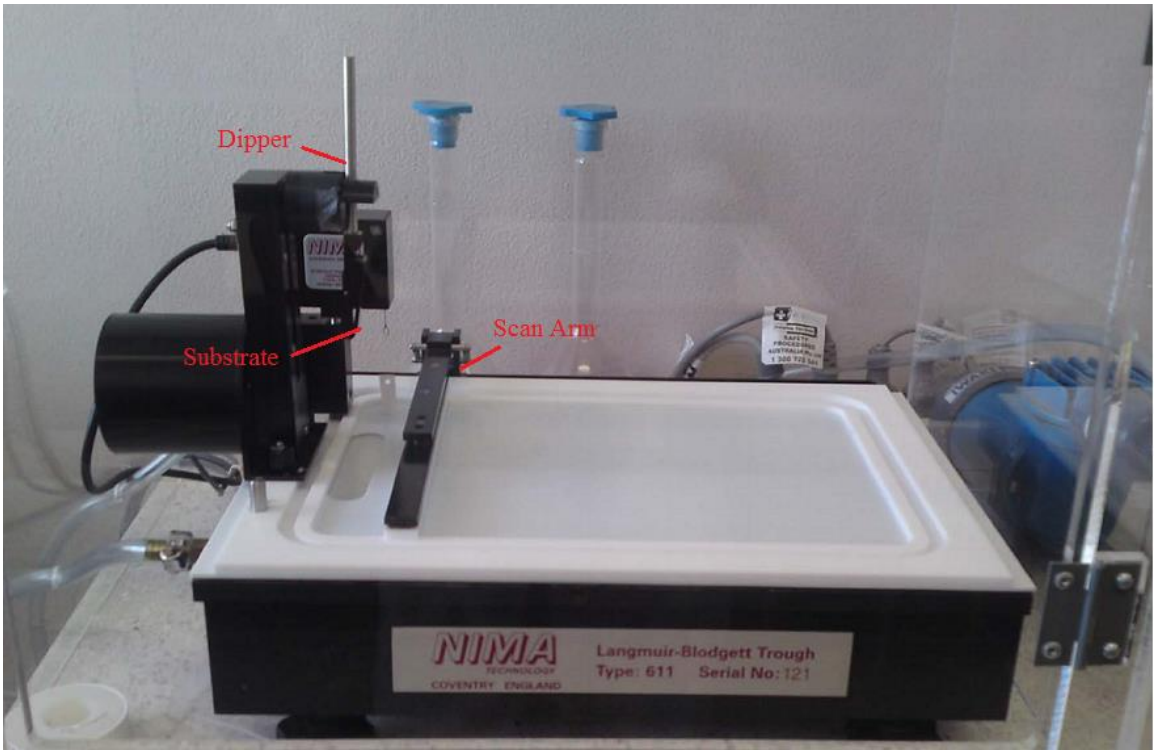

Figure 2.3. Langmuir-Blodgett trough used in this dissertation.

In this dissertation Langmuir-Blodgett deposition technique has been applied to fabricate single monolayers of colloidal metal nanoparticles. In typical method colloidal metal nanoparticles are dissolved in a volatile organic solvent such as chloroform or toluene (sometimes mixed with methanol) and then dispersed onto the surface of a water. Then volatile organic solvent evaporates in about 10-15mins leaving monolayer of nanoparticles stranded at water surface. Then the monolayer of nanoparticles can be transferred to a desired solid substrate, scanning arm allows for some control over the average separation between nanoparticles on the substrate.

In a typical procedure used in this work to assemble the nanocatalysts into monolayers on the surface of the quartz substrate, the prepared nanoparticles in aqueous solution were transferred to chloroform. 100 mL from the nanocatalyst solution was precipitated by with centrifugation at 6,000 rpm for 10 minutes and re-dispersed in 2 mL methanol. The nanoparticles in methanol were diluted with 3 mL of chloroform. The

nanoparticles were then dispersed on top of the Nima 611D Langmuir-Blodgett trough using a micro-syringe filled with water sub layer. The nanocatalyst monolayer was dried for 30 minutes before being transferred to the surface of the quartz substrate by the vertical dipping technique. Eight quartz substrates of 1 cm x 2.5 cm were coated at simultaneously at surface pressure of 2 mN/m, which was measured by D1L-75 model pressure sensor.

Electron Microscopy, TEM, SEM

For imaging metal nanoparticle samples several microscopy methods were used. Colloidal solutions of synthesized nanoparticles were imaged using a JEOL 100CX-2 transmission electron microscope (TEM). Copper TEM grids used for imaging were purchased from Ted Pella. The JEOL 100CX-2 was located in the Renewable Bioscience Institute (former paper science institute) at Georgia Tech. The high-resolution TEM and energy-dispersive X-ray spectroscopy (EDS) elemental mapping carried out using a Tecnai F30 microscope. Scanning electron microscopy (SEM) was used to image the particles on a substrate that were fabricated by LB technique. Instrument a Zeiss Ultra 60 FE-SEM located in Microelectronics Research Center at Georgia Tech was used.

REFERENCES

1. Weng, G., M.A. Mahmoud, and M.A. El-Sayed, *Nanocatalysts Can Change the Number of Electrons Involved in Oxidation-Reduction Reaction with the Nanocages Being the Most Efficient.* Journal of Physical Chemistry C, 2012. **116**(45): p. 24171-24176.

2. Mahmoud, M.A. and G. Weng, *Nanocatalysis Production of Photoactive Radicals.* Catalysis Communications, 2013. **38**: p. 63-66.

3. Mahmoud, M.A. and M.A. El-Sayed, *Metallic Double Shell Hollow Nanocages: The Challenges of Their Synthetic Techniques.* Langmuir, 2012. **28**(9): p. 4051-4059.

4. Mahmoud, M.A., F. Saira, and M.A. El-Sayed, *Experimental Evidence For The Nanocage Effect In Catalysis With Hollow Nanoparticles.* Nano Letters, 2010. **10**(9): p. 3764-3769.

5. Freund, P.L. and M. Spiro, *Colloidal Catalysis - the Effect of Sol Size and Concentration.* Journal of Physical Chemistry, 1985. **89**(7): p. 1074-1077.

6. Mahmoud, M.A., *Optical Properties of Gold Nanorattles: Evidences for Free Movement of the Inside Solid Nanosphere.* The Journal of Physical Chemistry C, 2014. **118**(19): p. 10321-10328.

7. Sun, Y.G. and Y.N. Xia, *Shape-controlled synthesis of gold and silver nanoparticles.* Science, 2002. **298**(5601): p. 2176-2179.

8. Sun, Y., B. Mayers, and Y. Xia, *Metal Nanostructures with Hollow Interiors.* Advanced Materials, 2003. **15**(7-8): p. 641-646.

9. Mahmoud, M.A. and M.A. El-Sayed, *Time Dependence and Signs of the Shift of the Surface Plasmon Resonance Frequency in Nanocages Elucidate the Nanocatalysis Mechanism in Hollow Nanoparticles.* Nano Letters, 2011. **11**(3): p. 946-953.

CHAPTER 3

DETERMINING THE MECHANISM OF SOLUTION METALLIC NANOCATALYSIS WITH SOLID AND HOLLOW NANOPARTICLES: HOMOGENEOUS OR HETEROGENEOUS

Summary

Metallic nanocatalysis in solution can take place either on the nanoparticle surface (heterogeneous mechanisms) or in solution by leached atoms or ions from the nanoparticle surface (homogeneous mechanism). So far, it has been difficult to distinguish between the two mechanisms. We have addressed this problem using the model reaction of the reduction of 4-nitrophenol (4-NP) by sodium borohydride (BH) in aqueous solution by metallic nanoparticles. We studied the reaction yield as a function of the free surface area of the nanoparticle after partial poisoning by 4-nitrothiophenol (4-NTP). Due to the fact both mechanisms will be dependent on the available active surface, we made use of the plasmonic properties of gold nanoparticles. For surface catalysis, if the products or intermediates have different dielectric value from that of the reactants, the surface plasmon extinction band would shift in the course of the reaction if solid or hollow plasmonic nanoparticles are used for the catalysis. This is observed for the reaction being examined in which hydrogen gas is produced causing a blue shift of the surface plasmon band of the hollow gold nanospheres (AuHNSs) used as a catalyst. Hollow nanoparticles can also be used to test for the involvement of the atomic surface leach mechanism. They have two plasmonic surfaces, the coupling between their surface fields increases by decreasing the wall thickness of the hollow nanoparticle if surface atom leaching takes place. This leads to a red shift of the nanocatalyst plasmon band. In the present study, AuHNSs did not show any red shift of the LSPR during or after the 4-

NP-BH reduction. This agrees with a surface heterogeneous type mechanism not involving leached atoms in solution.[1]

Introduction

The effective catalytic properties of the metallic nanoparticles are based on their high surface area to volume ratio[2], the surface potential of the nanocatalyst facets which depends on their atomic density[3], the number of valency unsaturated surface atoms [4,5], the capping material surface density of the nanocatalyst, and the energy of the Fermi level in redox reactions[6].

Solution catalysis with metallic nanoparticles can either take place on the surface of the nanoparticle (heterogeneous mechanism) or in solution by atoms or ions leached from the nanoparticle surface (homogeneous mechanism).[7] It has been difficult to determine which mechanism is dominant in colloidal solution nanocatalysis.[8-10] It is easy to examine the dependence of the rate of the reaction on the available surface area of the nanoparticle. This can be done by partially poisoning the surface of gold nanoparticles with different amounts of thiol compound such as 4-nitrothiophenol (4-NTP) and studying the effect on the efficiency of the nanocatalyst. If dependence is observed is this evidence for the heterogeneous mechanism? This experiment does not completely rule out the involvement of the homogeneous mechanism. Since the amount of leached ions or atoms is dependent upon the amount of exposed nanoparticle surface, the homogeneous reaction will also depend on the amount of 4-NTP bound to the surface.

To develop an experiment which could distinguish between the two mechanisms we turned to the plasmonic properties of nanoparticles. If the products or intermediates of a catalyzed reaction have different dielectric function from those of the reactants, a shift in the surface plasmon band of the solid or hollow plasmonic nanocatalyst should be observed for a heterogeneous (surface type) mechanism. In addition, plasmonic hollow nanoparticles can be used to test for surface atom leaching (homogeneous type) mechanism. Hollow nanoparticles have interior and exterior wall surfaces with connecting pores.[11-14] These hollow nanocatalysts have shown efficient catalytic properties due to a number of properties: the confinement of the reactant inside the cavity

(nanoreactor cage effect)[15,16], the high surface area resulting from the presence of the additional inner surface, and the fact that the inner surface could be less capped and have rougher morphology than the outer surface[17] giving it higher catalytic activity. Our recent studies suggest that catalysis using hollow nanocatalyst can take place efficiently inside the cavity and that the cage effect can play a great role in improving the efficiency of the hollow nanocatalysts.[18] In addition to the catalytic properties of the plasmonic hollow nanocatalysts, they are characterized by the presence of localized surface plasmon resonance (LSPR) spectrum.[12] Like solid plasmonic nanoparticles, their LSPR band shifts as the dielectric function of the medium around their surfaces is changed. This makes it easy to track changes in the chemical composition of the nanocatalyst for heterogeneous reactions on the surface.[12] The LSPR extinction wavelength depends also on the shape, size, and the wall thickness of the of the plasmonic nanocatalyst.[19] This latter property results from the dependence of the coupling between the outer and the inner surface plasmons of the hollow nanoparticles on the wall thickness. This makes hollow plasmonic nanoparticles especially useful in detecting atomic leaching from the surface[10] and reshaping due to atomic migration[7]. If the mechanism is of the homogeneous type and atoms (or ions) indeed leach out of the nanocatalyst surface, the thickness of the nanoparticle wall decreases leading to stronger coupling between the two wall surface plasmons with a resulting red shift of the nanoparticle LSPR band.[19]

In the present study we investigated the mechanism of the nanocatalytic reduction of 4-nitrophenol (4-NP) by sodium borohydride (BH) using plasmonic hollow nanospheres. We used both the method of measuring the dependence of the reaction yield on the surface area of the nanocatalyst (by using the adsorption isotherm of binding 4-NTP) as well as the changes of the plasmonic extinction band position of the hollow plasmonic nanospheres during the course of the reaction. The first technique suggested dependence of the reaction yield on the fraction of the free surface of the gold hollow nanospheres. This alone does not uniquely prove that it is a surface mechanism since the

rate of atomic leaching. The wavelength of LSPR of the hollow gold nanosphere was measured during and after the catalytic reaction. A shift in the wavelength can either suggest a change in the dielectric constant of the nanoparticle medium around the nanoparticle surface or thinning of the nanoparticle's walls, both suggesting a surface type mechanism. Blue (not red) shift in the LSPR peak of the AuHNSs nanocatalyst is observed during the catalysis strongly supporting the heterogeneous mechanism and indicating that species with lower dielectric constants than that of the solvent (e.g. hydrogen gas) are produced.

The surface morphology of solid nanocatalysts can be easily determined by electronic imaging techniques. This is not possible for the inner surface of hollow nanoparticles. In this study we present a method to measure the surface area and the morphology of the inner surface of the hollow nanocatalyst based on the observed adsorption isotherm technique. At the end of the paper, we discuss in details the possible molecular mechanism for the reaction studied.

Experimental

Nanoparticle synthesis

Gold nanospheres (AuNSs) were prepared as reported earlier, by the reduction of $HAuCl_4.3H_2O$ using PVP (MW≈10,000).[20,21] Briefly, in a 150 mL flask, 100 mL of 0.085 mM gold salt solution in deionized water (DI) was heated until boiling. Under 500 rpm stirring, 0.5 g PVP was added. The reaction was allowed to proceed until the solution turned to red color and the LSPR peak became narrow.

Gold nanocages (AuNCs) with different sizes have been prepared from a silver nanocube (AgNC) template by the galvanic replacement technique. The size of the template particle should vary accordingly with the size of the nanocage wanted to prepare. Briefly the synthesis procedure of the AuNCs from AgNCs is; 10 mL from the 20 mL cleaned AgNCs was diluted to 200 mL with DI water and brought to boiling and

stirred with stirring rate of 300 rpm. Hydrogen tetrachloroaurate ($HAuCl_4$, Sigma-Aldrich) solution (0.1 g/L) was injected slowly into the hot AgNCs solution until the SPR spectrum peak of the solution shifted to desired wavelength.

Gold hollow nanospheres (AuHNSs) were prepared by the galvanic replacement of silver atoms in silver nanosphere (AgNS) template with gold ions. Briefly, AgNSs were prepared by heating of 50 mL of ethylene glycol (EG) in a 100 mL round bottom glass flask at 145 ^oC for 20 minutes. 0.4 g of PVP (MW~55,000) was then added to the hot EG solution. Then, 0.2 g of $AgNO_3$ dissolved in 5 mL EG was added at once at stirring speed of 500 rpm. After heating and stirring for 5 minutes, the reaction was stopped by quenching the solution with ice water. In order to separate the AgNSs from the by-product, 20 mL of AgNSs solution was diluted with 20 mL DI water and centrifuged at 14,000 rpm for 25 minutes. The precipitated AgNSs were dispersed in a solution of 0.01 g of PVP (MW~55,000) dissolved in 100 mL DI water. In order to prepare gold hollow nanospheres (AuHNSs), AgNSs solutions in water were heated and brought to boiling, then $HAuCl_4$ solution (0.01 g/L) was injected slowly into the hot silver solutions until the LSPR peak of the solution shifted to ~ 650 nm. The solution was cooled and cleaned by 10,000 rpm centrifugation as reported earlier.[17] Cleaned nanoparticle solutions were re-dispersed in DI water and the final optical densities were equilibrated to 1.25 for AuNSs and 1.1 for AuHNSs and AuNCs. These stock solutions of nanoparticles were used throughout the study. The cubical gold nanocages (AuNCs) of different sizes were prepared by the galvanic replacement technique.

JEOL TEM 100CX was used to image the AuNSs and AuHNSs, Figure 3.1 A and B shows the TEM images of AuNSs of size 44 ±7 nm and AuHNSs of a size 41±6 nm, respectively. The AuNCs were imaged as shown in Figure 3.1 C and D utilizing Zeiss ultra 60 SEM, the sizes of the two AuNCs samples were found to be 37±3 nm and 56±3 nm, respectively.

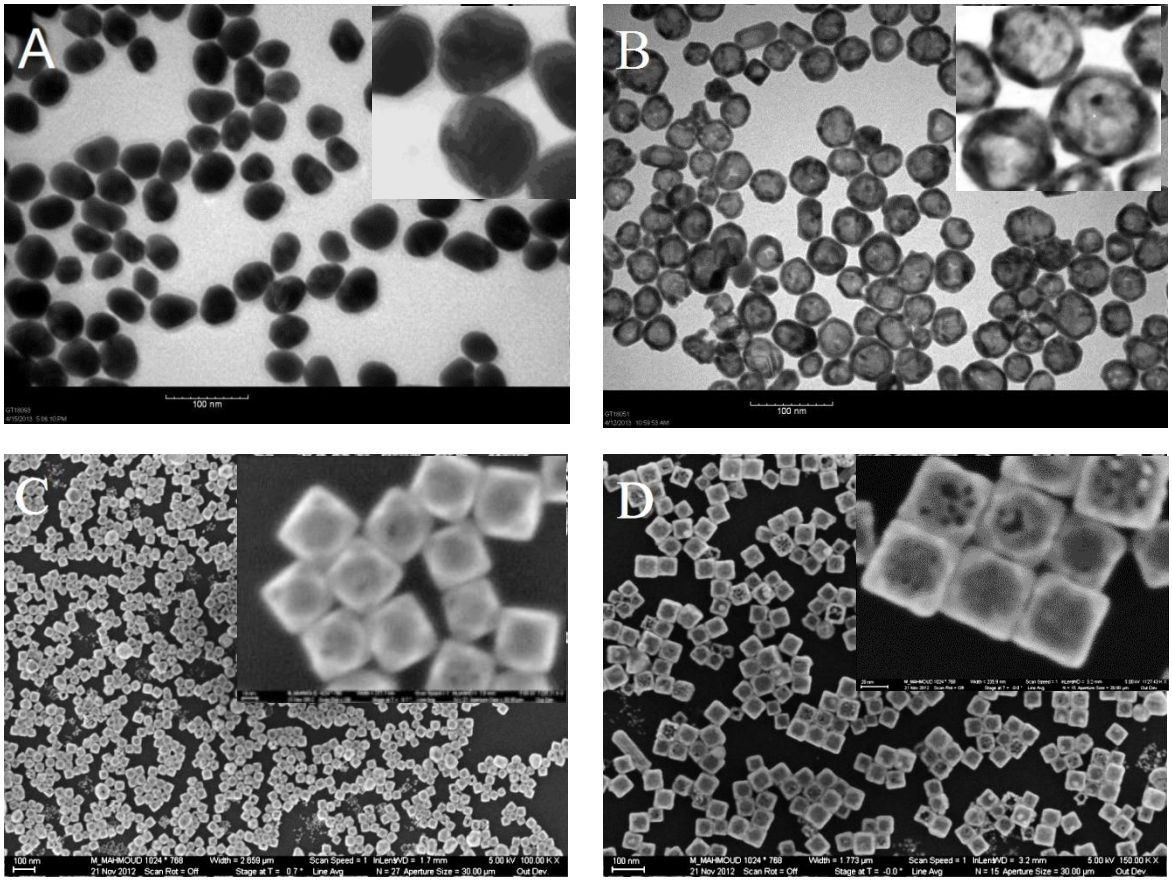

Figure 3.1. TEM images of: A) Solid Gold nanospheres (44 ±7 nm). B) Hollow Gold nanospheres (41 ±6 nm). SEM images of Gold nanocages with sizes of C) 37 ±3 nm D) 55 ±3 nm.

Adsorption isotherms and Langmuir plots

A solution of 0.1 mM 4-nitrothiophenol was prepared by sonication of the solid salt in DI water at pH=6.4 which was adjusted by 0.1 M sodium hydroxide solution. The resulting solution had an optical absorption peak at 410 nm. In eleven vials, 1 mL of gold nanospheres or gold nanocages solution were mixed with different amounts of 4-nitrothiophenol (4-NTP) and the final concentrations of 4-NTP after mixing were 0.5 - 10 x 10^{-5} M. The solutions were shaken by a mechanical shaker for 24 hours. The unadsorbed amount of 4-NTP was measured optically and calculated using the extinction coefficient of 4-NTP. The equilibrium concentration was calculated from the absorption peak intensity after adsorption. The moles of adsorbed 4-NTP per gram of nanoparticle

was calculated by dividing the total amount of adsorbed 4-NTP by the weight of gold present in 1 mL of gold nanoparticles solution. The weight of gold was measured by ICP-MS, after dissolving by aqua regia.

Calibration curve and extinction coefficient of 4-nitrothiophenol

4-nitrothiophenol (4NTP) was prepared with different concentration, and the absorption spectrum was measured for each solution. Figure 3.2 shows the relationship between the optical densities of the absorption spectrum of 4-NTP and the concentration. The relationship is linear obeying Beer's Law. The slope of the curve is the extinction coefficient which is 11,170.

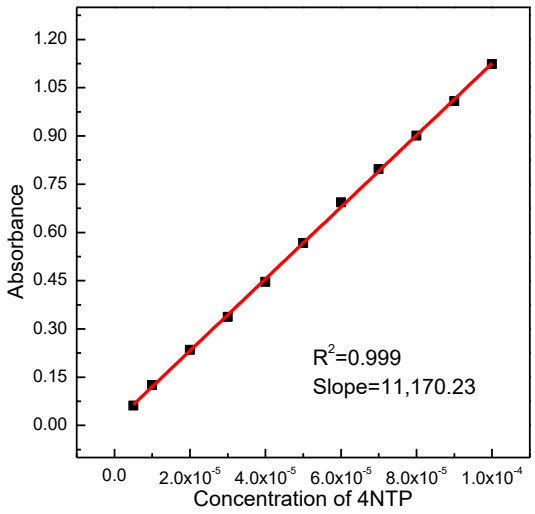

Figure 3.2. The relationship between the optical densities of the absorption spectrum of 4-NTP and the concentration. The relationship is linear obeying Beer's Law.

Determination of the effective surface area

The number of grams of gold present in 3mL of the nanoparticles solution (which used in the adsorption isotherm measurement), was determined as follow: The optical density of the cleaned AuNSs, AuHNSs, and AuNCs with 37 nm and 55nm sizes were measured and found to be 1.3, 0.73, 2.17, and 1.95 respectively. 5 mL of AuNSs, AuHNSs and 6 mL of AuNCs were dissolved in 20 mL *aqua regia*. Then the solutions

were boiled and evaporated in the fume hood until their volumes became to be 0.5 mL. The volumes of the resulting solution were completed to 5 mL for AuNSs, AuHNSs and to 6 ml for AuNCs by DI water. The grams of the gold in solutions of AuHSs, AuNSs and AuNCs with sizes 37 nm and 55 nm were measured by ICP-MS and found to be 0.96, 7.54, 5.84, and 10.2 mg/L respectively. From the plasmon peak absorbance inside the 3mL solution and ICP results we found the grams of particles inside the 3mL solution.

We plotted the Langmuir isotherm plot between the equilibrium concentrations of 4-NTP divided by adsorbed moles of 4-NTP per gram of particle versus the equilibrium concentrations of 4-NTP. The concentration of 4-NTP was determined optically using the calibration curve. The slope of isotherm plot will give us reciprocal of the number of moles of 4-NTP per grams of the particle so the active surface area will be equal to: Surface area = $1/(\text{slope}) \times (N_A) \times (0.187) \times 10^{-18}\ m^2$

Where the number $0.187 \times 10^{-18}\ m^2$ is the average surface area which each 4-NTP molecule occupies (calculated by using ChemDraw software) and N_A is Avogadro's number. By using equation above Active surface area for Au nanospheres, Au hollow spheres and Au nanocages were calculated.

Kinetics studies

0.5 ml of AuHNSs solution was mixed with five different concentrations of 4-NTP solutions in five different vials and left for 10 minutes. Then 0.15 ml of 2 mM 4-NTP solution and 1.5 mL of 0.06 M sodium borohydride (BH) solution were added. The decrease in the intensity of the peak at 410 nm from 4-nitrophenol (4-NP) was followed optically with time by Ocean optics UV spectrometer.

Experiments used for studying the mechanism

AuHNSs solution of 3 mL, 0.5 mL DI water and 4.5 mL of 0.1 mM 4-NTP solution were mixed and the changes in the plasmon peak position were studied. After two hours, the solution was centrifuged and re-dispersed in water, separated into two parts and plasmon peak position was measured. One half of solution was re-dispersed in water and 1.5 mL of 0.06 M $NaBH_4$ solution was added to it and to the other half 1.5 mL of DI water was added and this solution was used as the control. Time dependent absorbance of the plasmon peak was recorded. Shift in the plasmon peak with time was plotted and the induction period was calculated. 1 mL of AuHNSs solution and 1.5 mL of 0.06 M $NaBH_4$ solution were mixed and the plasmon peak position was measured with time. After two hours the solution was centrifuged, re-dispersed in water, and absorbance was measured.

Results and discussion

Studying the Morphology of the Hollow Gold Nanocatalyst and the Determination of Their Effective Surface Area

The efficiency of any nanocatalyst with a surface type mechanism depends greatly on its surface area exposed to the reacting materials and the number of the chemically unsaturated active atoms.[4,5] During the synthesis of the colloidal nanocatalysts, capping materials are used to control the shape and stabilize the nanocatalyst.[2] Although these capping molecules stabilize the nanocatalyst during the catalysis reaction, they can also reduce the available surface area of the nanocatalyst because of their binding to the surface atoms of the nanocatalysts.[22,23] This means that the value of the chemically active surface area of the nanocatalyst will not be the same as the calculated one. Hollow nanocatalysts have two surfaces which are catalytically active, but the inner surface is more efficient than the outer one.[16,24] It is not possible to determine the surface area and morphology of the inner surface of the hollow

nanocatalyst using current techniques. The traditional techniques used to determine the surface area, based on Brunauer–Emmett–Teller theory (BET), will not be accurate in our study since solution catalysis is different from gas phase catalysis. We suggest using adsorption isotherms to determine both the surface area and inner surface morphology of the nanocatalysts. The surface area of the gold nanospheres of solid and hollow structure is determined by the Langmuir isotherm. Thiols have high affinity for atomic gold due to the formation of a semi-covalent bond.[25] The adsorption isotherms of the 4-nitrothiophenol (4-NTP) on the surface of AuNSs and AuHNSs, are shown in Figure 3.3 A and B, respectively. This isotherm is a relationship between the number of moles of adsorbed 4-NTP per gram of nanoparticle and the equilibrium concentration of 4-NTP remaining after the adsorption process. The amount of adsorbed 4-NTP on the surface of AuNSs or AuHNSs is determined from the optical measurement using the extinction coefficient of 4-NTP ($\varepsilon_{4\text{-NTP}}$=1.78x$10^4$ L $mole^{-1}$ cm^{-1}). The adsorption isotherm for the solid nanoparticles is one stage. The adsorption isotherm for AuHNSs has two adsorption stages. The reason is due to the presence of two different surfaces with different adsorption coefficients dye to different morphological properties. The adsorption isotherm of the hollow nanoparticles has an S-shape like porous silica.[26]

A Langmuir linear plot was used in order to determine the effective surface area per gram of nanoparticle. Figure 3.3 C shows the Langmuir plot of the adsorption of 4-NTP on the surface of AuNSs. For solid gold nanoparticle, a straight line is obtained with a slope of 453.51 g/mole (Figure 3.3 C), while for gold hollow nanoparticles it has two straight lines with slopes of 15.911 g/mole and 2.6230 g/mole (Figure 3.3D) respectively. The presence of two slopes again is due to the presence of two different surfaces with different surface binding properties. In order to calculate the surface area of the nanocatalysts from the Langmuir isotherm, the reciprocal of the slope of the Langmuir plot was multiplied by Avogadro's number and the cross section of 4-NTP molecule. According to our calculation, the actual surface area of AuNSs which were available for

catalysis is 248.2 m^2/g while the hollow AuHNSs have two different values: 7050 m^2/g for the outer surface and 42777 m^2/g for the inner surface. The large effective surface area of the AuHNSs is expected because of two reasons. First, as observed from the TEM images, the outer surface of AuHNSs is not completely smooth. Moreover, the presence of pores in the walls of AuHNSs could add to the value of the effective surface area. The second possible reason could be because some of the 4-NTP accumulates inside the cavity which decreases the actual equilibrium concentration. This supports our former reported studies for the nanoreactor cage effect in catalysis with hollow nanocatalysts.[18,20] However, during the catalysis with nanocatalysts of the hollow structures the reacting materials diffuses in and out through the pores on the surface and accumulate inside the cavity of the nanocatalyst. Although the confinement of the reactant inside the cavity of the hollow nanocatalyst increases the efficiency of the nanocatalysts[20], it causes decrease in the accuracy of our surface area measurement.

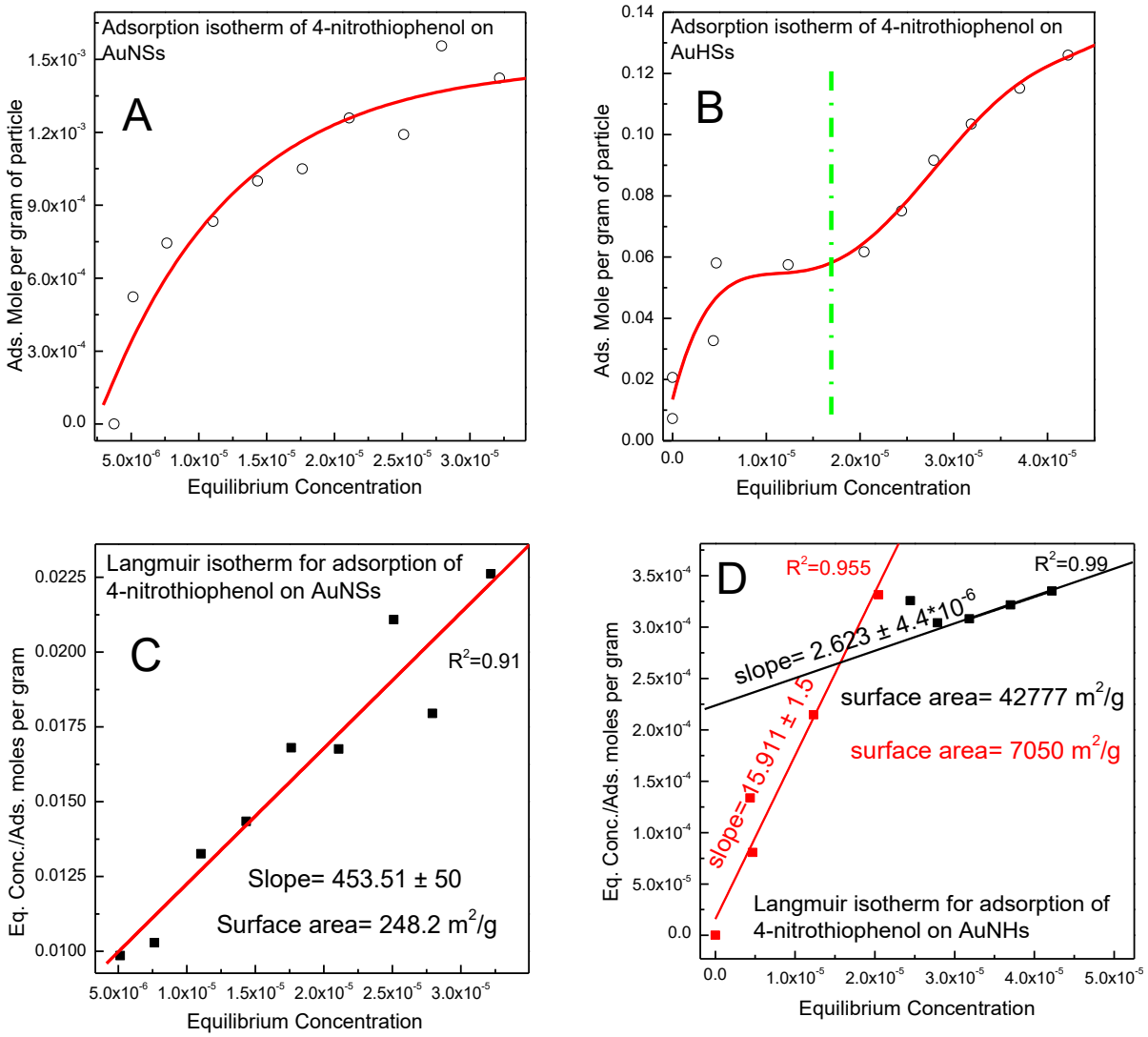

Figure 3.3. Adsorption isotherms of 4-nitrothiophenol on: A) Gold nanospheres, B) Gold hollow spheres. The isotherm is constructed by mixing fixed amounts of the nanoparticles with different amount of 4-nitrothiophenol, the adsorbed moles per gram of nanoparticle is in the vertical axis and the unabsorbed amount (equilibrium concentration) is in the horizontal axis. Langmuir isotherms of the adsorption of 4-nitrothiophenol on: C) Gold nanospheres, D) Gold hollow spheres. This suggests that the surface morphology of the hollow nanoparticles is not the same as for solid shapes especially the inner surface.

In order to confirm the idea that the morphology of the inner and outer surfaces of the hollow nanocatalysts is not identical, the adsorption isotherm of cubical gold nanocages of sizes 37±3 nm and 56±3 nm were determined. As in the case of AuHNSs,

both sizes of AuNCs had adsorption isotherms with two stages (see Figure 3.4.). The Langmuir plot strongly suggested that each of AuNCs of the two different sizes has two different surfaces with different binding properties.

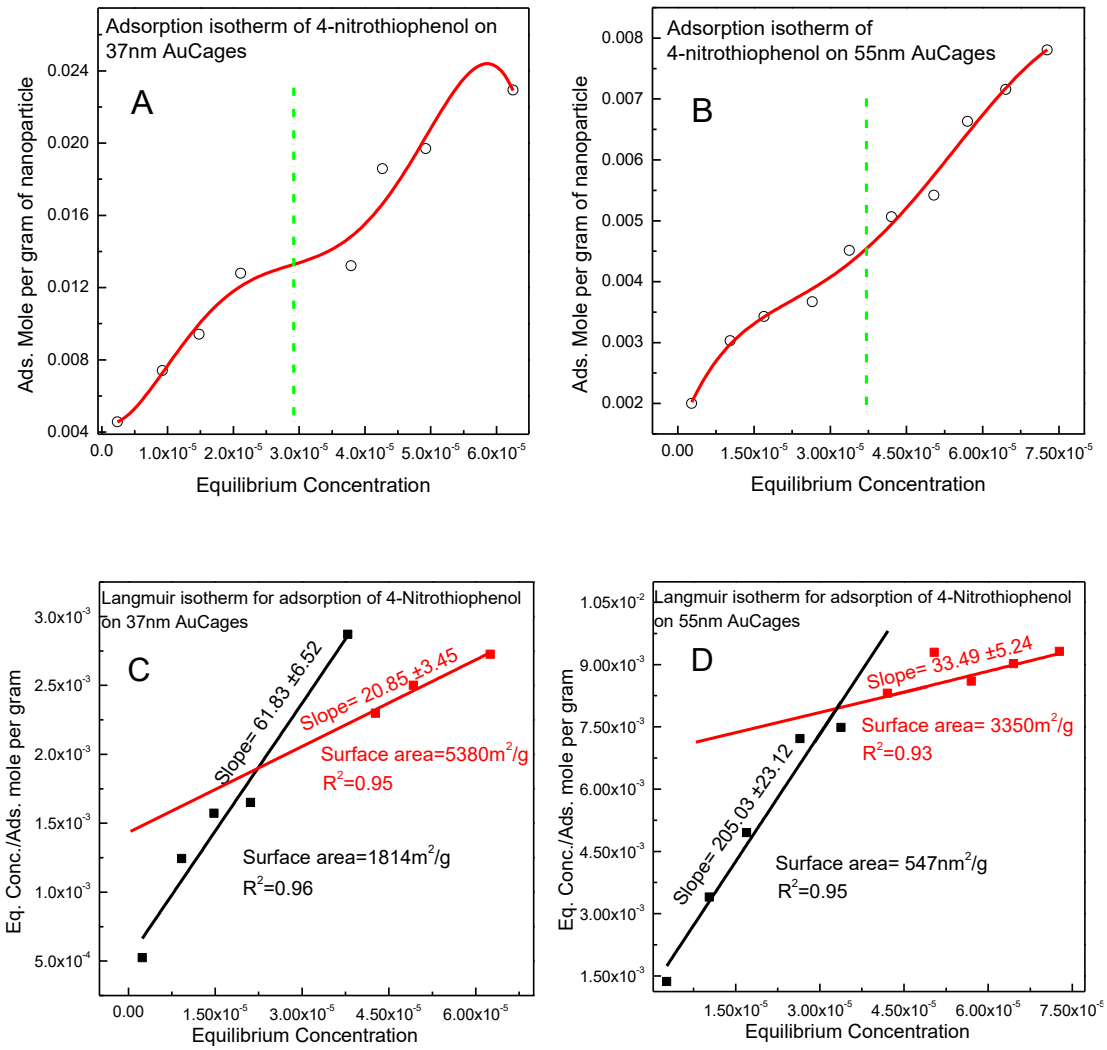

Figure 3.4. Adsorption isotherm of 4-nitrothiophenol on Gold Nanocages with size of: A) 37 ±3 nm B) 55 ±3 nm. The isotherm is constructed by mixing the fixed amount of the nanoparticles with different amount of 4-nitrothiophenol, the adsorbed moles per gram of nanoparticle is in the vertical axis and the unabsorbed amount (equilibrium concentration) is in the horizontal axis. Langmuir isotherm of the adsorption of 4-nitrothiophenol on Gold Nanocages with size of: C) 37 ±3 nm D) 55 ±3 nm.

Dependence of the Reaction Rate on the Nanoparticle's Available Surface Area

The effective surface area of the nanocatalyst can be decreased either by decreasing the size of nanocatalyst or by poisoning its surface with chemically bound materials. As shown above the 4-NTP strongly binds to the gold nanoparticles. Gold nanoparticles, like most of the metallic nanoparticles, can catalyze the reduction of 4-nitrophenol (4-NP) by sodium borohydride (BH).[27,28] The effective surface area of the nanocatalyst can be reduced either by decreasing the size of nanocatalyst or by poisoning a fraction of its surface with chemically bound materials. As shown above 4-NTP strongly binds to the gold nanoparticles. 4-NTP is the thiol analogue of 4-NP, unlike 4-NP, when 4-NTP is mixed with AuHNSs, the localized surface plasmon resonance (LSPR) red-shifts due to bond formation with the surface of the nanoparticles. In order to study the relationship between the decrease on the chemically active surface area of the nanocatalyst and the rate of the catalysis reaction, the catalytic reduction of 4-NP by BH in presence of nanocatalyst AuHNSs was taken as a model reaction. 4-NTP of different concentrations was added to the reaction mixture. The available surface area of the nanocatalyst depends on the amount of added 4-NTP. Figure 3.5. A shows the relationship between the natural logarithms of the concentration of 4-NP and the reaction time at different concentration of 4-NTP (0, 1.1, 3.3, 5.5, and 7.7 μM). The 4-NTP is mixed with the AuHNSs and left for 10 minutes. The inset panel in figure 3.5. A has similar features as the other curves in figure 3.5. A, but the 4-NTP is mixed with the AuHNSs and left for several days before being used in the catalysis reaction. It is observed that the reaction has an initial induction period (an incubation step involving no change in the concentration of 4-NP).[29] The relationship after the induction period is linear and the slope is equal to the negative value of the reaction rate constant, since the reaction proceeds by pseudo-first-order kinetics. The induction period increases as the amount of 4-NTP increases, while the rate constant of the reaction decreases (see Table

3.1). The LSPR of the AuHNSs blue shifts during the reaction, especially during the induction period; once it passed no further shift is observed in the LSPR.

Figure 3.5. B shows the relationship between the LSPR peak positions of the AuHNSs during the catalytic reduction of 4-NP by BH in the presence of different concentrations of 4-NTP. The LSPR peak of the AuHNSs red shifts due to binding of the 4-NTP to their surfaces and the value of the red shift increases as the amount of 4-NTP added is increased. In fact, when the AuHNSs, coated with different amount of 4-NTP, is mixed with 4-NP and BH, its LSPR peak blue shifts. The plot of the values of the rate constant of the 4-NP and BH reaction versus the concentration of 4-NTP decreases exponentially, while the induction period increases linearly with increasing the concentration of 4-NTP (Figure 3.5. C and D respectively).

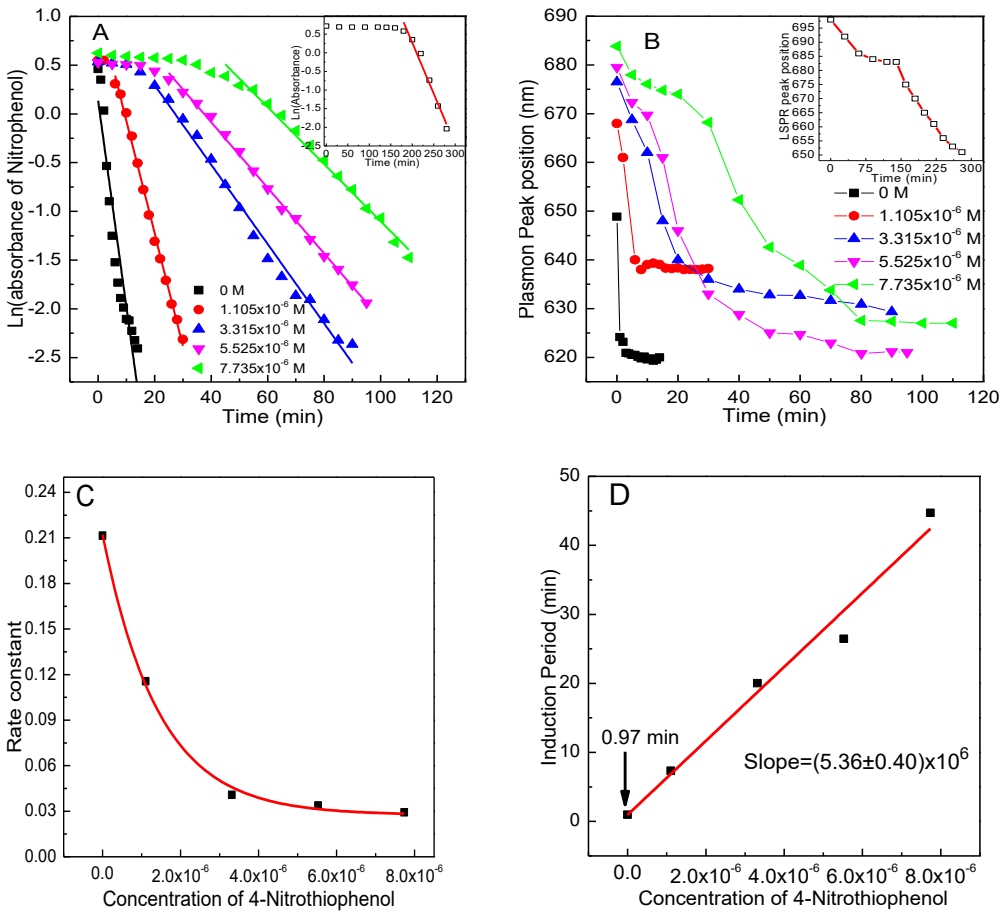

Figure 3.5. A) The relationship between the natural logarithm of the absorbance intensity of 4-nitrophenol and time, AuHNSs is covered with different amounts of 4-nitrothiophenol. B) The LSPR peak position of AuHNSs coated with different amount of 4-nitrothiophenol and measured at different time during the 4-nitrophenol-borohydride reaction. C) The relationship between the rate constant of the 4-nitrophenol-borohydride reaction catalyzed by AuHNSs with the concentration of 4-nitrothiophenol. D) The plot of the values of the induction period and the concentration of 4-nitrothiophenol. These results supports the idea that, as the effective surface area of the AuHNSs catalyst is decreased, by coating with 4-nitrothiophenol, the induction period increases while the reaction rate constant decreases.

Table 3.1. The rate constant and the induction period of the reduction of 4-nitrophenol by sodium borohydride catalyzed by AuHNSs coated with different amounts of 4-nitrothiophenol, and the values of the blue shift in the LSPR peak after catalysis reaction.

Conc. Thiophenol	**Rate constant**	**Induction Period (min)**	**Plasmon shift**
0	0.211±0.019	0.98	28.8
1.11×10^{-6}	0.116±0.002	7.34	29.8
3.32×10^{-6}	0.041±0.001	20.03	47.2
5.55×10^{-6}	0.034±0.001	26.47	58.5
7.74×10^{-6}	0.029±0.001	44.71	56.6
Saturated	0.027±0.001	180.00	48.0

Using the Plasmonic Properties in Determining the Nanoparticle Catalytic Mechanism

The dependence of the reaction rate constant and the induction period of the BH/4-NP reaction on the available surface area of the AuHNSs do not completely clarify whether the mechanism is homogenous or heterogeneous. Because both the surface reaction required for heterogeneous mechanism and the amount of leached atoms or ions that drive the homogenous mechanism depend on the available effective surface area of the AuHNSs. In order to determine the mechanism of the catalysis, the LSPR spectrum of the AuHNSs catalyst is followed during the catalysis reaction.

1. Sensitivity of the surface plasmon band wavelength to changes of the dielectric function of the surface medium during the reaction:

The advantage of the catalytic reaction being examined is that the by-product is H_2 gas. The dielectric constant of the medium around the nanoparticle surface of the plasmonic gold nanocatalyst changes from ~1.33 for water to ~1 for H_2 gas.[12] As a result,

the surface plasmon band should shift to the blue as shown in the present work (see figure 3.5. B). This allows the gold nanocatalyst to act as a probe for the changes taking place on or around the surface of the nanocatalyst.[29] This type of result could offer a strong evidence of surface heterogeneous type catalysis in agreement with the possible conclusions made in section above.

2. Testing for atomic leaching from the nanocatalyst surface:

The main difference between the hollow and solid nanoparticles is that when solid plasmonic nanoparticles lose surface atoms (size reduction) their LSPR peak blue shifts, while the hollow nanoparticles LSPR red shift.[30] We followed the shift in the LSPR peak of AuHNSs after binding of 4-NTP and BH. Figure 3.6. A shows the LSPR peak position of AuHNSs before and after mixing with 4-NTP. The LSPR peak of AuHNSs red shifts with time after mixing with 4-NTP, the maximum shift is obtained after 2 h when the peak position is shifted from 679 nm to 705 nm. The absorption peak intensity of 4-NTP at 410 nm is decreased 2 h after mixing due to binding to the surface of the AuHNSs. The LSPR peak position of AuHNSs does not change after moving from the 4-NTP solution to water medium by centrifugation because the 4-NTP binds strongly with surface of the nanoparticles. The peak corresponding to the free 4-NTP disappeared. Similar experiments carried out for BH adsorption on AuHNSs. Figure 3.6. B shows the LSPR spectrum of AuHNSs before and after mixing with BH. The blue shift in the LSPR peak position of AuHNSs increases with time. After 2 h the LSPR peak shifts from 679 to 628 nm. Then, the AuHNSs are moved to water medium by centrifugation, the LSPR peak of the AuHNSs shifts from 628 nm to 658 nm. When the AuHNSs are dispersed in aqueous medium for 1 hour, the LSPR peak shifts to the original peak position of 679 nm. These results strongly suggest that no atoms are leached from the AuHNSs surface during the reaction with BH since the initial plasmon peak position is recovered. Thus the

nanocatalyst mechanism in this reaction is heterogeneous (surface type) in nature in support of the results of the Langmuir isotherm surface coverage technique.

In order to confirm whether or not the BH reacts with the surface of AuHNSs while it is completely coated with a layer of 4-NTP, AuHNSs were coated with a layer of 4-NTP and then the BH was added. This was followed by a time dependent measurement for the LSPR of the AuHNSs (Figure 3.6 C). The LSPR peak position of the AuHNSs after coating with 4-NTP was at 705 nm, which after the addition of BH has blue-shifted with time, and the maximum shift was observed after 50 minutes when the LSPR peak position was at 650 nm. This result suggests that BH can penetrate or displace the 4-NTP adsorbed on the surface of AuHNSs or that the 4-NTP binds to specific sites and not all the surface sites of the nanoparticle surface. The shift in the LSPR peak of AuHNSs coated with a layer of 4-NTP after mixing with BH is shown in Figure 3.6. D.

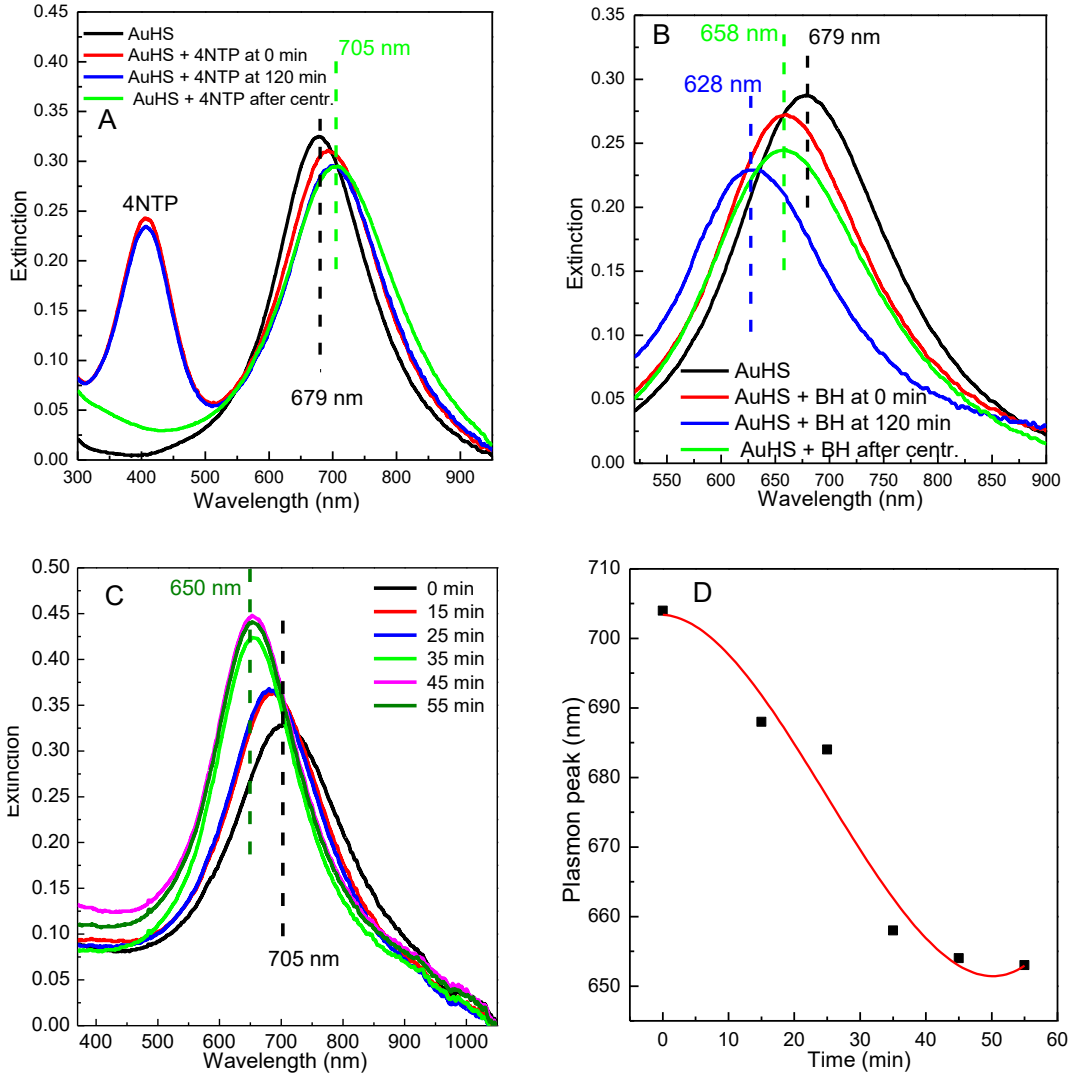

Figure 3.6. A) The LSPR spectrum of AuHNSs before and after mixing with 4-NTP measured at different time scale and the LSPR spectrum of AuHNSs after centrifugation, re-dispersed in DI water. B) The LSPR spectrum of AuHNSs after mixing with BH and after transferring to DI water. C) The LSPR spectrum of AuHNSs coated with a layer of 4-NTP and mixed with BH at different times. D) The time dependent measurement for the LSPR peak position of the AuHNSs coated with a layer of 4-NTP after mixing with BH.

Molecular Mechanism of the Reaction Studied

Our previous studies showed that the reaction of BH with the nanocatalyst takes place mainly during the induction period for the 4-NP-BH catalysis reaction.[12] However,

when the BH is mixed separately with the nanocatalyst for a period of time equal to the induction period the reaction proceeds immediately after the 4-NP is added. It has been reported that BH reacts with the metallic nanocatalyst producing hydrogen gas.[31] The hydrogen is not responsible for the reduction of 4-NP since AuHNSs exposed to H_2 gas for two hour could not catalyze the reduction of the 4-NP. BH catalytically decomposes in aqueous medium by metallic nanocatalysts due to the reaction with water through multiple steps of different oxidation potentials.[32]

The presence of multiple oxidized forms of borohydride have been detected by *in situ* FTIR measurements[32,33] BH is oxidized into different forms on the surface of Pt electrodes at different oxidation potentials. Each oxidation stage is accompanied with H_2 gas evolution and the oxidized BH species adsorb on the surface of the platinum electrode.[27,28] Therefore BH reacts with water on the surface of nanocatalyst producing hydrogen and an oxidized form of borohydride. 4-NP has no role during the reaction of BH with the surface of the AuHNSs forming hydrogen. First-principle calculations have shown that the BH and its oxidized forms bind to the surface of the gold through the H.[34]

As discussed above, the nanocatalysis occurs on the surface of the catalyst (i.e. the involvement of the heterogeneous mechanism). The reduced form of BH is formed on the surface of AuHNSs, the hydrogen gas evolves around their surface and gives the observed blue shift of the LSPR peak as its dielectric constant is much smaller than that of water. Then, the 4-NP molecule approaches the surface of AuHNSs and gets reduced by the adsorbed oxidized BH species. If 4-NTP is present, it will cover part of the surface of the AuHNSs nanocatalyst and increases the induction period and decreases the rate of the reaction, due to decreasing the available surface area.

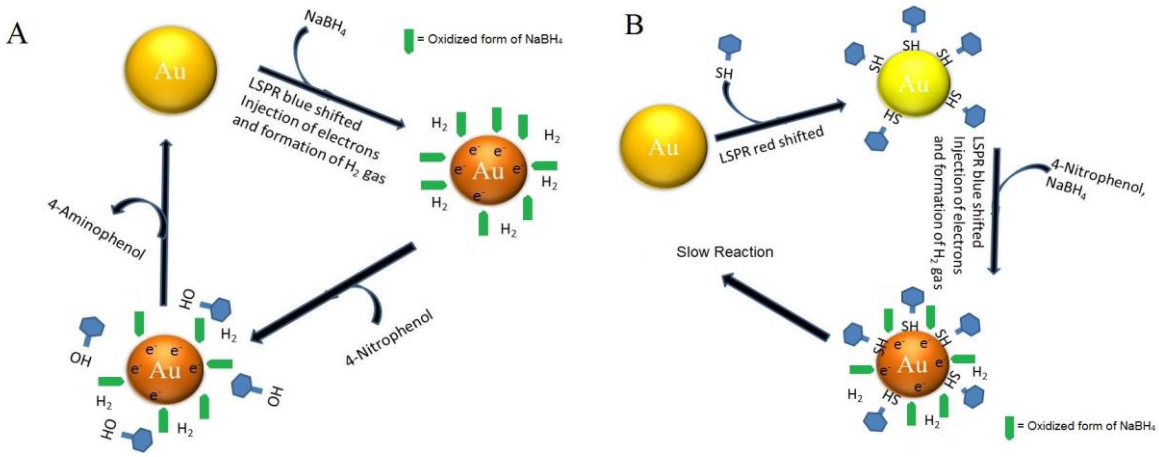

Figure 3.7. Possible schematic description for the reduction of 4-NP by BH catalyzed by AuHNSs: A) In absence 4-NTP the reaction proceeds rapidly, B) The rate of the reaction is reduced when the available surface of the nanocatalyst is decreased due to the binding of different amounts of 4-NTP, due to the involvement of the heterogeneous catalytic mechanism.

Conclusion

These results support our earlier studies reporting the high catalytic efficiency of the inner surface of the hollow nanocatalysts. In our former studies, we suggested that the strong catalytic properties of the hollow nanocatalyst are not only due to the cage effect but also to the fact that the morphology of the inner surface is more catalytic. The adsorption isotherm of the chemically bound 4-nitrothiophenol on the surface of the hollow and solid gold nanospheres showed a one stage isotherm for solid shape and a two stage isotherm for the hollow shape. The presence of two regions of the hollow shape isotherm confirmed the difference in the adsorption properties of the inner and outer surfaces of the hollow nanoparticles. The Langmuir isotherm is used to determine the surface area of the nanocatalysts. This method was applied to gold nanospheres, hollow nanospheres, and gold nanocages with consistent results.

The mechanism of the reduction of 4-nitrophenol by borohydride on the surface of gold nanocatalyst was discussed. The LSPR of hollow nanoparticles usually red-shifts as the wall thickness decrease. The LSPR of AuHNSs did not show any red shift during

or after the reaction indicating no atomic leaching from the surface of the nanocatalyst. Three different methods have been used which confirmed that the mechanism of the catalytic reduction of 4-NP by BH in presence of gold hollow nanospheres occurs on the surfaces (the heterogeneous mechanism): 1) The reaction rate constant and the induction period, which depend on the available effective surface area of the nanocatalyst, decreases by covering parts of the surface of the nanocatalyst with 4-nitrothiophenol; 2) the plasmonic band wavelength shifted to the blue as the reaction produced more hydrogen; and, 3) no red shift was observed for the surface plasmon band of the gold hollow nanosphere during the reaction eliminating the atomic leaching from the nanocatalyst surface, thus ruling out the homogeneous mechanism.

REFERENCES

1. Mahmoud, M.A., B. Garlyyev, and M.A. El-Sayed, *Determining the mechanism of solution metallic nanocatalysis with solid and hollow nanoparticles: homogeneous or heterogeneous.* The Journal of Physical Chemistry C, 2013. **117**(42): p. 21886-21893.

2. Burda, C., et al., *Chemistry and properties of nanocrystals of different shapes.* Chemical Reviews, 2005. **105**(4): p. 1025-1102.

3. Bratlie, K.M., et al., *Platinum nanoparticle shape effects on benzene hydrogenation selectivity.* Nano Letters, 2007. **7**(10): p. 3097-3101.

4. Narayanan, R. and M.A. El-Sayed, *Shape-dependent catalytic activity of platinum nanoparticles in colloidal solution.* Nano Letters, 2004. **4**(7): p. 1343-1348.

5. Mahmoud, M.A., et al., *A new catalytically active colloidal platinum nanocatalyst: The multiarmed nanostar single crystal.* Journal of the American Chemical Society, 2008. **130**(14): p. 4590-+.

6. Bukhtiyarov, V.I. and M.G. Slin'ko, *Metallic nanosystems in catalysis.* Uspekhi Khimii, 2001. **70**(2): p. 167-181.

7. Narayanan, R., C. Tabor, and M.A. El-Sayed, *Can the observed changes in the size or shape of a colloidal nanocatalyst reveal the nanocatalysis mechanism type: Homogeneous or heterogeneous?* Topics in Catalysis, 2008. **48**(1-4): p. 60-74.

8. Mahmoud, M.A., *Proposed molecular mechanism for the colloidal nanocatalysis of the hexacyanoferrate III-thiosulfate electron transfer reaction: On the involvement of a Prussian blue analogue complex intermediate.* Journal of Catalysis, 2010. **274**(2): p. 215-220.

9. Landman, U., et al., *Factors in gold nanocatalysis: oxidation of CO in the non-scalable size regime.* Topics in Catalysis, 2007. **44**(1-2): p. 145-158.

10. Wunder, S., et al., *Catalytic Activity of Faceted Gold Nanoparticles Studied by a Model Reaction: Evidence for Substrate-Induced Surface Restructuring.* Acs Catalysis, 2011. **1**(8): p. 908-916.

11. Zeng, J., et al., *A Comparison Study of the Catalytic Properties of Au-Based Nanocages, Nanoboxes, and Nanoparticles.* Nano Letters, 2010. **10**(1): p. 30-35.

12. Mahmoud, M. and M. El-Sayed, *Time dependence and signs of the shift of the surface plasmon resonance frequency in nanocages elucidate the nanocatalysis mechanism in hollow nanoparticles.* Nano letters, 2011. **11**(3): p. 946-953.

13. Mahmoud, M.A. and M.A. El-Sayed, *Aggregation of Gold Nanoframes Reduces, Rather Than Enhances, SERS Efficiency Due to the Trade-Off of the Inter- and Intraparticle Plasmonic Fields.* Nano Letters, 2009. **9**(8): p. 3025-3031.

14. Schwartzberg, A.M., et al., *Synthesis, characterization, and tunable optical properties of hollow gold nanospheres.* Journal of Physical Chemistry B, 2006. **110**(40): p. 19935-19944.

15. Yen, C., M. Mahmoud, and M. El-Sayed, *Photocatalysis in Gold Nanocage Nanoreactors†.* The Journal of Physical Chemistry A, 2009. **113**(16): p. 4340-4345.

16. Mahmoud, M.A., F. Saira, and M.A. El-Sayed, *Experimental Evidence For The Nanocage Effect In Catalysis With Hollow Nanoparticles.* Nano Letters, 2010. **10**(9): p. 3764-3769.

17. Mahmoud, M.A. and M.A. El-Sayed, *Metallic Double Shell Hollow Nanocages: The Challenges of Their Synthetic Techniques.* Langmuir, 2012. **28**(9): p. 4051-4059.

18. Mahmoud, M.A., R. Narayanan, and M.A. El-Sayed, *Enhancing Colloidal Metallic Nanocatalysis: Sharp Edges and Corners for Solid Nanoparticles and Cage Effect for Hollow Ones.* Accounts of chemical research, 2013.

19. Mahmoud, M., B. Snyder, and M. El-Sayed, *Surface Plasmon Fields and Coupling in the Hollow Gold Nanoparticles and Surface-Enhanced Raman Spectroscopy. Theory and Experiment†.* The Journal of Physical Chemistry C, 2010. **114**(16): p. 7436-7443.

20. Weng, G., M.A. Mahmoud, and M.A. El-Sayed, *Nanocatalysts Can Change the Number of Electrons Involved in Oxidation-Reduction Reaction with the Nanocages Being the Most Efficient.* Journal of Physical Chemistry C, 2012. **116**(45): p. 24171-24176.

21. Mahmoud, M.A. and G. Weng, *Nanocatalysis Production of Photoactive Radicals.* Catalysis Communications, 2013. **38**: p. 63-66.

22. Borodko, Y., et al., *Charge-transfer interaction of poly(vinylpyrrolidone) with platinum and rhodium nanoparticles.* Journal of Physical Chemistry C, 2007. **111**(17): p. 6288-6295.

23. Kim, C. and H. Lee, *Change in the catalytic reactivity of Pt nanocubes in the presence of different surface-capping agents.* Catalysis Communications, 2009. **10**(9): p. 1305-1309.

24. Mahmoud, M.A., W. Qian, and M.A. El-Sayed, *Following Charge Separation on the Nanoscale in Cu2O-Au Nanoframe Hollow Nanoparticles.* Nano Letters, 2011. **11**(8): p. 3285-3289.

25. Hakkinen, H., *The gold-sulfur interface at the nanoscale.* Nature Chemistry, 2012. **4**(6): p. 443-455.

26. Gelb, L.D. and K.E. Gubbins, *Characterization of Porous Glasses by Adsorption: Models.* 1998. **6**: p. 551-556.

27. Jana, S., et al., *Synthesis of silver nano shell-coated cationic polystyrene beads: A solid phase catalyst for the reduction of 4-nitrophenol.* Applied Catalysis a-General, 2006. **313**(1): p. 41-48.

28. Pradhan, N., A. Pal, and T. Pal, *Silver nanoparticle catalyzed reduction of aromatic nitro compounds.* Colloids and Surfaces a-Physicochemical and Engineering Aspects, 2002. **196**(2-3): p. 247-257.

29. Mahmoud, M.A. and M.A. El-Sayed, *Time Dependence and Signs of the Shift of the Surface Plasmon Resonance Frequency in Nanocages Elucidate the Nanocatalysis Mechanism in Hollow Nanoparticles.* Nano Letters, 2011. **11**(3): p. 946-953.

30. Mahmoud, M.A. and M.A. El-Sayed, *Gold Nanoframes: Very High Surface Plasmon Fields and Excellent Near-Infrared Sensors.* Journal of the American Chemical Society, 2010. **132**(36): p. 12704-12710.

31. Amendola, S.C., et al., *An ultrasafe hydrogen generator: aqueous, alkaline borohydride solutions and Ru catalyst.* Journal of Power Sources, 2000. **85**(2): p. 186-189.

32. Mirkin, M.V., H.J. Yang, and A.J. Bard, *BOROHYDRIDE OXIDATION AT A GOLD ELECTRODE.* Journal of the Electrochemical Society, 1992. **139**(8): p. 2212-2217.

33. Concha, B.M., et al., *In Situ Infrared (FTIR) Study of the Mechanism of the Borohydride Oxidation Reaction on Smooth Pt Electrode.* Journal of Physical Chemistry C, 2011. **115**(25): p. 12439-12447.

34. Arevalo, R.L., et al., *Structure and stability of borohydride on Au(111) and Au3M(111) (M = Cr, Mn, Fe, Co, Ni) surfaces.* Dalton Transactions, 2013. **42**(3): p. 770-775.

CHAPTER 4

CONTROLLING OF THE CATALYTIC EFFICIENCY ON THE SURFACE OF HOLLOW GOLD NANOPARTICLES BY INTRODUCING INNER THIN LAYER OF PLATINUM OR PALLADIUM

Summary

The heterogeneous catalysis of electron-transfer reactions on the surface of gold nanoshells was changed by adding an inner platinum or palladium nanoshell in the double shells nanocatalysts. The reduction of 4-nitrothiophenol (4NTP) by borohydride was studied as model reaction when bound to the hollow gold nanocatalysts in the presence and absence of inner platinum and palladium nano shells . To confirm the heterogeneous catalytic mechanism, the nanocatalysts were assembled into a monolayer on the surface of a quartz substrate using the Langmuir-Blodgett technique, and the 4NTP is allowed to bind to the surface of gold through a strong thiol bond. The stages of the reduction reaction of 4NTP on the surface of gold were successfully followed in real time by time-resolved surface-enhanced Raman spectroscopy (SERS). Although the double shell nanocatalysts have two different catalytically active surfaces, the SERS measurement is able to probe the changes on the gold surface where the plasmon field is strongly focused. The mechanism of the reduction reaction of 4NTP was found to proceed through two stages consisting of the formation of an azo-dimer intermediate which was further reduced into 4-aminophenol. Palladium was found to increase the catalytic efficiency of the gold surface due to the presence of a new Fermi level of the

palladium-gold alloy, while platinum decreased its catalytic efficiency due to the electron sinkage which resulted from the difference in the electrochemical reduction potentials. Interestingly, the intermediate azo-dimer and the final product were both formed in the early stages of the reaction and increased with time, but the intermediate was found to decrease after reaching a threshold concentration.

Introduction

Nanoparticles are characterized by their high surface to volume ratio; this large surface area of the nanoparticles increases their efficiency when used for catalysis.[1-3] Introducing sharp corners and edges to the shape of the nanocatalysts further increases their catalytic efficiency.[4] As the activity of the nanocatalyst depends on the number of high energy active centers,[5] atoms located at the sharp tips are thermodynamically and catalytically active because they are unsatisfied in valency.[6] Although the nanocatalysts with sharp tips present well-enhancement of the catalytic efficiency, their sharp ends become rounded after the catalytic reaction, which causes a remarkable decrease in the catalytic efficiency.[7] The shape change of the nanocatalyst could be due to leaching or rearrangement of the atoms located on its sharp ends.[7]

Confinement of the reacting materials within the nanocatalysts has been found to improve their catalytic efficiency.[8-15] This confinement is acquired either by designing the nanocatalyst to have a cavity, or by fixing the catalyst on the surface of the inside wall of an inert support of containing voids. Nanocage catalysts made of a single metal such as gold, platinum, and palladium or two metals, such as double shell structures of gold-platinum, gold-palladium, and platinum-palladium have presented high catalytic efficiency due to the cage effect.[8-11] The idea of cage catalysis was supported by comparing the catalytic efficiency of gold nanocages with that of the solid nanocatalyst of similar shape, and the gold nanocages were found to have a higher catalytic efficiency than the solid nanocatalyst.[16,17] The cage effect was also observed for palladium nanotubes, which showed a high catalytic efficiency for the Suzuki reaction.[12]

Additionally, silver oxide prepared in situ on the interior wall of gold nanocages showed high photocatalytic activity for the decomposition of an organic dye as the reactive radicals were confined inside the gold nanocage.[18] High catalytic performance was also observed for hydrogen generation from formic acid on the surface of gold nanoparticles encapsulated in silica nanospheres.[13] The density functional theoretical calculation related the high catalytic efficiency of the hollow nanocatalysts to the electronic confinement effect.[19] Nanocatalysts fixed on the inner wall of porous metal-organic frameworks (MOFs) showed high catalytic activity due to the confinement of the reactant inside the voids present in the structure of the MOFs.[20] Polymer nanofibers when used as a support for platinum and ruthenium nanocatalysts showed high catalytic efficiency due to the cage effect.[21] Nickel, cobalt, iron and their respective oxides encapsulated inside SiO_2 nanoshell showed an exciting catalytic performance and thermal stability during the catalytic run at high temperature.[14] High electrocatalytic efficiency was also observed in hybrid inorganic nanostructures such as ruthenium and Cu_2S due to their high surface area and exciting electronic properties.[22]

Due to the small size of the nanocatalysts, which in some cases approaches the size of the reacting materials, the mechanism of the nanocatalysis is not clearly understood. In fact, heterogeneous catalysis is suggested when the catalysis takes place on the surface of the nanocatalyst, while a homogenous mechanism is favored when the catalysis proceeds through the formation of a complex, either on or far from the surface of the catalysts. Raman spectroscopy presents finger print vibrational spectra for molecules. Plasmonic nanoparticles are characterized by the presence of an electromagnetic field when they interact with light of resonant frequency; this plasmon

field is able to enhance the Raman signal of molecules located in its domain, as in surface-enhanced Raman spectroscopy (SERS). SERS is a sensitive technique which is able to sense concentrations down to the zeptomolar range (10^{-21}).[23] The high sensitivity of SERS has made it possible to use this technique to probe the catalytic reaction as it proceeded on the surface of the plasmonic nanocatalyst.[24,25]

This article aims to study the mechanism of the heterogeneous catalysis on the surface of gold nanoshells when present as a single nanoshell and when combined with an inner platinum or palladium nanoshell into a double-shell nanostructure. As it is not easy to differentiate between homogenous and heterogeneous catalysis by the colloidal nanoparticles, three considerations were taken into account to assure a heterogeneous mechanism during the design of the experiment: 1) In order to fix the nanocatalysts, they were assembled into a monolayer on the surface of a quartz substrate by the Langmuir-Blodgett technique, 2) The reduction of 4NTP by borohydride was used as a model reaction with the 4NTP bound to the surface of the nanocatalyst through a strong gold-thiol bond, and 3) The highly sensitive SERS technique was used to follow the reaction on the surface of the gold nanoparticles so the Raman signal recorded will be for the molecules bound to or near the surface of the gold, where the plasmon field is strong. This experimental design made it possible to study the mechanism of the heterogeneous catalysis on the surface of the gold nanoshells, and also to study the effect of hybridizing of the electronic properties of gold, with either platinum or palladium, on the catalytic efficiency of the gold surface. Cyclic voltammetry measurements were used to confirm the kinetic results obtained from the catalysis experiments.

Experimental

Silver Nanocubes

Briefly the synthesis of silver nanocubes, in a 100 mL round-bottomed flask, 35 mL of anhydrous ethylene glycol (Sigma Aldrich) was stirred at 400 rpm and heated at 140 °C for 1 h in an oil bath. After 1 h heating 0.35 g polyvinyl pyrrolidone (PVP) (molecular weight of ~55 000 g) dissolved in 5 mL ethylene glycol was added at once to the reaction mixture. The temperature of the reaction mixture was then raised gradually until it reached 155 °C. At this temperature, 0.4 mL of a 3 mM solution of sodium sulfide in ethylene glycol was added after 5 min from the addition of PVP. 2 ml of $AgNO_3$ solution (0.48 g $AgNO_3$ dissolved in 10 mL ethylene glycol) was added. The solution was stirred briefly under constant heating until the solution turned a yellow/auburn color, at which point the single crystal silver seeds are produced. Growth of these particles into large cubes was achieved through careful monitoring of both the stir speed and temperature until a turbid yellow/greenish solution is produced. The silver nanocubes were cleaned of excess polymer and solvent by dilution to three times its original volume with an acetone-water mixture and centrifugation at 14,000 rpm for 5 minutes. The precipitated particles were then re-dispersed and stored in deionized (DI) water. For gold nanocages 10 mL from the 20 mL cleaned silver nanocubes was diluted to 200 mL with DI water and brought to boiling and stirred with stirring rate of 300 rpm. $HAuCl_4$ solution (0.1 g/L) was injected slowly into the hot silver nanocube solution until the LSPR peak of the solution shifted to 600 nm. The gold nanocages solutions were then continuously refluxed until their absorption spectrum became stable. Then the solution was cooled down to room temperature and left for 2 days to allow the AgCl byproduct to settle down

and precipitate. The AgCl precipitate was removed by decantation of the gold nanocages solution. In order to clean the gold nanocages cavity from the AgCl salt, if any are left, the solution of gold nanocages was sonicated for 30 min, and then left for a day until all of the AgCl precipitates settled to the bottom of the solution. The solution was centrifuged at 10 000 rpm for 10 min. and the gold nanocages were dispersed in DI water.

Gold-Platinum Hybrid Nanocages

In order to synthesize Au−Pt shell−shell nanocages solution of K_2PtCl_4 (0.05 g/10 mL) was added to the gold nanocages solution, after cleaning as shown above. The LSPR peak of gold nanocages shifted to red as the amount of K_2PtCl_4 increased due to the replacement of the remaining silver inside the gold nanocages with formation of Pt inner shell. The LSPR peak position was measured as a function of the volume added from the salt solution. Solution was left until the LSPR peak position became constant and was not shifting any more.

Gold nanocage, gold-platinum double-shell, and gold-palladium double-shell nanocatalysts were prepared from silver nanocubes template by the galvanic replacement technique, as previously reported (for detailed procedure see supporting info.).[8] In order to assemble the nanocatalysts into monolayers on the surface of the quartz substrate, the prepared nanoparticles in aqueous solution were transferred to chloroform. 100 mL from the nanocatalyst solution was precipitated by with centrifugation at 6,000 rpm for 10 minutes and re-dispersed in 2 mL methanol. The nanoparticles in methanol were diluted with 3 mL of chloroform. The nanoparticles were then dispersed on top of the Nima 611D Langmuir-Blodgett trough using a micro-syringe filled with water sub layer. The

nanocatalyst monolayer was dried for 30 minutes before being transferred to the surface of the quartz substrate by the vertical dipping technique. Eight quartz substrates of 1 cm x 2.5 cm were coated at simultaneously at surface pressure of 2 mN/m, which was measured by D1L-75 model pressure sensor. In order to coat the surface of the nanocatalysts with 4-nitrothiphenol (4NTP), substrates coated with nanocatalysts were immersed in 0.1 mM aqueous solution of 4NTP and left overnight. The substrates were washed five times in deionized (DI) water by immersion and gently shaking. The substrates were then immersed in a 1 mM sodium borohydride solution and removed after different soaking times for Raman analysis using a Renishaw In via Raman microscope. For the cyclic voltammetry measurements, 10 mL of aqueous nanocatalyst solutions were mixed with 1 mL aqueous 4NTP solution and left overnight. Then, the solution was centrifuged twice at 6,000 rpm for 10 minutes to remove excess 4-NTP. The nanoparticles with 4-NTP on the surface were drop-casted on a glassy carbon electrode. AgCl/Ag electrode was used as the reference electrode and platinum was used as a counter electrode. All of the cyclic voltammetry measurements were carried out in 0.5 M H_2SO_4 at a scan rate of 50 mV/sec. A Zeiss Ultra 60 microscope was used for the scanning electron microscopy (SEM) imaging. A Tecnai F30 microscope was used for high-resolution transmission electron microscopy (HR-TEM) imaging and energy-dispersive X-ray spectroscopy (EDS) mapping.

Results and Discussions

Characterization and Monolayer Assembly of the Hollow Nanocatalysts

The efficiency of heterogeneous catalysts depends on the crystal structure and the surface potential energy. The reactions in this study take place on the surface of gold even in case of AuPdNCs and AuPdNCs. It is useful to study the crystal structures of the double shell nanocatalysts and monitor how the two metal shells are arranged. Figure 4.1A shows a high-resolution TEM image of part of the wall of a single AuNC. One gold shell was observed in the image. AuPdNCs, alternatively, seem to have three different layers. The outer layer is pure gold; the inner layer is pure palladium while the middle layer is gold-palladium alloy (see Figure 4.1B). Gold and palladium have face-centered-cubic (fcc) lattice, the *d*-spacing of the {111} facet of gold is 0.23 nm which is comparable with that of palladium (0.2 nm). The comparable lattice parameters of gold and palladium make their alloying quite possible. Figure 4.1C shows the TEM image of the wall of AuPtNC, the gold atoms in the outer gold layer are well organized while the interfacial layer between the platinum and gold is rough because platinum and gold do not form a homogenous alloy. Indeed, platinum has fcc lattice, the *d*-spacing of the {111} facet is 0.27 nm which is much larger than that of gold preventing the alloy formation, and generates a strong lattice strain in the interfacial layer. For more careful characterization of the hollow nanocatalysts, EDS mapping was carried out for AuPdNCs (see Figure 4.1 D). As shown from the EDS elemental mapping image, AuPdNC composed of palladium and gold metals, where the gold appears as an outer shell with green color in the image. While, the palladium inner shell appeared with red color is located inside the cage, and the alloy between the inner and outer shells is shown by

yellow color. EDS mapping images of the individual metals are shown in the center of Figure 4.1D.

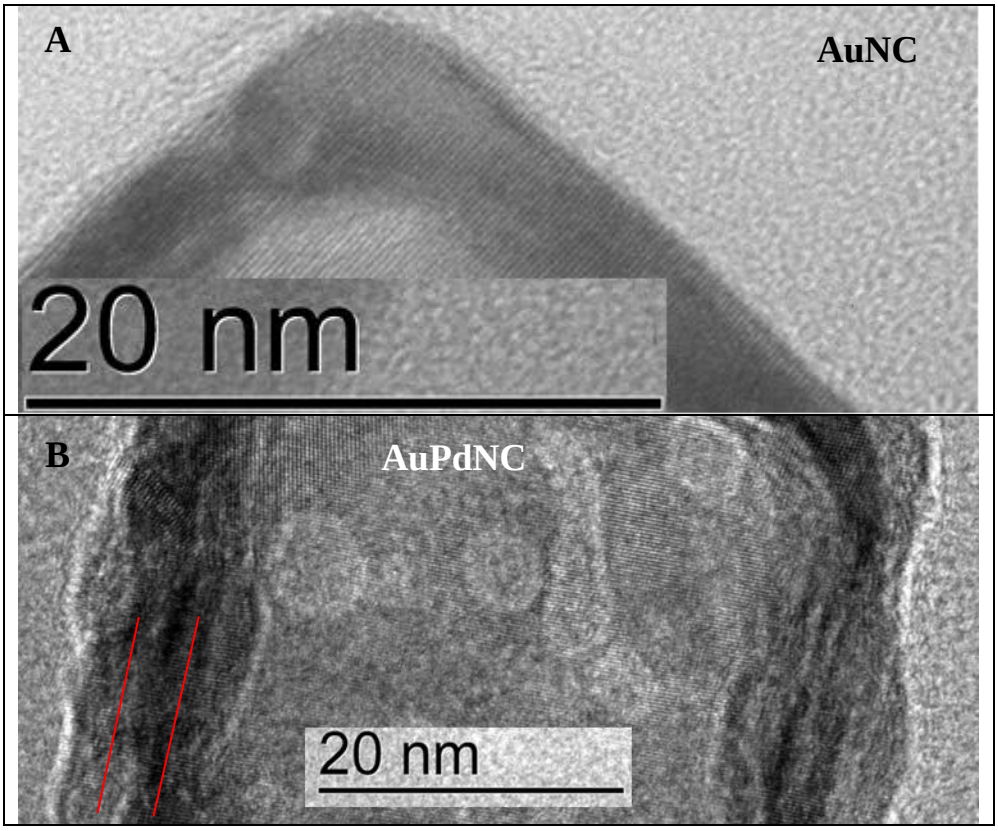

Figure 4.1. High resolution TEM images of the wall of: A) gold nanocage, B) gold palladium double shell nanoparticle, C) gold platinum double shell nanoparticle. It is clear that gold nanocage has one crystalline wall, while gold palladium double shell has three different layers, two of them for pure gold and pure palladium shells and an alloy layer in between, the alloy layer located between the two red lines in the image. In case of gold platinum double shell nanocage, two layers are observed which separated by the green line because platinum and gold cannot form homogenous alloy, while palladium and gold mix well because they have comparable crystal lattice parameters. D) EDS elemental mapping of AuPdNC of bright color (left image), the gold atoms of green color appears as an outer shell while palladium atoms of red color is shown as an inner shell (right image). The EDS mapping image of the individual palladium and gold before convolution are in the center.

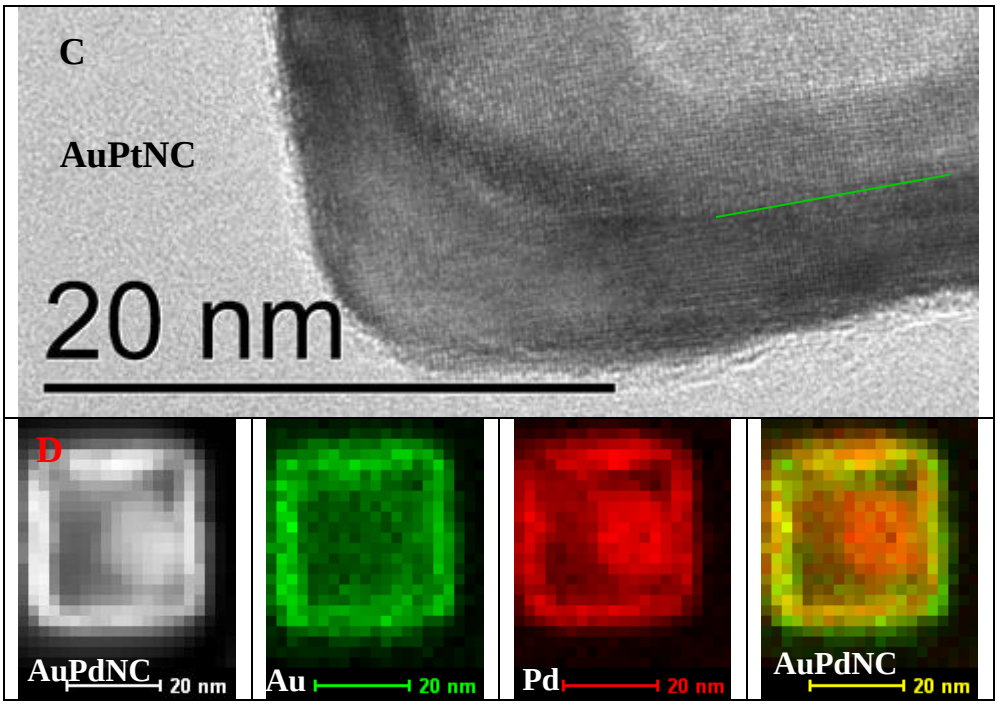

Figure 4.1. Continued

In order to increase the accuracy of the heterogeneous catalysis experiments, the Langmuir-Blodgett (LB) technique was used to assemble the nanocatalysts into a monolayer on the surface of a quartz substrate. The LB assembly keeps the nanocatalyst fixed in an organized way during the catalysis experiment. Figure 4.2 (A-C) shows the SEM images of AuNCs, AuPdNCs, and AuPtNCs monolayer assembled on the surface of quartz substrates at a surface pressure of 2 mN/m. Localized surface plasmon resonance extinction spectrum of the nanocatalysts after assembling on the surface of quartz substrate are shown in Figure 4.3.

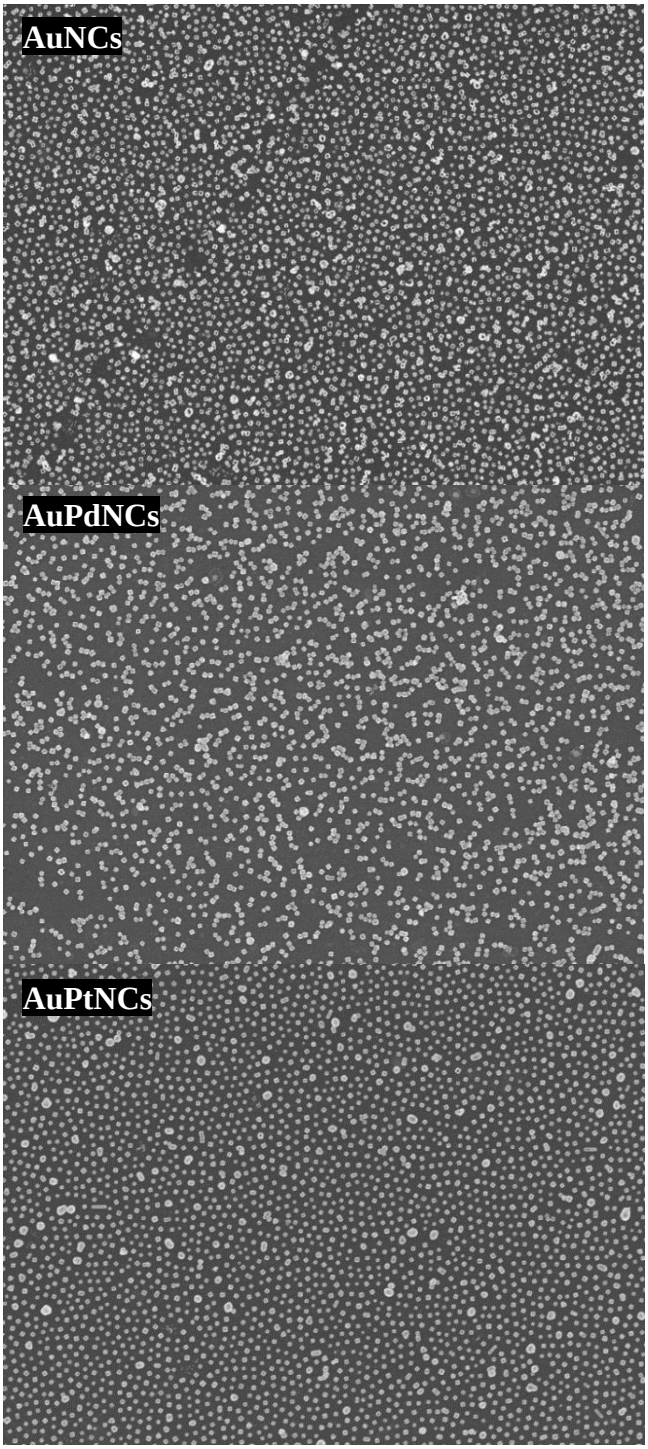

Figure 4.2. SEM images of Langmuir-Blodgett monolayer assembled on the surface of quartz substrate at surface pressure of the trough of 2 mN/m for: A) gold nanocage, B) gold palladium double shell nanoparticle, C) gold platinum double shell nanoparticle.

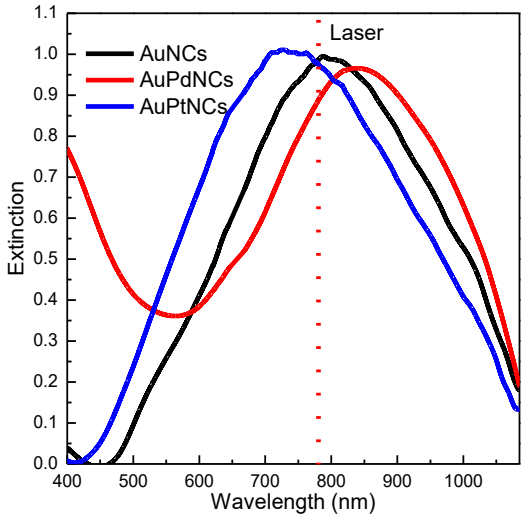

Figure 4.3. Localized surface plasmon resonance extinction spectrum of gold nanocages (black), gold palladium double shell nanoparticles (red), and gold platinum double shell nanoparticle (blue) assembled into monolayer on the surface of quartz substrate.

Spectroscopic Study of Catalytic Reactions on the Surface of Gold Nanoshell

Borohydride reduces 4-nitrothiophenol (4NTP) into 4-aminothiophenol on the surface of certain metal catalysts. Based on theoretical simulations, this reaction likely proceeds through the formation of an intermediate dimeric *azo* compound. This slightly persistent intermediate may undergo further reduction into 4-aminothiophenol (4ATP). The *azo* dimer was observed experimentally arising from a photochemical reaction rather than through a thermal mechanism.[26] In order to eliminate the photochemical reaction that could take a place as a result of the Raman laser irradiation, 4NTP adsorbed on the surface of the nanocatalysts was exposed to the laser for different periods of time. No change was observed in the SERS spectrum of 4NTP due to the irradiation, which suggested that no photochemical reaction is possible by such low energy excitation photons (see Figure 4.4). In multiple step electron transfer reactions each step proceeds at a certain electrochemical potential.

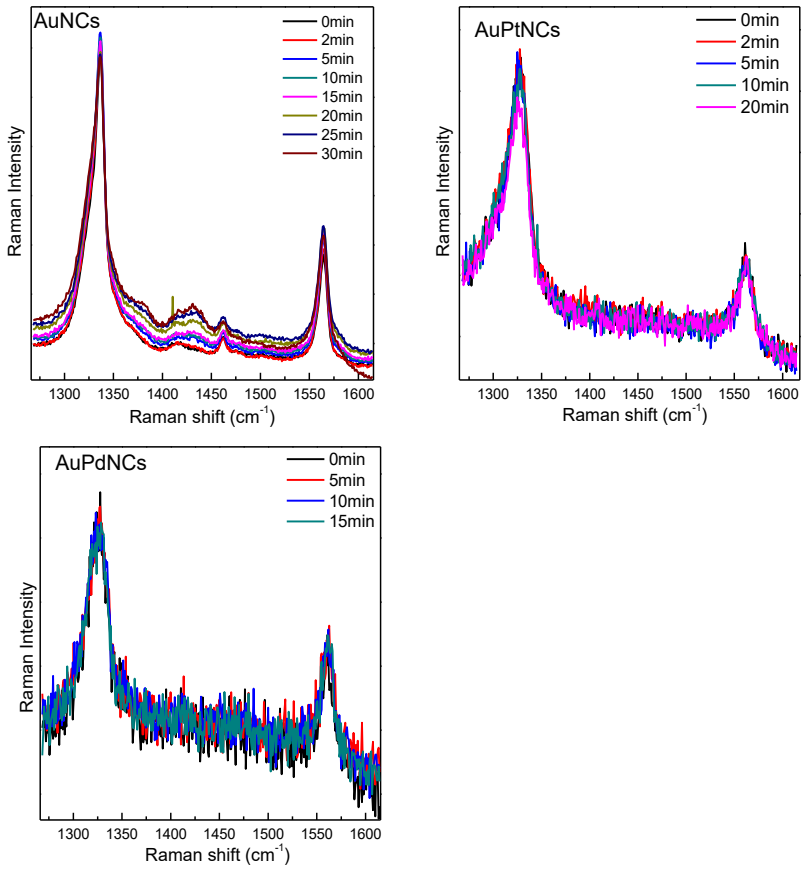

Figure 4.4. Surface-enhanced Raman spectrum measured for 4-nitrothiophenol adsorbed on the surface of Langmuir-Blodgett monolayer of: A) gold nanocages (AuNCs), B) gold-platinum double shell nanoparticles (AuPtNCs), and C) gold-palladium double shell nanoparticles (AuPdNCs) after Raman Laser irradiation for different time. It is observed that no change in the SERS spectrum of the 4-nitrothiophenol as a result of laser irradiation.

The reduction of 4NTP by BH is a promising system to study the different catalytic performance on the surface of gold in hollow nanoparticles when platinum or palladium is combined as an inner shell. Surface-enhanced Raman spectroscopy (SERS) was used to monitor the reduction stages of the 4NTP bound to the surface of AuNCs, AuPdNCs, and AuPtNCs. The Raman signal is expected to come primarily from the molecules adsorbed on the gold because the surface enhancement tails off quickly with distance. Figure 4.5 A-C show the SERS spectra of 4NTP bound to the surface of AuNCs, AuPtNCs, and AuPdNCs monolayers on the surface of quartz substrates after

being exposed to BH solution with various time delays. The SERS spectrum measured immediately after adding the BH solution corresponds to pure 4NTP which has SERS bands at 1570 and 1331 cm^{-1} which are assigned to ν(CC) and $\nu_s(NO_2)$ modes, respectively. After the reaction proceeded a short time new SERS bands appeared at 1431 and 1387 cm^{-1} corresponding to ν(-N=N-) of the intermediate dimer. When the reaction proceeded further, the 4NTP bands decreased with time and a band at 1594 cm^{-1} ν(CC) for 4ATP[27] increased. The band intensities are plotted against time in Figure 4.5 D-F. The SERS band intensities were calculated after subtracting the background spectrum which is located under the SERS spectrum. First origin software was used to create base line and the intensity of the peak was measured in the middle from the baseline to the maximum point. In order to determine the intensity of the SERS band of the product, the band at ~ 1590 cm^{-1} was deconvoluted into two bands since the reactant has SERS band interfering with that of an amino product. For all three hollow nanocatalysts the product and intermediate formed simultaneously. Initially the rate of formation of the intermediate was higher than that of the product. However, when the concentration of the intermediate reached a threshold amount, it further reduced into the final product (Figure 4.5 D- F). It is important to highlight the low value of the band intensity of the final product compared with the band intensities of the reactant and the intermediate compound in case of using AuNCs nanocatalyst, especially when the band intensities was compared at their maximum value. The opposite trend was observed when using AuPdNCs or AuPtNCs, the band intensities of the final product are higher than that of the reactant. One plausible reason for this result can is based on the fact that there are two different mechanisms for SERS enhancement, electromagnetic and chemical. The

chemical enhancement mechanism depends on the charge transfer between the adsorbed molecules and the nanoparticles which is expected to be high in case of AuPtNCs and AuPdNCs.[11] The electromagnetic mechanism depends on the strength of the plasmon field. AuNCs are have strong plasmonic fields so the Raman signal enhancement is related to the electromagnetic mechanism.[11] Since different vibrational modes are affected differently by the two SERS mechanisms, it is reasonable to think that amino. In summary, the SERS measurements showed that the 4NTP-BH when catalyzed by AuNCs surface in the presence and absence of platinum and palladium inner shell proceeds through *azo* dimer intermediate, which is further reduced to an amino compound *via* a thermal mechanism. We ensured that the photochemical reaction did not occur by using low laser fluency. Additionally, when the 4NTP adsorbed on the surface of AuNCs, AuPdNCs, and AuPtNCs was exposed to the laser in the absence of BH, no change in the SERS spectrum was observed with time (see Figure 4.4).

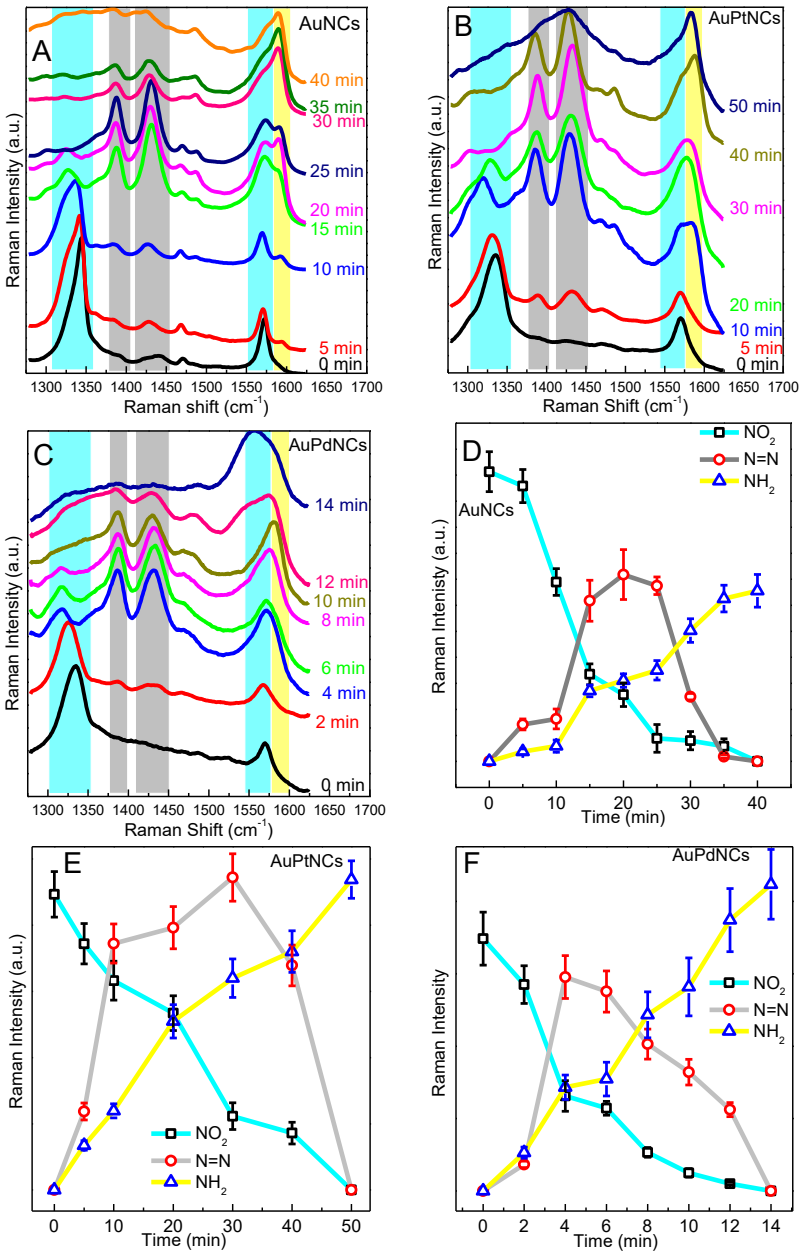

Figure 4.5. Surface-enhanced Raman spectrum collected at different time during the borohydride reduction of 4-nitrothiophenol reaction when catalyzed by a Langmuir-Blodgett monolayers on the surface of quartz substrate from: A) gold nanocages (AuNCs), B) gold-platinum double shell nanoparticles (AuPtNCs), and C) gold-palladium double shell nanoparticles (AuPdNCs). For better observation of the changes that takes place on the surface of the nanoparticles, the time dependent formation of intermediate, product and disappearance of reactant for the reduction of 4 nitrothiophenol by sodium borohydride were calculated from band intensities of the SERS spectrum using: D) AuNCs, E) AuPtNCs, and F) AuPdNCs.

Kinetics of Catalysis with Hollow Nanoparticles

The Raman measurements succeeded to present information about the reduction of 4-NTP by BH on the surface of the single gold nanoshell and when platinum and palladium are combined with gold as an inner shell. Time-dependent band intensities corresponding to the product and reactant in the Raman spectrum shown in Figure 4.5 were used to study the kinetics of the reduction reaction. The catalytic study was limited to focus on the catalysis on the surface of gold nanoshell as we planned, because the plasmon filed is concentrated on the surface of gold.[11] The concentration of BH used during the reduction reaction was sufficient excess to make the reduction of 4NTP pseudo first order. In order to confirm the order of the reaction, the first order expression was examined for both the appearance of the product and disappearance of the reactant, straight lines were obtained. Figure 4.7 A-C) show the linear relationship between the natural logarithm of the SERS band intensity of the 4NTP and 4ATP versus time calculated for AuNCs, AuPtNCs, and AuPdNCs, respectively. The slope of these linear expressions yields the apparent rate constant for the particular concentration of borohydride. The order or the reaction was confirmed by examining the second order graph, since two molecules of 4NTP were involved in the reaction to form the intermediate dimer. The second order plot which is the relationship between the reciprocal of the Raman band intensity of either 4NTP or 4ATP and the time of the reaction did not fit linearly for all three nanocatalysts, see Figure 4.6A-C.

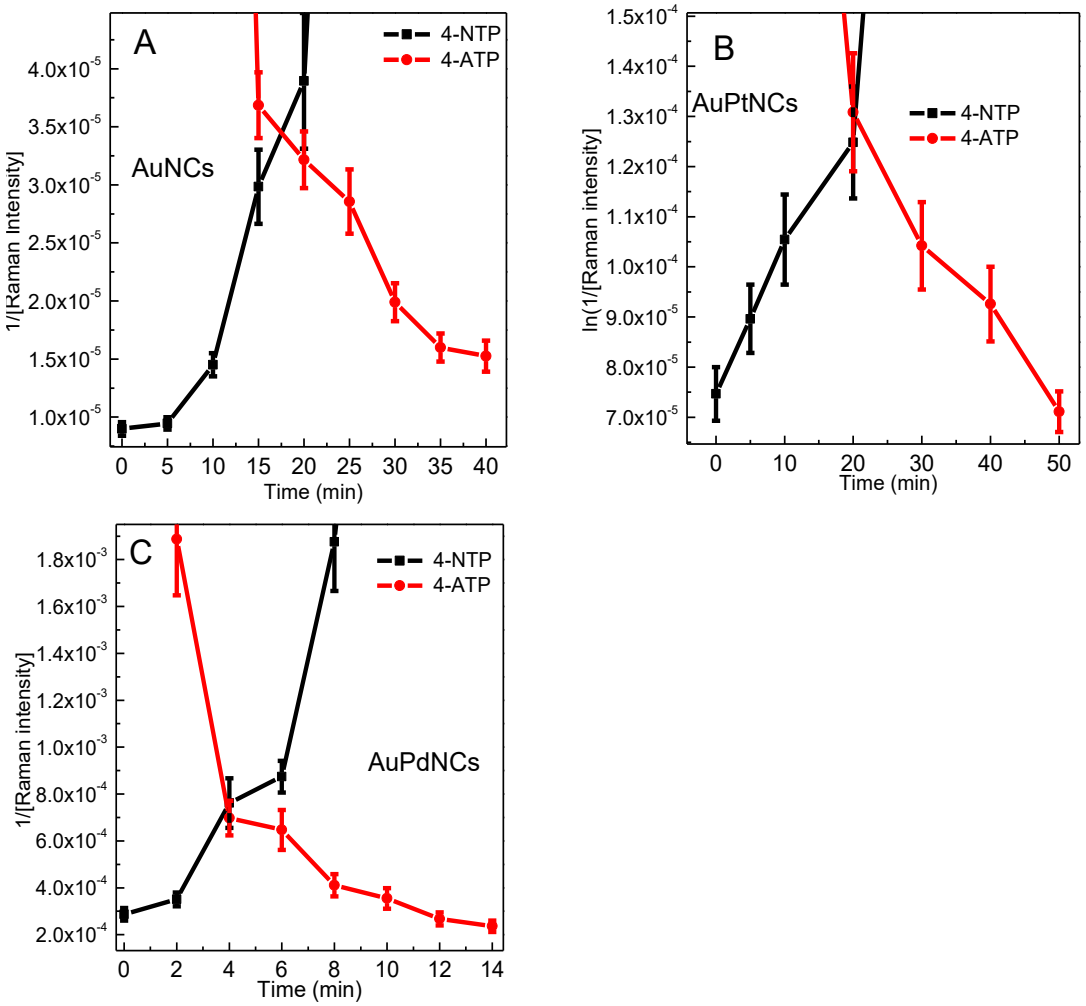

Figure 4.6. The second order graph for the catalytic reduction of 4-nitrothiophenol by borohydride catalyzed be AuNCs (A), AuPtNCs (B), and AuPdNCs (C). The second order plot which is the relationship between the reciprocal of the Raman band intensity of either 4NTP or 4ATP and the time of the reaction did not fit linearly for all three nanocatalysts.

In traditional colloidal nanocatalysis, the values of the reaction rate constant depend on the concentration of the nanoparticles which makes it difficult to compare the catalytic efficiencies using the value of the rate constants. As known, when the concentration is increased the probability of collision with surface of the catalyst increases, which increase the value of rate of the reaction. Interestingly, in our experiment, the reactant is chemically bound to the surface of the nanocatalysts and the

coverage density of the reactant on the gold surface is fixed, so the reaction rate constants can be used in the comparison of the catalytic efficiency. The values of the rate constants of the appearance of the product and the disappearance of the reactants are reported in table 4.1. In all cases herein studied the value of the appearance rate constant was found to be half of the disappearance rate constant. This supports the idea that the reaction proceeds in two stages through formation of a persistent intermediate. The second exciting observation is that the relative values of the rate constants proceed as AuPdNCs > AuNCs > AuPtNCs. This can be attributed to the alloying of gold and palladium. As seen in Figure 4.1 C, the interfacial layer between the Pt and Au in the AuPtNCs is rough and there is no alloy layer as in case of AuPdNCs.[28] The AuPd alloy has density of states which is intermediate between Au and Pd. Since Pd has greater density of states than gold, the alloy will be more active than unalloyed gold.[29]

In order to confirm the effect of inner Pt or Pd nanoshell in catalytic activity of the Au outer surface in the double shell nanocatalysts, the electrocatalytic reduction of 4NTP on the surface of AuNCs, AuPtNCs, and AuPdNCs was examined by cyclic voltammetry. Figure 4.7D shows the cyclic voltammogram of the reduction of 4NTP on the surface of the double shell nanocatalysts. It is clear that the value of the reduction potential of 4NTP follows the increasing trend of AuPdNCs < AuPtNCs < AuNCs (see table 4.1). The results of the electrocatalytic measurement for AuNCs and AuPdNCs agreed well with the kinetic results and supported the presence of a new Fermi level in the case of AuPdNCs, which lowered the value of the reduction potential. While, the value of the reduction potential of 4NTP on the surface of AuPtNCs was found to be slightly lower than that on the surface of AuNCs. This is because unlike the regular

catalysis followed by Raman spectroscopy which senses the catalysis on the surface of Au nanoshell, the electrocatalytic measure the catalysis on both the surface of gold and platinum. The lattice strain occurs between the platinum and gold nanoshells resulting from the lattice mismatch will also enhance the electrocatalytic properties of AuPtNCs.[30,31]

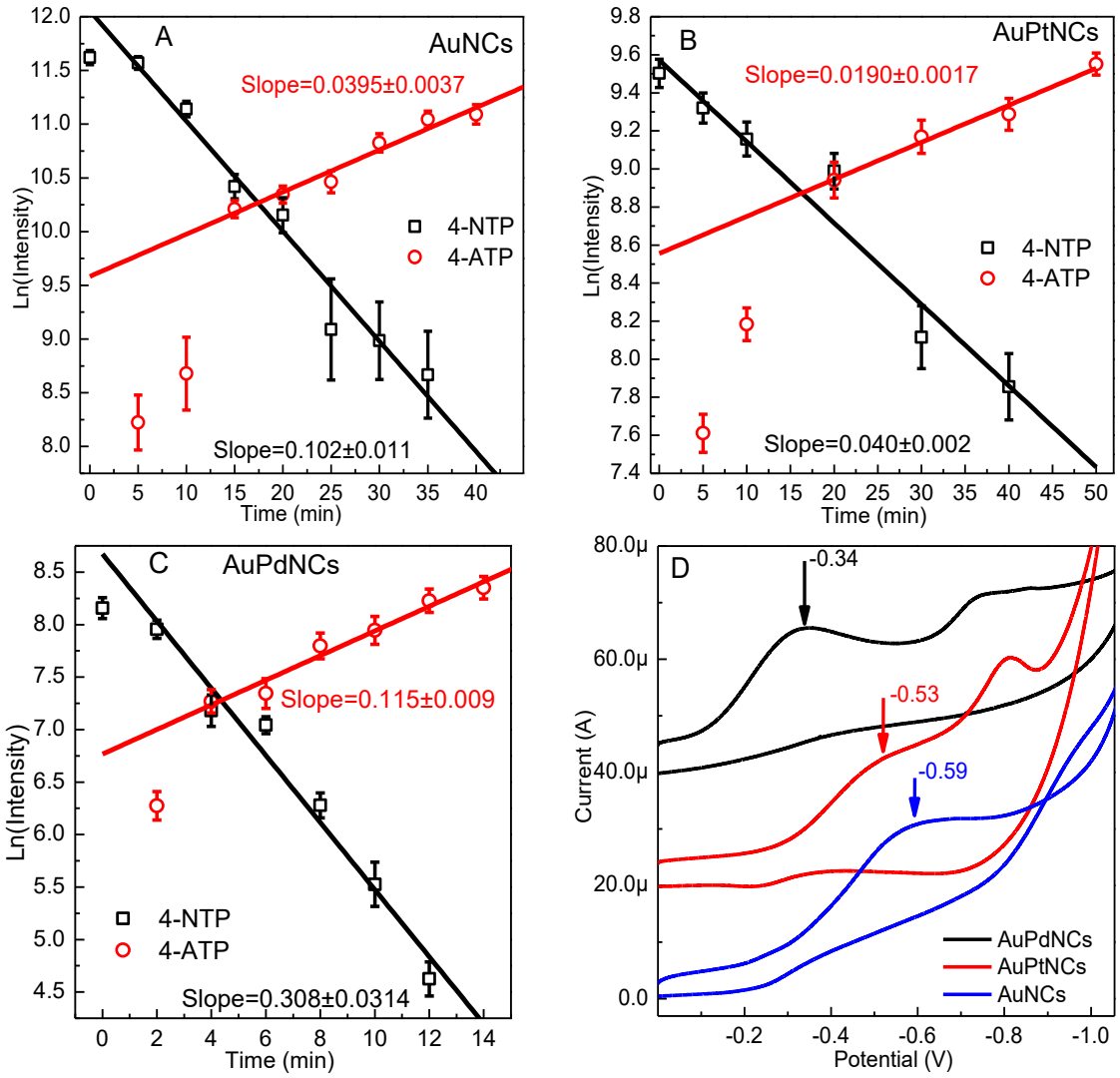

Figure 4.7. Linear relationship between the natural logarithm of the SERS band intensity of the 4NTP (reactant) and 4ATP (product) and the reaction time for: A) AuNCs, B) AuPtNCs, C) AuPdNCs. The slope of the straight-line is the rate constant which found to be increased in the following order AuPdNCs, AuNCs, and AuPtNCs, for both the reactant and product. D) Cyclic voltammogram for the reduction of 4NTP on the surface of AuNCs, AuPtNCs, and AuPdNCs in 0.5M H_2SO_4. The reduction potential increases in the order of AuPdNCs AuPtNCs, and AuNCs.

Table 4.1. Rate K constant for formation of product and disappearance of reactant, and oxidation, reduction potentials (vs. AgCl/Ag electrode) observed from CV measurements for 4 nitrothiophenol reduction by sodium borohydride in the presence of different nanocages.

Catalyst	Rate constant of reactant (K_{Re}, min^{-1})	Rate constant of product (K_{Re},min^{-1})	Reduction Potential (V)
AuPtNCs	0.040±0.002	0.0190±0.0017	0.53
AuNCs	0.102±0.011	0.0395±0.0037	0.59
AuPdNCs	0.308±0.031	0.1150±0.0090	0.34

Conclusion

In conclusion, the mechanism of heterogeneous redox catalysis on the surface of gold nanoshell was spectroscopically studied. The surface-enhanced Raman measurement made it possible to detect any small change that took place on the surface of the catalyst and monitor the rate of reaction due to the presence of plasmonic gold surface. The effect of introducing platinum and palladium inner shells on the catalytic efficiency of gold outer shell was discussed. The palladium inner nanoshell was found to increase the catalytic efficiency of the gold surface while the platinum nanoshell did the opposite. The reason of enhancing the catalytic efficiency of gold nanoshell by introducing an inner palladium nanoshell was the formation of palladium-gold nanoalloy layer between the pure palladium and gold nanoshells. This alloy layer has a new Fermi level of high density of states which increases the reactivity of gold-palladium double shell nanocatalyst. This alloy layer was not observed in case of gold-platinum double shell nanocatalyst, but a rough interface layer was observed instead. The unfavorable mixing between gold and platinum layers decreased the catalytic performance of gold-platinum

double shell nanocatalyst. In order to increase the accuracy of the catalysis study, the catalysts were assembled into monolayer on the surface of quartz substrate, and the reactant was allowed to bind strongly with the surface of the gold nanocatalysts. Cyclic voltammetry was used to confirm the presence of Fermi level in case of gold palladium double shell nanocatalyst.

REFERENCES

1. Lewis, L.N. and N. Lewis, *Platinum-catalyzed hydrosilylation - colloid formation as the essential step.* Journal of the American Chemical Society, 1986. **108**(23): p. 7228-7231.

2. Freund, P.L. and M. Spiro, *COLLOIDAL CATALYSIS - THE EFFECT OF SOL SIZE AND CONCENTRATION.* Journal of Physical Chemistry, 1985. **89**(7): p. 1074-1077.

3. Rioux, R.M., et al., *High-surface-area catalyst design: Synthesis, characterization, and reaction studies of platinum nanoparticles in mesoporous SBA-15 silica.* Journal of Physical Chemistry B, 2005. **109**(6): p. 2192-2202.

4. Narayanan, R. and M.A. El-Sayed, *Shape-Dependent Catalytic Activity of Platinum Nanoparticles in Colloidal Solution.* Nano Letters, 2004. **4**(7): p. 1343-1348.

5. Abbet, S., et al., *Pd1/MgO(1 0 0): a model system in nanocatalysis.* Surface Science, 2002. **514**(1–3): p. 249-255.

6. Burda, C., et al., *Chemistry and properties of nanocrystals of different shapes.* Chemical Reviews, 2005. **105**(4): p. 1025-1102.

7. Narayanan, R. and M.A. El-Sayed, *Changing Catalytic Activity during Colloidal Platinum Nanocatalysis Due to Shape Changes: Electron-Transfer Reaction.* Journal of the American Chemical Society, 2004. **126**(23): p. 7194-7195.

8. Mahmoud, M.A., F. Saira, and M.A. El-Sayed, *Experimental Evidence For The Nanocage Effect In Catalysis With Hollow Nanoparticles.* Nano Letters, 2010. **10**(9): p. 3764-3769.

9. Mahmoud, M.A. and M.A. El-Sayed, *Time Dependence and Signs of the Shift of the Surface Plasmon Resonance Frequency in Nanocages Elucidate the Nanocatalysis Mechanism in Hollow Nanoparticles.* Nano Letters, 2011. **11**(3): p. 946-953.

10. Mahmoud, M.A., R. Narayanan, and M.A. El-Sayed, *Enhancing colloidal metallic nanocatalysis: sharp edges and corners for solid nanoparticles and cage effect for hollow ones.* Accounts of chemical research, 2013. **46**(8): p. 1795-1805.

11. Mahmoud, M.A., *Surface-Enhanced Raman Spectroscopy of Double-Shell Hollow Nanoparticles: Electromagnetic and Chemical Enhancements.* Langmuir, 2013. **29**(21): p. 6253-6261.

12. Sun, Y.G., B. Mayers, and Y.N. Xia, *Metal nanostructures with hollow interiors.* Advanced Materials, 2003. **15**(7-8): p. 641-646.

13. Yadav, M., et al., *Strong metal-molecular support interaction (SMMSI): Amine-functionalized gold nanoparticles encapsulated in silica nanospheres highly active for catalytic decomposition of formic acid.* Journal of Materials Chemistry, 2012. **22**(25): p. 12582-12586.

14. Park, J.C., et al., *Ni@SiO2 yolk-shell nanoreactor catalysts: High temperature stability and recyclability.* Journal of Materials Chemistry, 2010. **20**(7): p. 1239-1246.

15. Chen, C., et al., *Highly Crystalline Multimetallic Nanoframes with Three-Dimensional Electrocatalytic Surfaces.* Science, 2014. **343**(6177): p. 1339-1343.

16. Zeng, J., et al., *A Comparison Study of the Catalytic Properties of Au-Based Nanocages, Nanoboxes, and Nanoparticles.* Nano Letters, 2010. **10**(1): p. 30-35.

17. Weng, G., M.A. Mahmoud, and M.A. El-Sayed, *Nanocatalysts Can Change the Number of Electrons Involved in Oxidation–Reduction Reaction with the Nanocages Being the Most Efficient.* The Journal of Physical Chemistry C, 2012. **116**(45): p. 24171-24176.

18. Yen, C.W., M.A. Mahmoud, and M.A. El-Sayed, *Photocatalysis in Gold Nanocage Nanoreactors†.* The Journal of Physical Chemistry A, 2009. **113**(16): p. 4340-4345.

19. de la Hoz, J.M.M. and P.B. Balbuena, *Geometric and Electronic Confinement Effects on Catalysis.* Journal of Physical Chemistry C, 2011. **115**(43): p. 21324-21333.

20. Eddaoudi, M., et al., *Systematic design of pore size and functionality in isoreticular MOFs and their application in methane storage.* Science, 2002. **295**(5554): p. 469-472.

21. Graeser, M., et al., *Polymer core-shell fibers with metal nanoparticles as nanoreactor for catalysis.* Macromolecules, 2007. **40**(17): p. 6032-6039.

22. Macdonald, J.E., et al., *Hybrid nanoscale inorganic cages.* Nature Materials, 2010. **9**(10): p. 810-815.

23. Rodríguez-Lorenzo, L., et al., *Zeptomol Detection Through Controlled Ultrasensitive Surface-Enhanced Raman Scattering.* Journal of the American Chemical Society, 2009. **131**(13): p. 4616-4618.

24. Heck, K.N., et al., *Using Catalytic and Surface-Enhanced Raman Spectroscopy-Active Gold Nanoshells to Understand the Role of Basicity in Glycerol Oxidation.* ACS Catalysis, 2013. **3**(11): p. 2430-2435.

25. Li, J.F., et al., *Shell-isolated nanoparticle-enhanced Raman spectroscopy.* Nature, 2010. **464**(7287): p. 392-395.

26. Zhao, L.-B., et al., *A DFT study on photoinduced surface catalytic coupling reactions on nanostructured silver: selective formation of azobenzene derivatives from para-substituted nitrobenzene and aniline.* Physical Chemistry Chemical Physics, 2012. **14**(37): p. 12919-12929.

27. Yin, P.G., et al., *Surface-enhanced Raman spectroscopy with self-assembled cobalt nanoparticle chains: Comparison of theory and experiment.* Physical Chemistry Chemical Physics, 2010. **12**(36): p. 10781-10785.

28. Tran, D.T. and R.L. Johnston, *Study of 40-atom Pt-Au clusters using a combined empirical potential-density functional approach.* Proceedings of the Royal Society a-Mathematical Physical and Engineering Sciences, 2011. **467**(2131): p. 2004-2019.

29. Ramirez-Caballero, G.E. and P.B. Balbuena, *Confinement effects on alloy reactivity.* Physical Chemistry Chemical Physics, 2010. **12**(39): p. 12466-12471.

30. Hammer, B. and J.K. Norskov, *Why gold is the noblest of all the metals.* Nature, 1995. **376**(6537): p. 238-240.

31. Strasser, P., et al., *Lattice-strain control of the activity in dealloyed core–shell fuel cell catalysts.* Nat Chem, 2010. **2**(6): p. 454-460.

CHAPTER 5
WAVELENGTH SELECTIVE PHOTOCATALYSIS USING GOLD-PLATINUM NANO-RATTLES

Summary

The selectivity of a thermal catalyzed reaction with multiple products, catalyzed on the surface of a catalyst exhibiting different surface facets and surface energy, is controlled by the temperature. Manipulating the temperature makes one product more dominant than the other. The selectivity of the photochemical reaction on the surface of plasmonic nanocatalyst of multiple plasmon modes is controlled by changing the wavelength of the exciting light. Gold nanospheres (AuNSs) located inside of gold-platinum double shell nanoparticles in a rattle structure were prepared with different sizes and showed two plasmon spectral modes. The high energy plasmon mode corresponds to the photo-excitation of the small nanosphere, while the low energy plasmonic mode is related to both the gold-platinum double shell plasmon and the inside nanosphere, as assigned by calculation using the discrete dipole approximation (DDA) simulation technique. Photodimerization of 4-nitrothiophenol (4NTP) adsorbed on the surface of gold platinum nanorattles (AuPtNRTs) was studied using the surface-enhanced Raman spectroscopy technique. When the AuPtNRTs are photo-excited at the high energy band at 532 nm, which selectively excites the AuNS, 4NTP is photodimerized into an *azo* compound only on the surface of AuNS. The 4NTP adsorbed on the surface of the outer gold-platinum double shell did not react. Despite the fact that 785 nm photons excite both the AuNS and the outer shell of the AuPtNRTs, no photodimerization is observed with such low energy photons.

Introduction

Plasmonic nanoparticles are characterized by their strong interaction with light of resonant frequency due to the localized surface plasmon resonance (LSPR) phenomena.[1] The LSPR involves generation of a strong plasmon field which decays by enhanced absorption and scattering processes.[2] The scattered photons have been used in plasmon imaging[3], enhanced Raman scattering[4], plasmonic nanolensing[5]. The absorbed photons have been used to induce photochemical reactions such as energy transfer in hydrogen production[6] or initiating photodimerization of aromatic nitro compounds into *azo* dimers[7, 8]. The photons absorbed by the nanoparticles can also decay generating heat as in case of the photothermal therapy[3] and photothermal enhanced catalytic reactions[9].

According to the electromagnetic mechanism of surface enhanced Raman spectroscopy (SERS)[4], the plasmon field of the plasmonic nanoparticles enhances the exciting light and the Raman signal of any analyte located in its domain. The SERS enhancement factor[10] can approach the value of 10^{10}, which improves the sensitivity of SERS as an analytical technique[7, 11]. Previously, in order to improve the detection by SERS, the plasmon field intensity has been maximized[12, 13] and the scattering spectrum of the nanoparticles has been enhanced[14]. Gold and silver nanoparticles of different shapes[15, 16], sizes[17, 18], and structure[19, 20] have been prepared and examined in SERS[21-24]. Asymmetric nanoparticles have proven to provide stronger and more concentrated plasmon field intensity compared to highly symmetric shapes.[1, 14] The asymmetric nanoparticles have more than one plasmon mode[25, 26] which made it possible to use different laser excitations[27]. Hollow particles with spherical symmetry can also exhibit multiple modes as in case of gold nanorattles .[28]

Controlling the selectivity of the catalyst is an important goal of catalysis research.[29-32] This can be accomplished by designing the catalyst to include different surface facets with different atomic density and surface energy. The hydrogenation of benzene on the surface of Pt (111) produces cyclohexane and cyclohexene, while only cyclohexene was obtained on the surface of Pt (100).[33]

This study aims to induce and selectively control plasmonic photocatalysis on the surface of gold nanospheres in gold-platinum nanorattle nanoparticles. Gold platinum nanorattles (AuPtNRTs) composed of gold nanosphere located inside a larger gold-platinum double shell of different diameters were prepared. AuPtNRTs were characterized by the presence of two LSPR peaks; discrete dipole approximation (DDA) simulations showed that the high energy peak of the AuPtNRTs is for the gold nanosphere (AuNS) and the lower energy one is for gold-platinum double shell and AuNS. In order to examine the selective plasmonic photocatalytic property on the surface AuPtNRTs, 4-nitrothiophenol (4NTP) was allowed to adsorb on their surfaces. When the AuPtNRTs are photo-excited by high energy photons at 532 nm that only excite the interior AuNSs, 4NTP photodimerizes into the *azo* dimer only on the surface of AuNSs. Upon excitation of the AuPtNRTs with the lower energy photons of wavelength of 785 nm that excites both the gold-platinum double shell and the AuNS, no plasmonic photodimerization was observed.

A 532 nm laser was used to monitor the reactions on the surface of inner AuNSs *via* SERS. While the changes on both surfaces of the outer gold-platinum double shell and the inner gold nanosphere surface were investigated using the 785 nm laser. The

newly prepared AuPtNRTs were well-characterized using both high-resolution imaging and elemental mapping techniques.

Experimental

AuPtNRTs were synthesized by preparing AuNSs by the citrate reduction approach.[34] 500 mL of 1% hydrogentertrachloroaurate trihydrate aqueous solution was brought to boiling. Under gentle stirring and heating, 5 mL of 4% trisodium citrate trihydrate was added; the heating and stirring were continued until the color of the solution turned to red wine color. After cooling, the AuNSs were cleaned by centrifugation at 12000 rpm for 10 min and re-dispersed in 100 mL deionized (DI) water. The second step in the synthesis of AuPtNRTs was the synthesis of silver gold core-shell nanoparticles (Ag-AuNSs), and this was carried out by depositing a silver layer of different thicknesses on the surface of AuNSs.[28] Briefly, 400 mL solution of the cleaned AuNSs of OD=0.35 was brought to boiling, and 4 mL of trisodium citrate trihydrate (2%) was added followed by 1.2 mL silver nitrate (0.2 M). The solution was boiled and stirred for 4 min until color turned to yellow. The resulting particles were coated with a thin shell of silver. The thickness of the silver nanoshell was increased by the following steps. After the solution of Ag-AuNSs cooled down, its OD was adjusted to be 0.44. The Ag-AuNSs (OD=0.44) solution of volume of 200, 150, 100, and 75 mL was diluted with 0, 50, 100, 125 mL DI water, respectively. 0.05 g of polyvinyl pyrrolidone (MW = 55 000) dissolved in 10 mL was added to the resulting diluted Ag-AuNSs solution. Under slow stirring, 0.1 M $AgNO_3$ solution and 0.078 M L-Ascorbic acid solution of volume of 0.5, 1, 1.5, and 2 mL was added to the Ag-AuNSs solutions resulting from the dilution of concentrated Ag-AuNSs with volumes of 200, 150, 100, and 75 mL, respectively. The

stirring was continued for 5 minutes. The resulting Ag-AuNSs with silver shells of different thicknesses were cleaned by centrifugation at 9,000 rpm for 5 minutes and redispersed in 100 mL DI water. Finally, the AuPtNRTs were prepared by galvanic replacement technique.[15, 16] The silver nanoshell surrounding the surface of AuNSs converted into a gold-platinum double shell by a procedure similar to the early reported technique.[35] 0.05 g of PVP dissolved in 5 mL DI water was added to the cleaned solutions of Ag-AuNSs, and the solution was heated until the temperature reached 80 ^{o}C. Under stirring, an aqueous solution of $HAuCl_4.3H_2O$ (0.001g/10 ml) was added dropwise until the LSPR peak shifted to 600 nm. After 24 hours, the resulting nanoparticles were decanted from the precipitated AgCl. In order to add an internal platinum nanoshell to the gold nanorattle, 10 mL of ammonium tetrachloroplatinate (II) (0.05g/10 mL) was added dropwise to the solution of nanoparticles resulting from the final step. After each drop added from the platinum salt solution, the solution of the nanoparticles was vigorously shaken. The AuPtNRTs solution was kept for 24 hours and decanted from the AgCl precipitate, and then centrifuged at 6,000 rpm for 10 minutes and the residue was re-dispersed in 20 mL DI water. The gold nanorattles were prepared as reported.[28] In order to coat the surface of AuPtNRTs with 4-nitrothiphenol, 2 mL of a 0.1 mM aqueous solution was mixed with 10 mL of the cleaned AuPtNRTs or AuNSs and incubated for 6 hours. Then the free 4NTP was removed by centrifugation of the AuPtNRTs and re-dispersion in DI water. Finally, the AuPtNRTs coated with 4NTP were drop cast on a glass substrate and exposed to 532 nm or 785 nm laser for 2 minutes. A Renishaw In via Raman microscope with a 50x objective and 532 nm and 785 nm lasers were used for surface Raman measurements. An Ocean Optics HR4000Cg-UV-NIR was used for the

optical extinction measurements. The low resolution characterization of the nanoparticles was conducted by JEOL 100C transmission electron microscope (TEM). While the high-resolution TEM and energy-dispersive X-ray spectroscopy (EDS) elemental mapping carried out using a Tecnai F30 microscope.

The DDA simulation carried out using DDSCAT 6.1, the shape file of the AuNRT and AuPtNRTs is assumed to have three holes and 4 dipoles per 1 nm. The dielectric function of the surrounding medium is the average of polyvinyl pyrrolidone and water. The electromagnetic plasmon field were calculated for the plane of y= 0.6x length of the nanorattle.

Results and Discussion

Characterization of the Nanorattles

The gold-platinum nanorattles are composed of a gold nanosphere located inside of a gold-platinum double shell with gold on the exterior. TEM, high-resolution TEM imaging, and EDS elemental mapping were used to characterize these nanoparticles. Figure 5.1 A through D show the TEM images of AuPtNRTs with inner gold nanosphere of fixed diameter and different outer gold-platinum double shell. The majority of the nanorattles are spherical, and each nanorattle contains only one gold nanosphere. Statistical analysis carried-out using imageJ software for over 150 nanoparticles taken from TEM images showed that, the diameter of the outer shell of the AuPtNRT of Figure 5.1 A to D is 24.3±2.7, 29.6±3.3, 37.2±4.7, and 47.3±6.6 nm, respectively. The inside diameters of the AuNSs were found to be 15.2±1.9 nm in all of the AuPtNRTs.

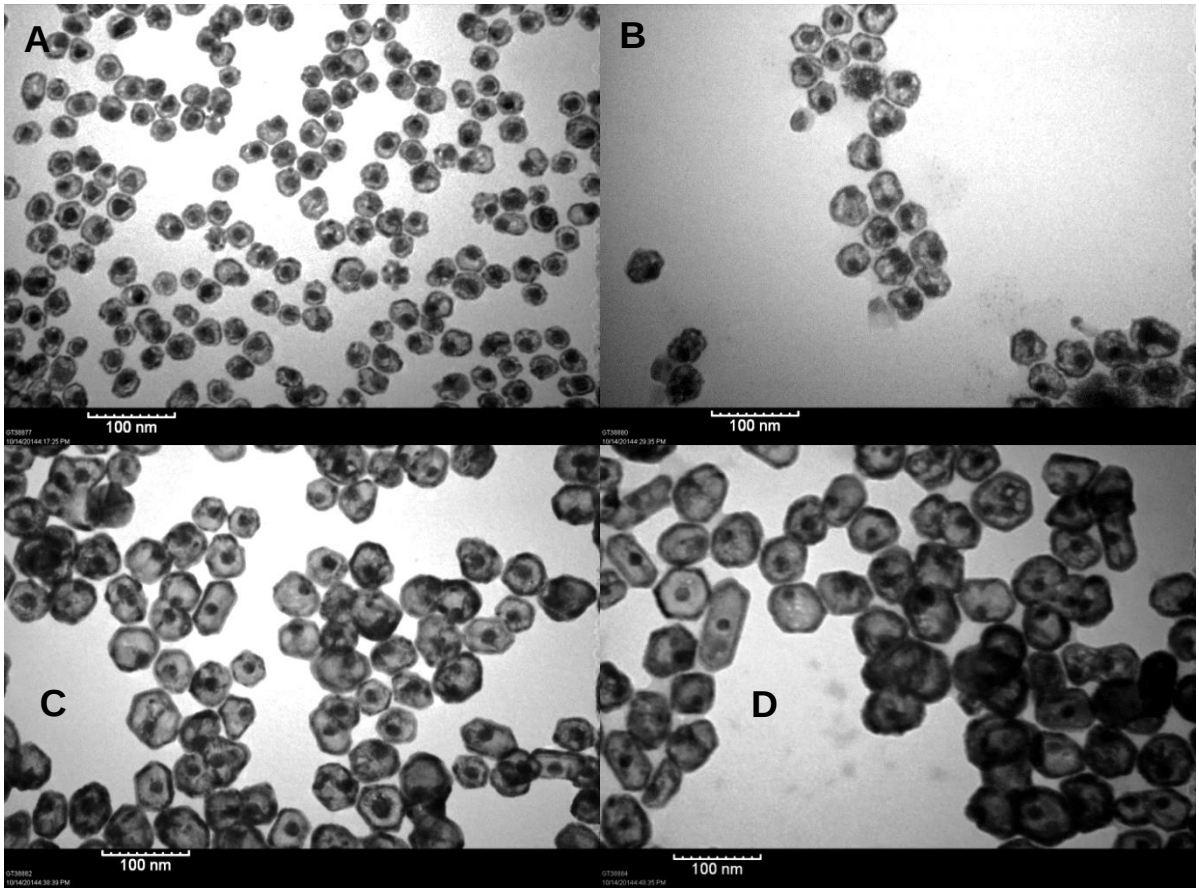

Figure 5.1. TEM images of gold-platinum nanorattles composed of small gold nanosphere of 15.2±1.9 nm in diameter located inside gold-platinum double shell of diameter of: A) 24.3±2.7, B) 29.6±3.3, C) 37.2±4.7, and D) 47.3±6.6 nm.

The AuPtNRTs are comprised of two metals (gold and platinum) which are arranged in a complex structure. Consequently, HR-TEM was used to examine the fine structure. Figure 5.2A shows the HR-TEM of AuPtNRT of 24.3±2.7 diameter and AuNS of 15.2±1.9 nm diameter. The AuNS is clearly separated from the outer shell. The outer shell seems to be smooth. The TEM images showed that the diameter of the AuNSs did not change after introducing the outer gold-platinum double shell of different diameters. This suggests that the platinum or gold did not deposit on the surface of inner AuNS during the nanorattles synthesis. In order to analyze the distribution of the gold and platinum metals in the nanorattle's shell, elemental analysis was carried out using EDS

mapping. Figure 5.2 B-D show the EDS elemental mapping of gold and platinum when they are separated and after they convoluted. It is clear that, the hollow shell of the AuPtNRT composed of an outer gold nanoshell and an inner platinum nanoshell.

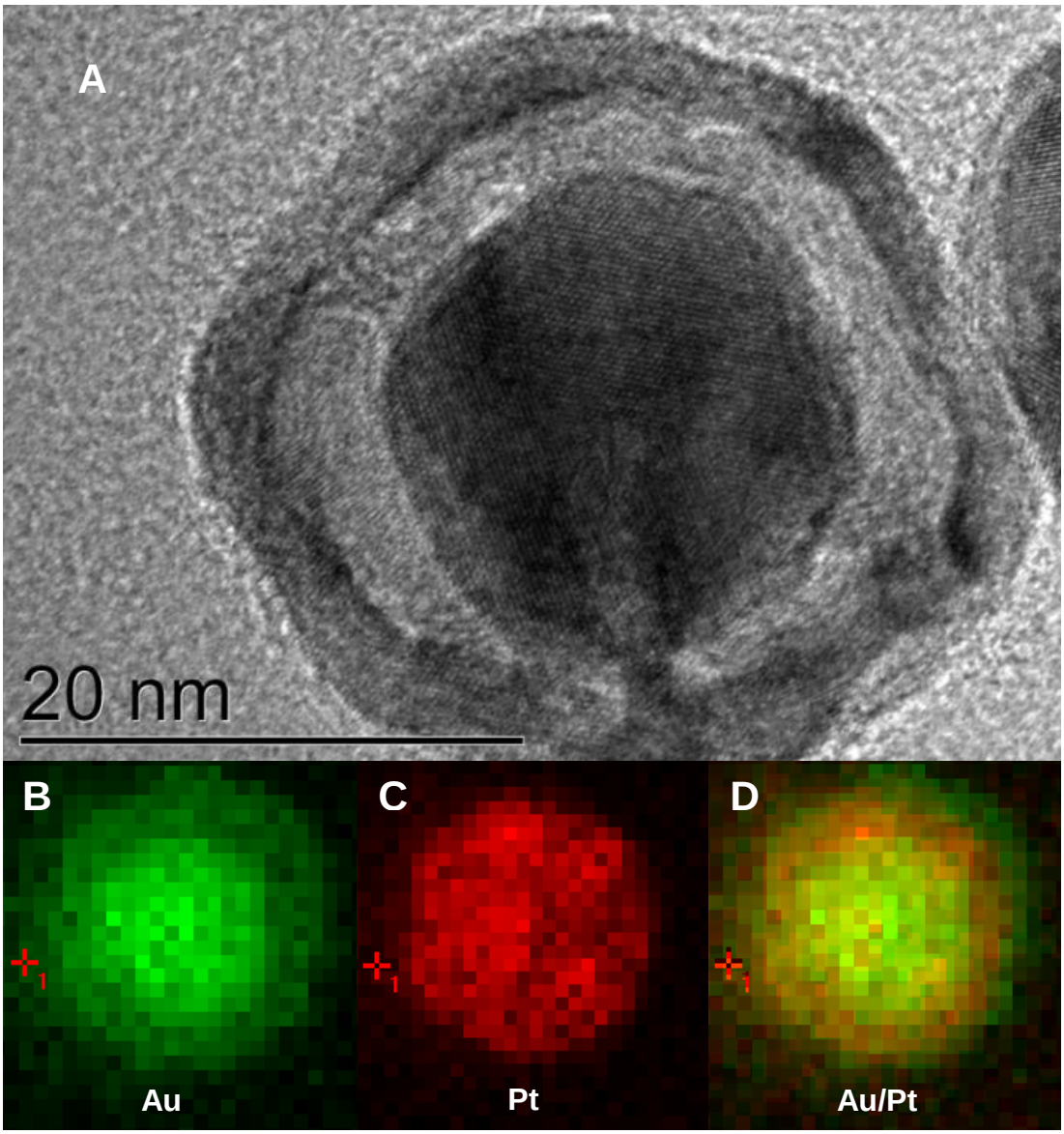

Figure 5.2. A) High-resolution TEM image of a single gold platinum nanorattle showing a gold nanosphere located inside gold-platinum double shell. EDS elemental mapping showing: B) the individual exterior gold nanoshell of the AuPtNRT, C) Individual interior platinum nanoshell of the AuPtNRT, D) combined gold and platinum layers forming the outer double shell of the AuPtNRT. The EDS elemental mapping suggested that, the shell of the AuPtNRT is composed of gold outer layer and platinum inner layer.

Optical Properties of the Nanorattles

The plasmon field and the LSPR spectrum of plasmonic nanoparticles are useful in many applications.[8, 9, 36] Plasmonic nanoparticles with multiple peaks improve the applicability of the nanoparticles. Recently, gold nanorattles with multiple peaks were prepared.[28] A lower energy and intense plasmon mode corresponding to the LSPR spectrum of the outer gold nanoshell and a higher energy and less intense plasmon mode resulting from the excitation of the inner gold nanosphere.[28] Figure 5.3A shows the LSPR spectrum of 17.2±2.6 nm gold nanospheres measured while it is free and after placed inside 38.4±4.2 nm gold nanoshell in a rattle structure (TEM is shown in Figure 5.4). As it has been reported[28], AuNRTs show two sharp LSPR peaks at 523 and 800 nm, while a single peak at 518 nm was observed for the AuNSs.

Palladium or platinum inner nanoshells are shown to manipulate the optical[36], mechanical[37], and catalytic[38] properties of the gold nanoshells when they are combined in double shell nanostructures. Upon examining the optical properties of such double shell plasmonic metallic nanoparticles, their LSPR peak became much broader[36], which indicated the reduction of the coherence time of the oscillating conduction band free electrons during the interaction with the electromagnetic radiation.[36, 37] Platinum and palladium hollow nanoparticle are characterized by their broad LSPR spectrum which extends into the UV and visible region.[39-41] The broad plasmon mode of the palladium nanoshell overlaps and hybridizes with the sharp plasmon mode of the gold nanosphere.[41] Figure 5.3 B shows the LSPR spectrum of the AuPtNRTs of 15.2±1.9 nm diameter AuNSs and outer gold-platinum double shell with diameters of 24.3±2.7, 29.6±3.3, 37.2±4.7, 47.3±6.6 nm. The LSPR spectrum of the AuPtNRTs has broad features and the

peaks are unresolved. Consequently, Gaussian deconvolution fitting was carried out to determine the LSPR peak positions. Two characteristic LSPR peaks were obtained for each AuPtNRT, one at 520 nm, and the other at 840, 750, 698, and 705 nm, for AuPtNRTs with outer diameters of 24.3±2.7, 29.6±3.3, 37.2±4.7, 47.3±6.6 nm, respectively. Both the LSPR peak position and the ratio between the intensity of the two peaks depend on the diameter of the outer AuPt double shell. The ratio between the intensity of the high energy peak and the low energy peak was found to decrease as the diameter of the outer shell was increased. The higher energy LSPR peak of the AuPtNRTs was found to shift to higher energy as the diameter of the outer shell is increased. As expected, introducing the platinum nanoshell increased the broadness of the LSPR peak.

DDA calculations were used to study the effect of adding an inner Pt shell to the AuNRTs. Figure 5.3C shows the LSPR spectrum of 47 nm AuNRT and AuPtNRTs of diameter of 47 and 24 nm. The wall thickness of the 47 nm AuNRT and AuPtNRT is 5 nm which splits in case of AuPtNRT into 2.5 nm for Au and 2.5 nm for Pt. The wall thickness of the 24 nm AuPtNRT is 1.5 nm for Au and 1.5 nm for Pt. In all three nanorattles, the inside AuNS is considered to be 15 nm in diameter. As it was observed experimentally, the LSPR spectrum of the AuPtNRT is broader than that of the AuNRT and the LSPR spectrum of AuNRTs appears at energy lower than that of AuPtNRT of similar dimensions. The lower energy LSPR peak of the smaller AuPtNRT (24 nm) appears at wavelength higher than the larger one (47 nm). Ultimately, the intensity ratio of the high energy LSPR peak to the low energy one is increased as the diameter of the AuPtNRT decreases.

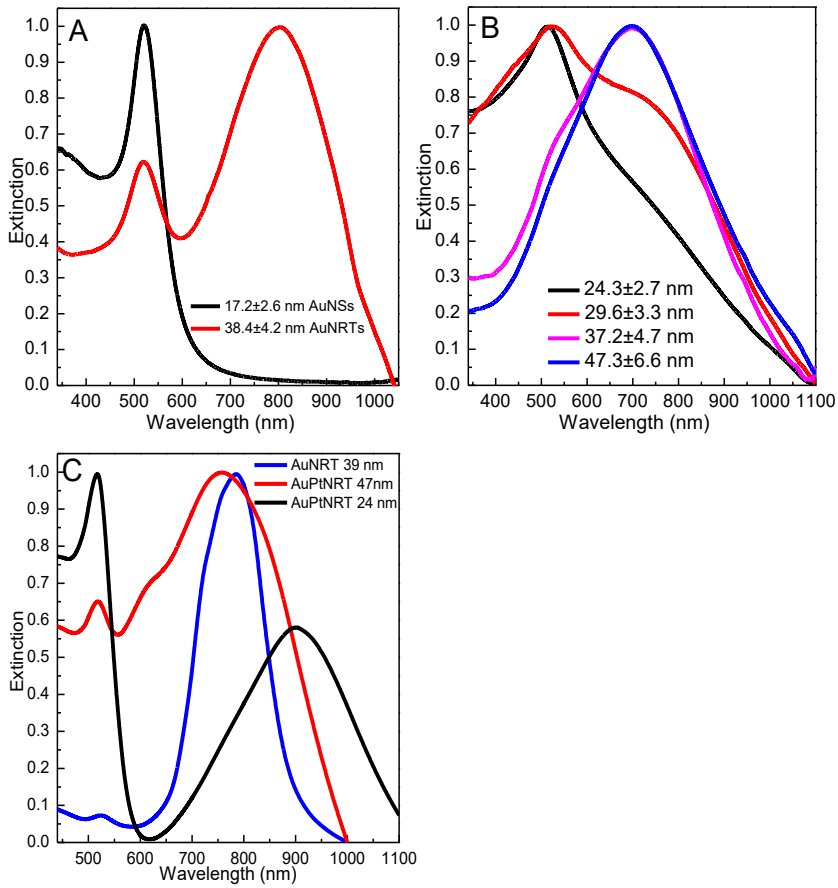

Figure 5.3. LSPR extinction spectrum measured for: A) 17.2±2.6 nm diameter gold nanospheres (black) and gold nanorattles of 17.2±2.6 nm gold nanosphere located inside 38.4±4.2 nm gold nanoshell (red), B) gold-platinum nanorattles of 15.2±1.9 nm gold nanosphere and outer gold-platinum double shell of diameter of 24.3±2.7, 29.6±3.3, 37.2±4.7, and 47.3±6.6 nm. C) Simulated LSPR spectrum of AuNRT (blue) and AuPtNRT (red) of 47 nm diameter and 5 nm wall thickness, and 24 nm AuPtNRT of 3 nm wall thickness. The inside AuNS is 15 nm in all of the three nanorattles and half of the wall of the AuPtNRT is Pt. The ratio between the intensity of the high energy peak and the low energy peak in the AuPtNRTs of identical gold nanosphere was found to decrease as the diameter of the outer gold-platinum nanorattles was increased in both the experimentally measured and simulated spectrum. The LSPR spectrum of the AuNRT became much broader and shift to higher energy upon introducing an inner Pt nanoshell.

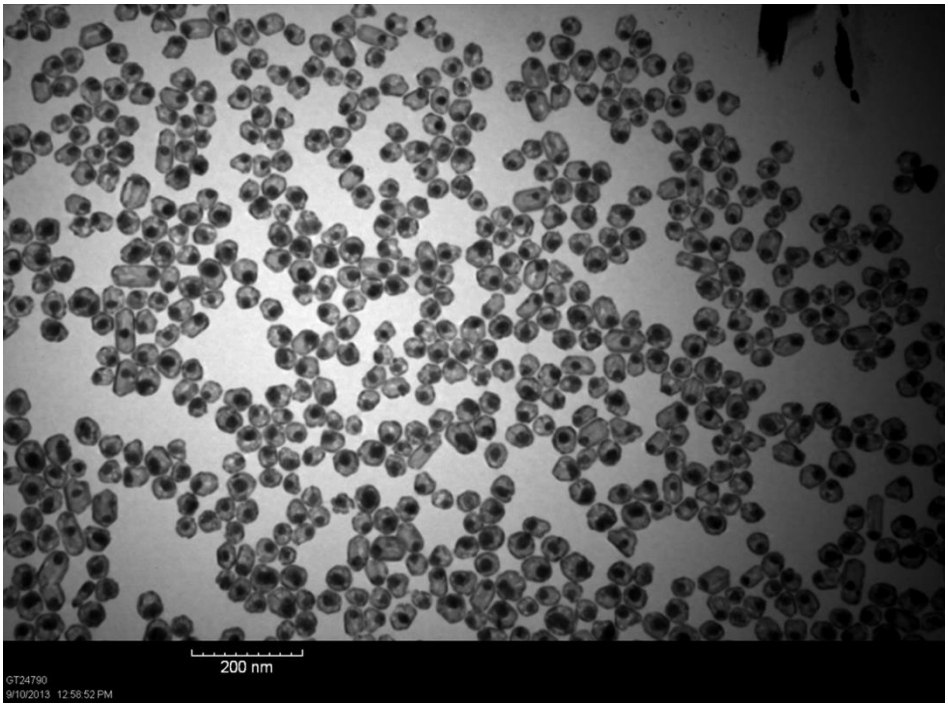

Figure 5.4. TEM image of gold nanorattle of 17.2±2.6 nm gold nanospheres located inside 38.4±4.2 nm gold nanoshell in a rattle structure.

Selective Plasmonic Photodimerization of 4NTP on the Surface of Nanorattles

The efficiency of any photocatalyst depends on its ability to capture photons with sufficient energy to induce the photochemical reaction, and then transfer such photons to the reactant.[42] 4NTP adsorbed on the surface of plasmonic nanoparticles undergoes photodimerization into the *azo* dimer upon photo-excitation by high energy photons.[8] If the LSPR peak of the nanoparticles was located at longer wavelengths, and therefore excited by a lower energy photons, no dimerization was observed.[38] SERS is the most accurate technique for examining the photodimerization of 4NTP adsorbed on the surface of plasmonic nanoparticles. Fortunately, the Raman laser can be used for SERS detection as well as for inducing the photodimerization. The SERS spectrum of 4NTP adsorbed on the surface of 15.2±1.9 nm gold nanosphere after irradiation with a 532 nm laser for 2 minutes is shown in Figure 5.5. Sharp SERS bands at 1331 and 1573 cm^{-1} corresponding

to symmetric nitro stretching mode $\nu_s(NO_2)$ and parallel C-C stretching mode of 4NTP are obtained, respectively.[38] Two SERS bands appeared at 1431 and 1387 cm^{-1} assigned to ν(-N=N-) and a SERS band at 1140 cm^{-1} for ν(CN) was also obtained.[38] These three SERS bands characterize the *azo* dimer formation,[38] which results from the plasmon-induced photochemical dimerization of 4NTP. Figure 5.6 shows the SERS spectrum of 4NTP adsorbed on the surface of AuPtNRTs of different diameters after 2 minute irradiation with the 532 nm laser. 532 nm and 785 nm lasers were used for Raman detection. The SERS spectrum showed clear bands at 1140, 1431, and 1387 cm^{-1} corresponding to the *azo* dimer formation[38] when the 532 nm laser was used, while the intensity of such SERS bands is very small upon 785 nm Raman laser excitation. Based on the optical measurement of AuPtNRTs shown in Figure 5.3, the 532 nm laser is suggested to excite the internal AuNSs while the outer gold-platinum double shell could be excited by the 785 nm laser. However, for more complex plasmonic systems such as AuPtNRTs, it is hard to predict which surface of the AuPtNRTs is excited by the high energy photons and induces the photodimerization, and it also is not easy to confirm which surface provides the SERS signal. No significant change was observed when the 4NTP adsorbed on the surface of AuPtNRTs were irradiated with 785 nm wavelength laser. This is expected because even though the 785 nm excites the plasmon peak of the gold-platinum double shell of AuPtNRT it doesn't supply photons of sufficient energy that are required to dimerize the 4NTP molecules.

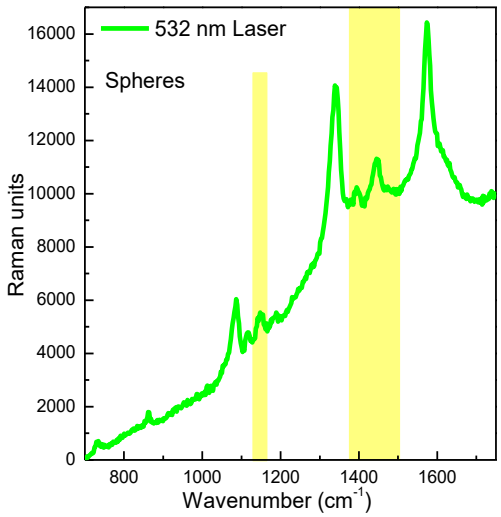

Figure 5.5. SERS spectrum of 4NTP adsorbed on the surface of AuNSs after irradiation with 532 nm laser for 2 minutes, the SERS measurements conducted by 532 nm laser excitation.

The frequency of the Raman band is used to monitor the dimer formation, and the concentrations of products and reactants are determined from the band intensities. The photodimerization conversion ratio by the AuPtNRTs of different outer shell sizes, after 2 minutes of 532 nm laser irradiation, is determined by comparing the ratio between the intensity of SERS bands of the *azo* dimers and of the monomer. The photodimerization conversion ratio was found to increase as the diameter of the outer shell of the AuPtNRTs increased (Figure 5.6A through D). Similar SERS results were obtained when the 4NTP adsorbed on the surface of the AuNRTs was irradiated with the 532 nm laser for 2 minutes. However, the SERS spectrum collected upon 532 nm excitation of AuNRTs showed characteristic sharp bands for the azo dimer, while weak SERS bands corresponding to the azo dimer formation is observed when 785 nm excitation is used.

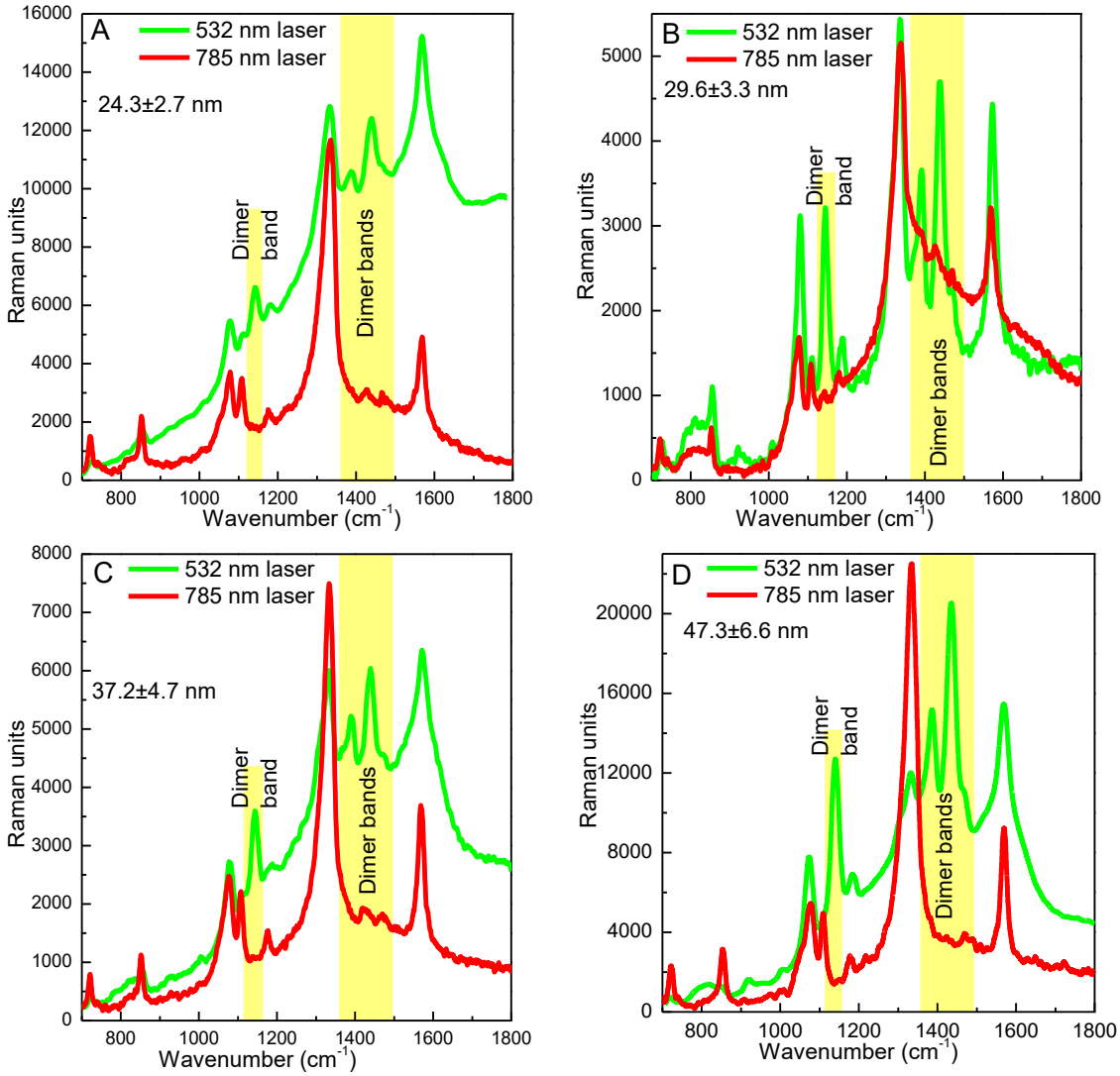

Figure 5.6. SERS spectrum of 4-nitrothiophenol adsorbed on the surface of AuPtNRTs after irradiation with 532 nm laser for 2 minutes, the SERS measurements after exciting at 532 nm laser excitation (green) and by using the 785 nm laser excitation (red). The AuPtNRTs of 15.2±1.9 nm AuNSs and outer gold-platinum double shell of diameter of 24.3±2.7 nm (A), 29.6±3.3nm (B), 37.2±4.7 nm (C), and 47.3±6.6 nm (D) were examined in the plasmonic photodimerization. SERS bands corresponding to the azo dimer formation was clearly observed when the 532 nm was used during the Raman measurement. The dimer formation was found to increase as the diameter of outer shell of the AuPtNRTs was increased. Weak SERS bands were obtained upon 785 nm Raman laser excitation.

Simulation of the Plasmon Field Intensity of Nanorattles using DDA Calculations

The photodimerization of 4NTP requires photons of sufficient energy; AuPtNRTs and AuNRTs have plasmon modes which can be excited by the 532 nm. It is useful to

examine whether such high energy photons are able to excite the internal AuNS selectively to induce the photodimerization on its surface. Moreover, it is also important to investigate the surface that produces the SERS enhancement.

The efficiency of SERS enhancement by a certain plasmonic nanoparticle depends greatly on the strength of its electromagnetic plasmon field.[43] It is possible to determine the location of the hotspots on the surface of plasmonic nanoparticles, either for individual particle or multiple particles using DDA calculations. However, for complicated systems, such as the plasmonic nanorattles where the outer shell has two surfaces in addition to the surface of the inner nanosphere, it is useful to determine the plasmon field intensity and the filed distribution on each surface upon excitation.

The plasmon field calculation of the nanorattles at the wavelength of the Raman laser makes it possible to determine which surface provides the SERS signal and to locate the surface that is excited with high energy photons and induces photodimerization. Figure 5.7 A and B show the plasmon field contour of AuNRTs of 47 nm diameter, 5 nm wall thickness, and 15 nm AuNS, calculated using DDA at the plasmon modes of 525 and 795 nm, respectively. The plasmon field intensity was found to be highest on the surface of the AuNS when the AuNRT is excited at 525 nm. Conversely, at 795 nm excitation the plasmon field intensity is high on the surface of AuNS and also on the inner and outer surfaces of gold nanoshell. DDA calculations for the plasmon field of AuPtNRT of similar dimensions to AuNRT were also carried out. However, the 5 nm outer shell of the AuPtNRT was proposed to be 2.5 nm of Au and 2.5 nm of Pt. The plasmon field contour of AuPtNRT calculated at the 520 nm and 730 nm plasmon modes are shown in Figure 5.7 C and D, respectively. Similar to the AuNRT, the AuPtNRT

plasmon field showed the highest intensity on the surface of the AuNS when calculated at the 520 nm plasmon mode. Unlike the AuNRT though, the plasmon field intensity on the inner shell surface of the AuPtNRT (Pt surface) is negligible upon 730 nm excitation, but the plasmon field on the surface of the AuNS and the outer surface of AuPtNRT is still high at 730 nm excitation.

The plasmon field calculation was carried out for smaller AuPtNRT (24 nm in diameter) of similar AuNS (15 nm) and wall thickness of 3 nm. Similar to the larger AuPtNRT, the plasmon field intensity was found to be high on the surface of AuNS only when calculated at the 520 nm plasmon mode, and the field at the 880 nm plasmon mode showed high intensity on the surface of the AuNS and the outer surface of the AuPtNRT. The plasmon field intensity of the smaller AuPtNRT was found to be higher than that of the larger one when calculated at the lower energy plasmon mode, while at the higher energy plasmon mode, the plasmon field intensity on the surface of AuNS in the larger AuPtNRT is stronger than that of the smaller AuPtNRT.

The results of the DDA plasmon field calculation make it easy to understand the SERS results. Exciting the higher energy plasmon mode of AuNRTs and AuPtNRTs by the 532 nm photons selectively excites the AuNS within the nanorattles and initiates the selective photodimerization of 4NTP on the AuNS surface. The SERS spectrum collected upon 532 nm excitation also arises from the surface of the AuNS inside the nanorattles. When the diameter of the AuPtNRTs is increased and the AuNS remains fixed, the plasmon field intensity on the surface of AuNS increases; this confirms the increase of the dimerization conversion ratio as the diameter of the AuPtNRTs is increased. Figure

5.8 shows a schematic diagram which summarizes the selective plasmonic photodimerization of 4NTP on the surface of AuPtNRTs.

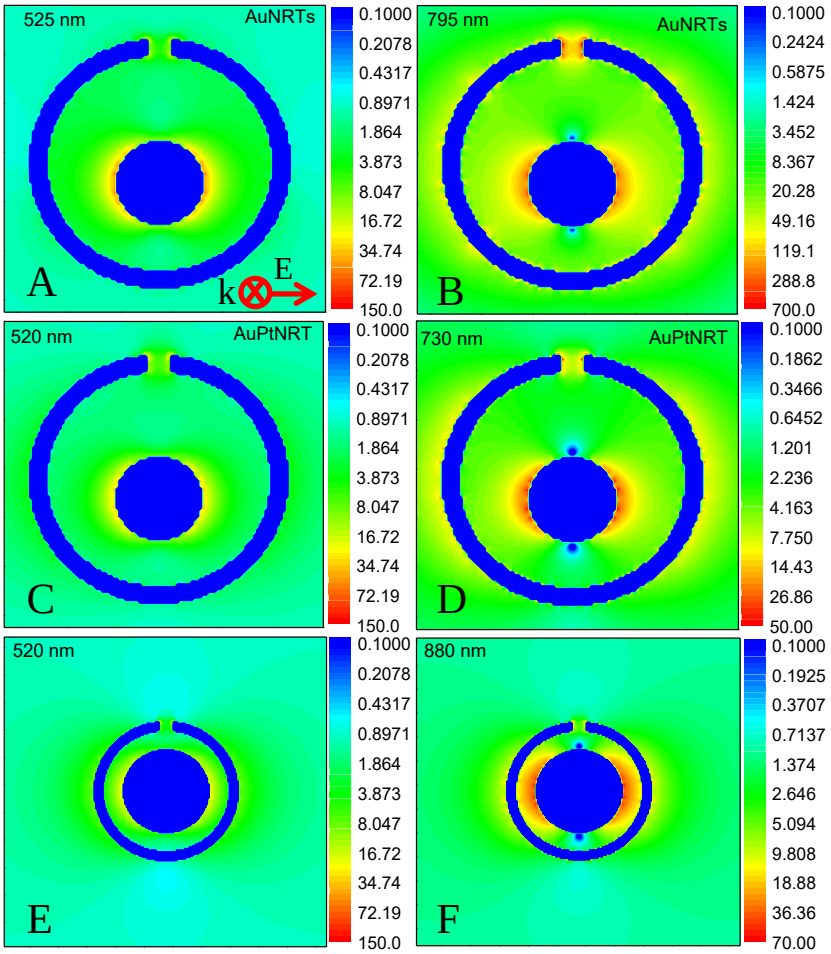

Figure 5.7. Plasmon field intensity contour calculated by the DDA technique for: A) AuNRT of diameter of 47 nm, 5 nm wall thickness, and 15 nm AuNS when excited at 525 nm. B) 47 nm AuNRT of 15 nm AuNS at 795 nm excitation. C) AuNS of 15 nm diameter located inside a 47 nm gold platinum double shell of 5 nm wall thickness in a rattle structure which is excited at 520 nm. D) AuPtNRT of 47 nm diameter and 15 nm AuNS is excited at 730 nm. E) AuPtNRT has diameter of 24 nm, wall thickness of 3 nm, and 15 nm AuNS calculated at 520 nm plasmon mode. F) The 24 nm AuPtNRT of 15 nm is excited at 880 nm. The plasmon field of AuNRT was found to have high intensity on the surface of AuNS when calculated at 525 nm excitation, while upon excitation at 795 nm, the plasmon field intensity is high on the surface of AuNS and the inner and outer surfaces of the gold nanoshell of AuNRT. For the AuPtNRT, the plasmon field intensity was found to be high on the surface of AuNS upon 520 nm excitation, while exciting the 47 nm AuPtNRT at 730 nm and the 24 nm AuPtNRT at 880 nm induced high field intensity on the exterior surface of the AuPtNRT in addition to the surface of AuNS. Unlike, the AuNRT where the plasmon field intensity is high on both the exterior and interior surfaces, the field intensity is negligible on the interior surface of AuPtNRT. The plasmon field intensity of AuPtNRT calculated at the lower energy plasmon mode of the smaller AuPtNRT is stronger than that of the larger AuPtNRT, although the field intensity calculated at the higher energy plasmon mode (520 nm) behaved oppositely.

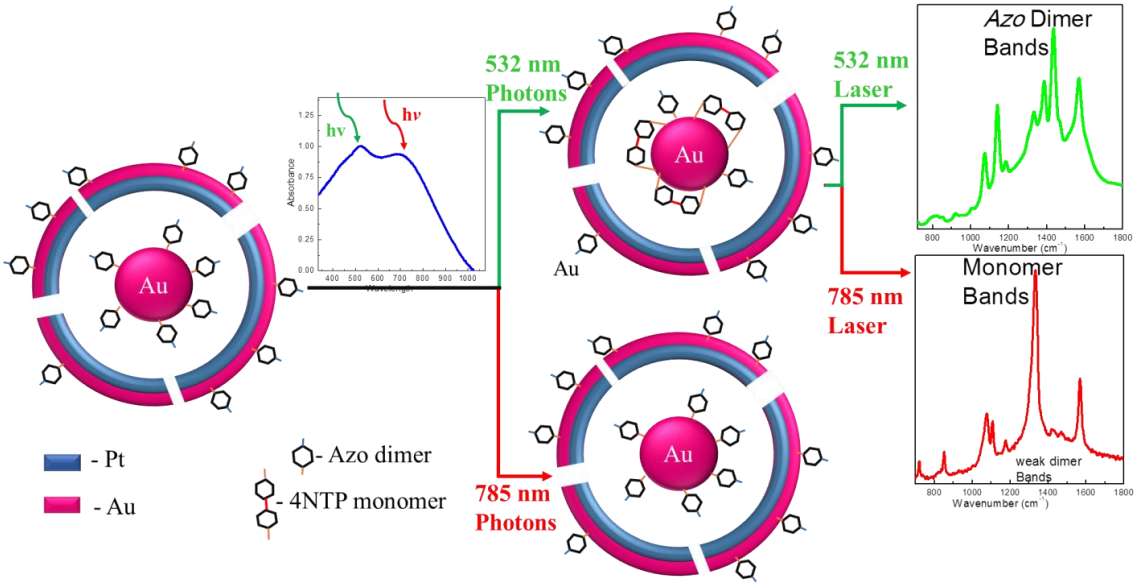

Figure 5.8. Schematic depiction of the selective plasmonic photodimerization of 4NTP on the surface of AuPtNRT after 532 nm laser irradiation. The *azo* dimer is formed on the surface of the internal AuNS and not on the surface of its gold-palladium double shell. The 532 nm photon selectively excites the AuNS and has sufficient energy to induce the plasmonic photodimerization of 4NTP. However, the SERS bands correspond to the *azo* dimer formation was observed when the Raman measurement collected upon 532 nm laser excitation. Although the 785 nm photons excite both the AuNS and the gold-palladium double shell of the AuPtNRT, this low energy photon is not sufficient to initiate the 4NTP photodimerization. The SERS spectrum collected under the 785 nm laser excitation monitors the adsorbed molecules on the surface of gold-palladium double shell and AuNS as well.

Conclusions

Gold-platinum nanorattles were prepared with gold nanospheres located inside gold-platinum double shells of different diameters. The AuPtNRTs showed two plasmon spectral peaks which were observed experimentally and confirmed by theoretical calculation using DDA simulations. The plasmon field calculation showed that the higher energy LSPR peak corresponds to the excitation of the AuNS and the lower energy peak relates to excitation of both the outer double shell and the AuNS. The plasmon field

intensity on the surface of the AuNS calculated at the lower energy plasmon mode of the AuPtNRT was found to increase as the outer shell radius increases.

4-nitrothiophenol adsorbed on the surface of AuPtNRTs was plasmonically photodimerized into the *azo* dimer when exposed to the 532 nm laser photons. Raman spectroscopy was used to selectively detect the changes that occurred on the surface of AuPtNRTs depending on the wavelength of the laser used during the measurement. The Raman measurement using the 532 nm laser that selectively excites the AuNS showed SERS bands for the dimers, while very weak SERS signal for the *azo* dimer was observed when the Raman measurement was carried out with 785 nm laser excitation. This suggests that the *azo* dimer was formed selectively on the surface of the inner AuNS but not on the outer gold-platinum double shell of the AuPtNRTs. This result was confirmed for all the AuNRTs of different diameters. The SERS measurements showed that, increasing the size of the AuPtNRTs while maintaining the AuNS diameter is found to increase the *azo* dimer to 4NTP conversion ratio. The SERS measurement correlated will with the plasmon field calculation carried out for the high energy plasmon mode that showed that the plasmon field intensity on the surface of AuNS increased as the size of the AuPtNRT increased.

REFERENCES

1. Kelly, K.L., et al., *The Optical Properties of Metal Nanoparticles: The Influence of Size, Shape, and Dielectric Environment.* J. Phys. Chem. B, 2003. **107**: p. 668-677.

2. Lee, K.S. and M.A. El-Sayed, *Dependence of the enhanced optical scattering efficiency relative to that of absorption for gold metal nanorods on aspect ratio, size, end-cap shape, and medium refractive index.* Journal of Physical Chemistry B, 2005. **109**(43): p. 20331-20338.

3. Huang, X., et al., *Cancer Cell Imaging and Photothermal Therapy in the Near-Infrared Region by Using Gold Nanorods.* Journal of the American Chemical Society, 2006. **128**(6): p. 2115-2120.

4. Jeanmaire, D.L. and R.P. Van duyne, *Surface Raman Spectroelectrochemistry .1. Heterocyclic, Aromatic, and Aliphatic-Amines Adsorbed on Anodized Silver Electrode.* Journal of Electroanalytical Chemistry, 1977. **84**(1): p. 1-20.

5. Mahmoud, M.A., et al., *Plasmonic Field Enhancement of the Exciton− Exciton Annihilation Process in a Poly (p-phenyleneethynylene) Fluorescent Polymer by Ag Nanocubes.* Journal of the American Chemical Society, 2010. **132**(8): p. 2633-2641.

6. Mubeen, S., et al., *An autonomous photosynthetic device in which all charge carriers derive from surface plasmons.* Nat Nano, 2013. **8**(4): p. 247-251.

7. Li, J.F., et al., *Shell-isolated nanoparticle-enhanced Raman spectroscopy.* Nature, 2010. **464**(7287): p. 392-395.

8. Zhao, L.-B., et al., *A DFT study on photoinduced surface catalytic coupling reactions on nanostructured silver: selective formation of azobenzene derivatives from para-substituted nitrobenzene and aniline.* Physical Chemistry Chemical Physics, 2012. **14**(37): p. 12919-12929.

9. Mahmoud, M.A. and M.A. El-Sayed, *Enhancing Catalytic Efficiency of Hollow Palladium Nanoparticles by Photothermal Heating of Gold Nanoparticles Added to the Cavity: Palladium–Gold Nanorattles.* ChemCatChem, 2014. **6**(12): p. 3540-3546.

10. Xu, H., et al., *Spectroscopy of Single Hemoglobin Molecules by Surface Enhanced Raman Scattering.* Physical Review Letters, 1999. **83**(21): p. 4357-4360.

11. Rodríguez-Lorenzo, L., et al., *Zeptomol Detection Through Controlled Ultrasensitive Surface-Enhanced Raman Scattering.* Journal of the American Chemical Society, 2009. **131**(13): p. 4616-4618.

12. Mahmoud, M.A., B. Snyder, and M.A. El-Sayed, *Surface Plasmon Fields and Coupling in the Hollow Gold Nanoparticles and Surface-Enhanced Raman Spectroscopy. Theory and Experiment†.* The Journal of Physical Chemistry C, 2010. **114**(16): p. 7436-7443.

13. McFarland, A.D. and R.P. Van Duyne, *Single silver nanoparticles as real-time optical sensors with zeptomole sensitivity.* Nano Letters, 2003. **3**(8): p. 1057-1062.

14. Mahmoud, M.A. and M.A. El-Sayed, *Different plasmon sensing behavior of silver and gold nanorods.* The Journal of Physical Chemistry Letters, 2013.

15. Sun, Y.G. and Y.N. Xia, *Shape-controlled synthesis of gold and silver nanoparticles.* Science, 2002. **298**(5601): p. 2176-2179.

16. Sun, Y., B. Mayers, and Y. Xia, *Metal Nanostructures with Hollow Interiors.* Advanced Materials, 2003. **15**(7-8): p. 641-646.

17. Sisco, P.N. and C.J. Murphy, *Surface-Coverage Dependence of Surface-Enhanced Raman Scattering from Gold Nanocubes on Self-Assembled Monolayers of Analyte†.* The Journal of Physical Chemistry A, 2009. **113**(16): p. 3973-3978.

18. Grzelczak, M., et al., *Shape control in gold nanoparticle synthesis.* Chemical Society Reviews, 2008. **37**(9): p. 1783-1791.

19. Xia, Y., et al., *Shape-Controlled Synthesis of Metal Nanocrystals: Simple Chemistry Meets Complex Physics?* Angewandte Chemie International Edition, 2009. **48**(1): p. 60-103.

20. Wilcoxon, J.P. and B.L. Abrams, *Synthesis, structure and properties of metal nanoclusters.* Chemical Society Reviews, 2006. **35**(11): p. 1162-1194.

21. Sajanlal, P.R., et al., *Electric field enhancement and concomitant Raman spectral effects at the edges of a nanometre-thin gold mesotriangle.* Journal of Materials Chemistry, 2010. **20**(11): p. 2108-2113.

22. Camden, J.P., et al., *Probing the Structure of Single-Molecule Surface-Enhanced Raman Scattering Hot Spots.* Journal of the American Chemical Society, 2008. **130**(38): p. 12616-12617.

23. Braun, G., et al., *Chemically Patterned Microspheres for Controlled Nanoparticle Assembly in the Construction of SERS Hot Spots.* Journal of the American Chemical Society, 2007. **129**(25): p. 7760-7761.

24. Hastings, S.P., et al., *Quadrupole-Enhanced Raman Scattering.* ACS Nano, 2014. **8**(9): p. 9025-9034.

25. Jana, N.R., L. Gearheart, and C.J. Murphy, *Wet chemical synthesis of high aspect ratio cylindrical gold nanorods.* Journal of Physical Chemistry B, 2001. **105**(19): p. 4065-4067.

26. Pastoriza-Santos, I. and L.M. Liz-Marzan, *Colloidal silver nanoplates. State of the art and future challenges.* Journal of Materials Chemistry, 2008. **18**(15): p. 1724-1737.

27. Orendorff, C.J., et al., *Aspect ratio dependence on surface enhanced Raman scattering using silver and gold nanorod substrates.* Physical Chemistry Chemical Physics, 2006. **8**(1): p. 165-170.

28. Mahmoud, M.A., *Optical Properties of Gold Nanorattles: Evidences for Free Movement of the Inside Solid Nanosphere.* The Journal of Physical Chemistry C, 2014. **118**(19): p. 10321-10328.

29. Zaera, F., *Shape-Controlled Nanostructures in Heterogeneous Catalysis.* ChemSusChem, 2013. **6**(10): p. 1797-1820.

30. Somorjai, G.A., et al., *Dynamics of Surface Catalyzed Reactions; the Roles of Surface Defects, Surface Diffusion, and Hot Electrons†.* The Journal of Physical Chemistry B, 2006. **110**(40): p. 20014-20022.

31. Lee, I., et al., *Tuning selectivity in catalysis by controlling particle shape.* Nat Mater, 2009. **8**(2): p. 132-138.

32. An, K. and G.A. Somorjai, *Size and Shape Control of Metal Nanoparticles for Reaction Selectivity in Catalysis.* ChemCatChem, 2012. **4**(10): p. 1512-1524.

33. Bratlie, K.M., et al., *Platinum Nanoparticle Shape Effects on Benzene Hydrogenation Selectivity.* Nano Letters, 2007. **7**(10): p. 3097-3101.

34. Freund, P.L. and M. Spiro, *Colloidal Catalysis - the Effect of Sol Size and Concentration.* Journal of Physical Chemistry, 1985. **89**(7): p. 1074-1077.

35. Mahmoud, M.A. and M.A. El-Sayed, *Time Dependence and Signs of the Shift of the Surface Plasmon Resonance Frequency in Nanocages Elucidate the Nanocatalysis Mechanism in Hollow Nanoparticles.* Nano Letters, 2011. **11**(3): p. 946-953.

36. Mahmoud, M.A., *Surface-Enhanced Raman Spectroscopy of Double-Shell Hollow Nanoparticles: Electromagnetic and Chemical Enhancements.* Langmuir, 2013. **29**(21): p. 6253-6261.

37. Mahmoud, M.A., P. Szymanski, and M.A. El-Sayed, *Different Methods of Increasing the Mechanical Strength of Gold Nanocages.* The Journal of Physical Chemistry Letters, 2012. **3**(23): p. 3527-3531.

38. Mahmoud, M.A., B. Garlyyev, and M.A. El-Sayed, *Controlling the Catalytic Efficiency on the Surface of Hollow Gold Nanoparticles by Introducing an Inner Thin Layer of Platinum or Palladium.* The Journal of Physical Chemistry Letters, 2014. **5**(23): p. 4088-4094.

39. Mahmoud, M.A. and M.A. El-Sayed, *Metallic Double Shell Hollow Nanocages: The Challenges of Their Synthetic Techniques.* Langmuir, 2012. **28**(9): p. 4051-4059.

40. Niu, Z., et al., *Pd nanocrystals with single-, double-, and triple-cavities: facile synthesis and tunable plasmonic properties.* Chemical Science, 2011. **2**(12): p. 2392-2395.

41. Mahmoud, M.A., *Plasmon Resonance Hybridization of Gold Nanospheres and Palladium Nanoshells Combined in a Rattle Structure.* The Journal of Physical Chemistry Letters, 2014. **5**(15): p. 2594-2600.

42. Bard, A.J., *Photoelectrochemistry.* Science, 1980. **207**(4427): p. 139-144.

43. Mahmoud, M. and M. El-Sayed, *Aggregation of gold nanoframes reduces, rather than enhances, SERS efficiency due to the trade-off of the inter-and intraparticle plasmonic fields.* nano letters, 2009. **9**(8): p. 3025-3031.

APPENDIX A
ELECTROCATALYTIC STUDY OF OXYGEN REDUCTION REACTION ON SILVER NANOPLATES WITH (111) AND (100) SURFACES

Summary

Study and development of the new electrocatalysts for oxygen reduction reaction (ORR) is of a great importance for fuel cell applications. Platinum metal is proved to be excellent catalyst for ORR but due to its high cost and scarcity on earth scientists are in search of better catalysts. Silver nanoplates of different sizes were synthesized and they have shown to have mainly (111) surface structure on top and bottom and mixture between (100) and (111) structures on the edge surface. Activity of two silver surfaces towards oxygen reduction reaction was measured and (111) surface structure was found to be more active compared to (100) surface structure.

Experimental

Silver nanoplates were prepared by a single-pot experiment as reported before[1]. For the cyclic voltammetry measurements, monolayer of Ag nanoplates were deposited on a glassy carbon electrode. Centrifuged Ag nanoplates were diluted with 3 mL of ethanol then were dispersed on top of the petri dish filled with DI water sublayer using a microsyringe. Ag nanoplates monolayer was transferred to the glass electrode by dipping surface of the glass electrode. Then glass electrode with Ag nanoplate monolayer was left for drying for 2 hours. AgCl/Ag electrode was used as the reference electrode, and platinum was used as a counter electrode. All of the cyclic voltammetry measurements were carried out in 0.1 M KOH at a scan rate of 50 mV/s. Oxygen gas was bubbled into KOH solution for 30 mins before cyclic voltammetry measurements.

Results and discussions

Characterization of Silver Nanoplates

Silver nanoplates are very thin in thickness and have large top and bottom surfaces. Synthesized Ag nanoplates were characterized by using TEM and high resolution TEM imaging. TEM images of Ag nanoplates of 5 different sizes are shown in figure A.1 A through E. Statistical shape and size analysis were carried out using imageJ software for more than 150 nanoparticles. On average the length of the Ag nanoplates shown in figure A.1 A to E is 27 ± 6.7 nm, 43 ± 7.8 nm, 96 ± 11 nm, 144 ± 26 nm, and 787 ± 108 nm, respectively. From the TEM images we observed three different shapes of Ag nanoplates round, hexagonal and triangular. Majority of the small 27 nm Ag nanoplates were round and some hexagonal shaped. For larger sizes the majority of the

shapes were triangular and hexagonal. Shape analysis was done by separating Ag nanoplates into 3 categories: round, hexagonal and triangular shaped nanoplates. Truncated triangles were also counted in hexagonal group. The histogram in the figure A.1 F shows abundance of each shape in a given size of Ag nanoplates.

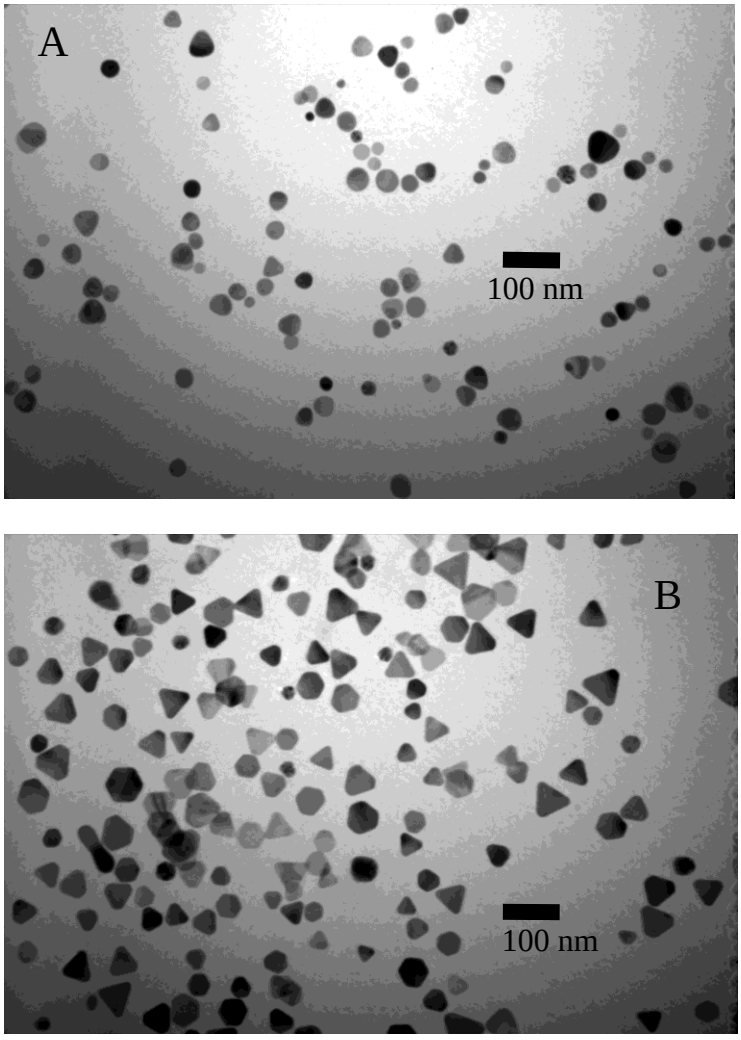

Figure A.1. TEM images of silver nanoplates of sizes A) 27 ± 6.7 nm B) 43 ± 7.8 nm C) 96 ± 11 nm D) 144 ± 26 nm E) 787 ± 108 nm F) Histogram of shape distribution with size of the Ag nanoplates.

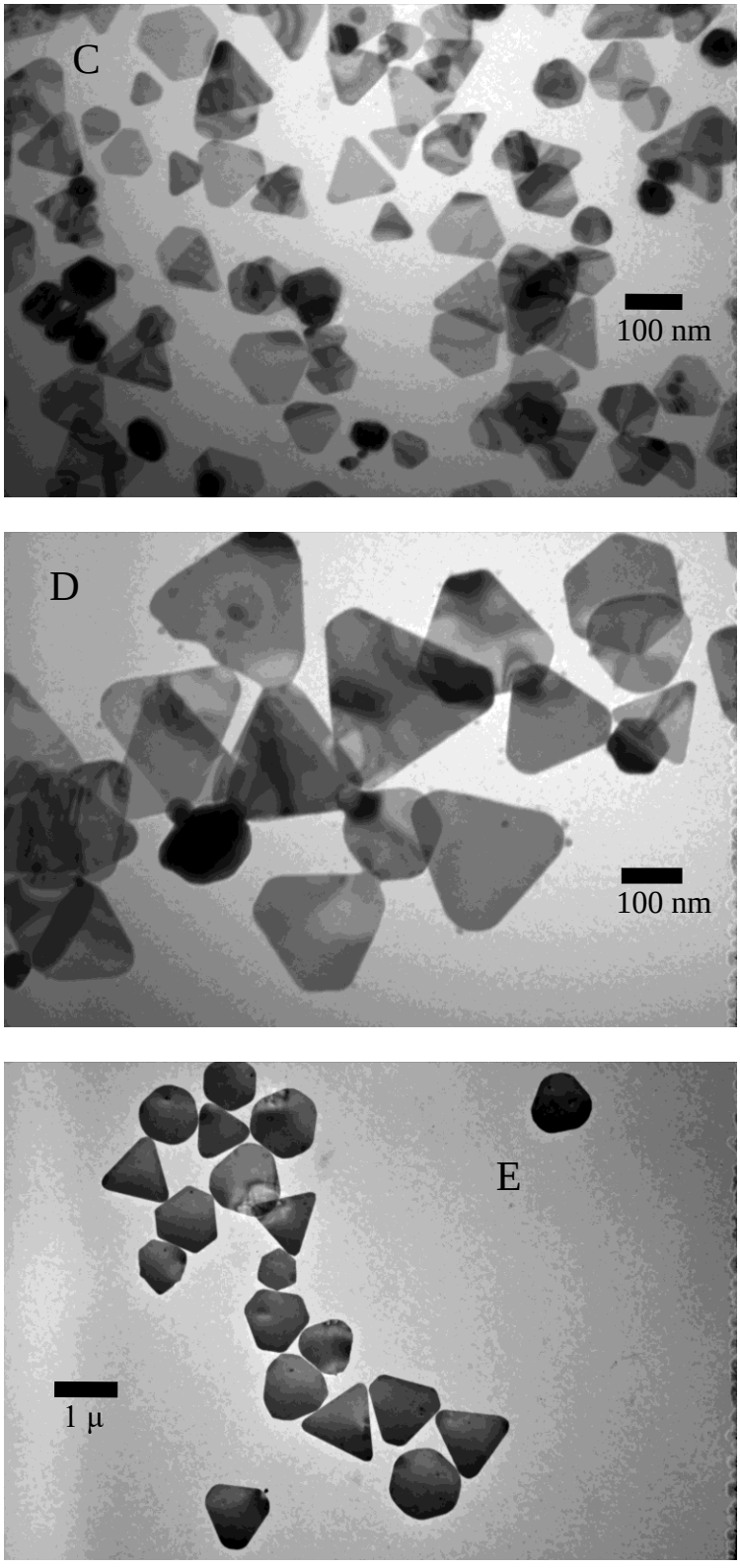

Figure A.1. Continued

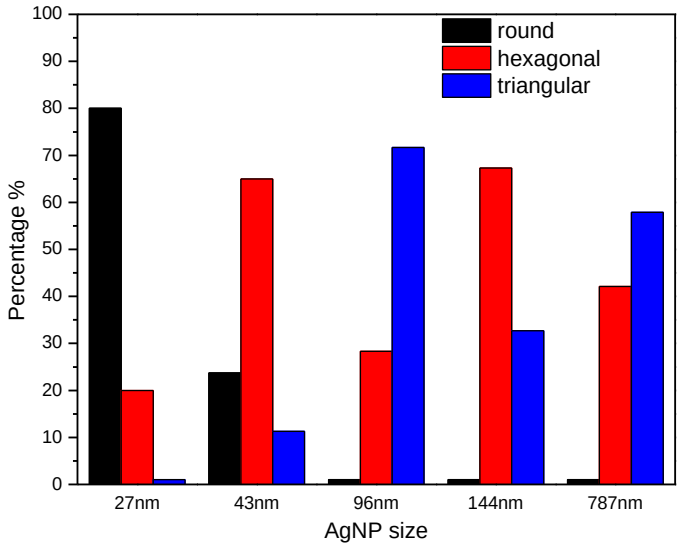

Figure A.1. Continued

High resolution TEM was used to determine fine structure of Ag nanoplates. Figure A.2 displays top and side view HR-TEM image of the 27 ± 6.7 nm Ag nanoplates. On the top view plane set with a spacing of 2.5 Å is assigned to the forbidden (1/3) {422} reflection,[2,3] which has been previously observed for Ag nanostructures in the form of thin nanoplates. We also observed fringes with d-spacing of 1.4 Å as shown in the top view of figure A.2 which are from the individual silver nanoplates corresponding to the {220} facet.[2] Observations from the HR-TEM images are consistent with the previous results for Ag nanoplates, in which each nanoplate is bound by {111} planes as the top and bottom faces and both {100}, {111} planes as the side faces alternating from edge to adjacent edge.

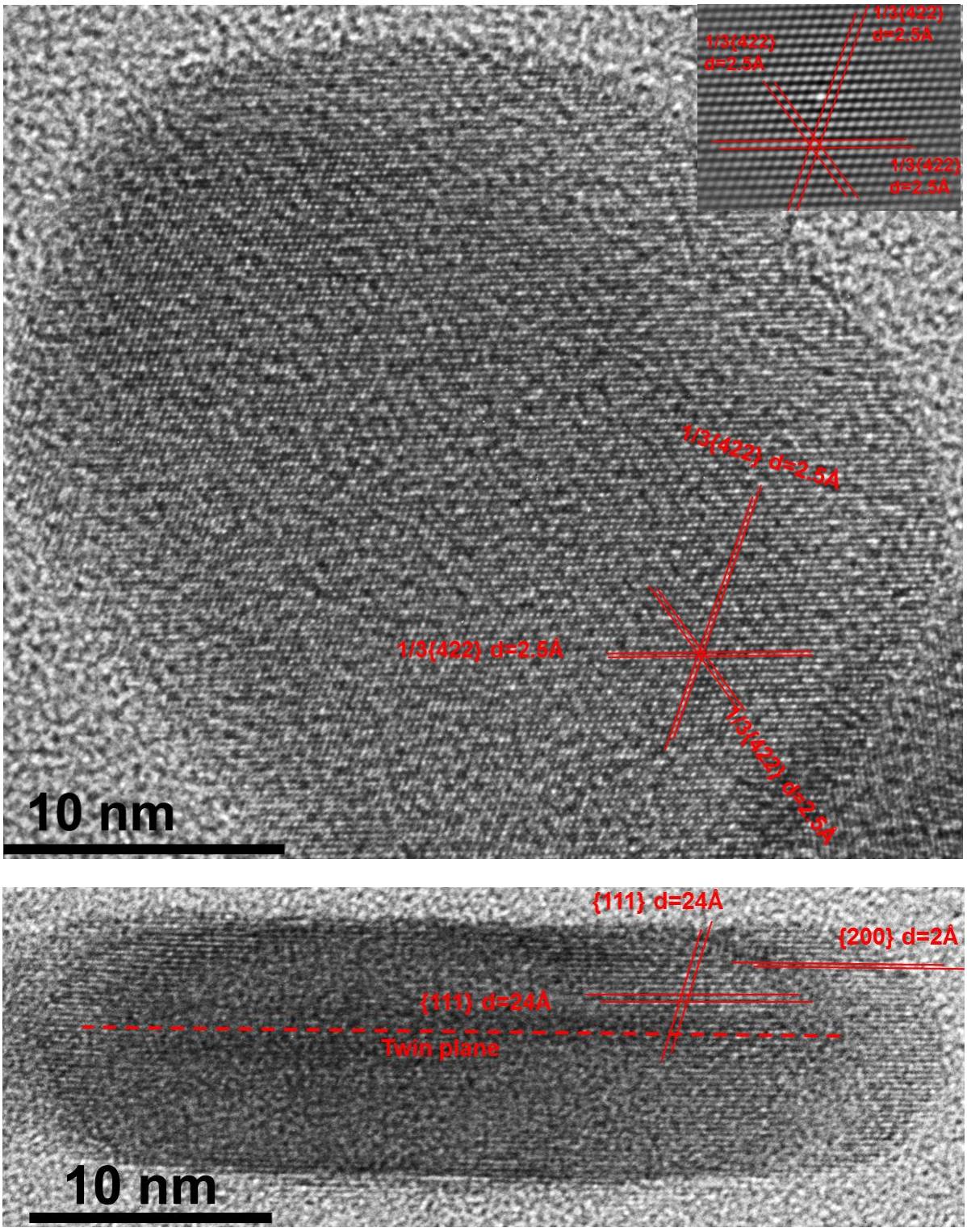

Figure A.2. HR-TEM of silver nanoplates measured from the top (upper image), and imaged from the side (lower image).

Optical Properties of Silver Nanoplates

Silver nanoplates can be considered as two-dimensional nanoparticles and when it interacts with resonant light, its conduction band electrons oscillate either perpendicular to the plane of the nanoparticle (out-of-plane) or along the plane of the nanoparticle (in-plane).[4,5] Optical properties of Ag nanoplates were measured by using Ocean Optics HR4000Cg-UV-NIR. In the UV spectrum for Ag nanoplates four peaks were observed in agreement with previously reported spectrums for Ag with nanoplate structures. Lowest energy peak is observed due to the in-plane dipole. Peaks are assigned from lowest energy to highest energy in following order; in-plane dipole, quadrupole, out-of-plane dipole and quadrupole plasmon resonance modes[4,5] (Figure A.3).

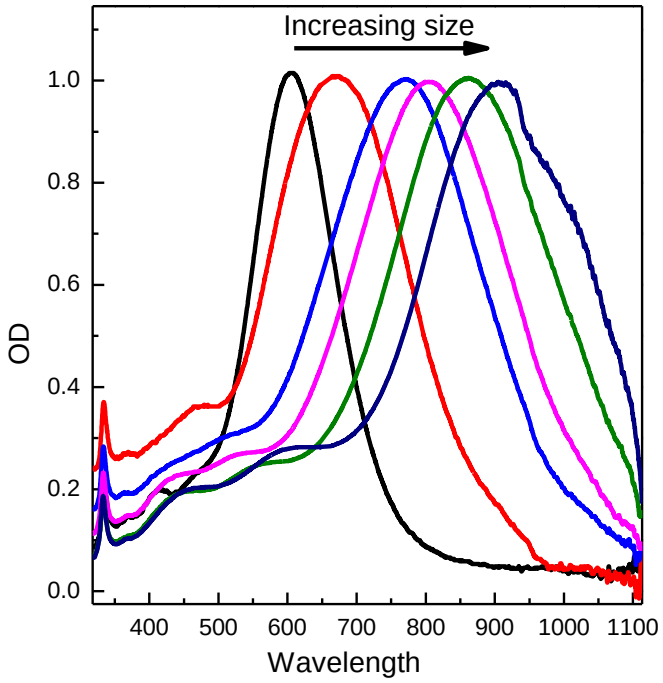

Figure A.3. Localized surface plasmon resonance spectrum of silver nanoplates with increasing sizes.

Cyclic Voltammetry Measurements

Cyclic voltammetry (CV) for each size of Ag nanoplates was recorded in 0.1 M KOH with a sweep rate of 50 mV/s. Monolayer of Ag nanoplates were deposited on glassy carbon electrode in order to prevent aggregation and to have uniform surface. Langmuir Blodget technique was used to make Ag nanoplate monolayer on the glassy carbon electrode. In an alkaline media oxygen reduction on the surface of Ag is known to follow 4-electron reduction pathway and known as a diffusion controlled reaction. Hydroxide ions in the solution will interfere with the reduction and will battle with dissolved oxygen molecules to bind to the silver active surface. Unlike in the case of platinum, binding of hydroxide to the silver surface is reversible.

Activity of the silver surfaces were found to be in order of (111) > (100) > (110) so in the cyclic voltammograms oxygen reduction on the (111) surface will happen at lower potential than reduction at (100) surface. In the figure A.4 we can see the cyclic voltammograms of oxygen reduction of the surfaces of silver nanoplates with different sizes.

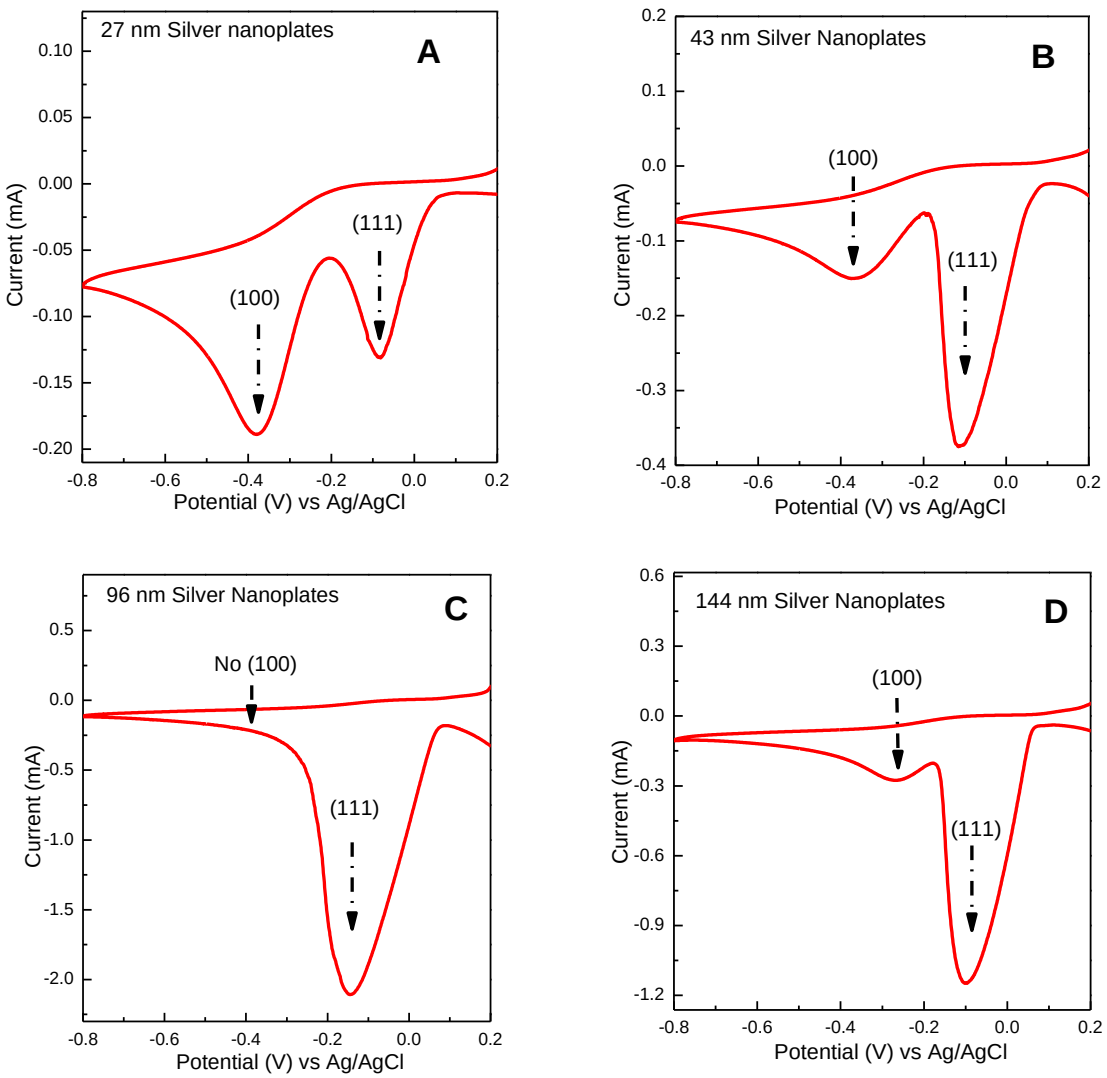

Figure A.4. Cyclic voltammograms of oxygen reduction in 0.1M KOH on Silver nanoplates with sizes of A) 27 ± 6.7 nm B) 43 ± 7.8 nm C) 96 ± 11 nm D) 144 ± 26 nm E) 787 ± 108 nm.

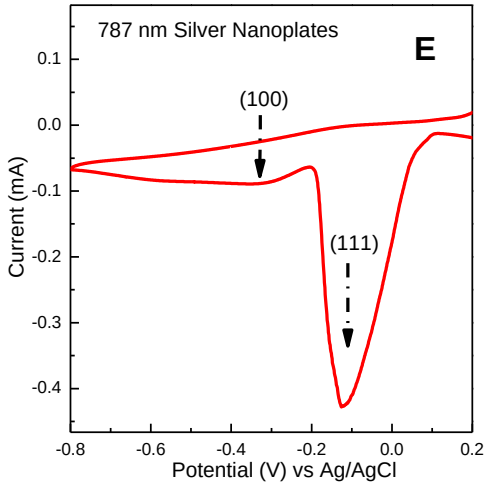

Figure A.4. Continued

Conclusion

In conclusion we were able to synthesize silver nanoplates with different sizes. They were structurally characterized by TEM and High- resolution TEM images. Silver nanoplates have shown to have mainly (111) surface structure on top and bottom surfaces and mixture between (100) and (111) structures on the edge surfaces. Activity of two silver surfaces towards oxygen reduction reaction was measured and (111) surface structure was found to be more active compared to (100) surface structure.

REFERENCES

1. Mahmoud, M.A., *Simultaneous Reduction of Metal Ions by Multiple Reducing Agents Initiate the Asymmetric Growth of Metallic Nanocrystals.* Crystal Growth & Design, 2015. **15**(9): p. 4279–4286.

2. Germain, V., et al., *Stacking faults in formation of silver nanodisks.* The Journal of Physical Chemistry B, 2003. **107**(34): p. 8717-8720.

3. Kirkland, A., et al. *Structural studies of trigonal lamellar particles of gold and silver*. in *Proceedings of the Royal Society of London A: Mathematical, Physical and Engineering Sciences*. 1993. The Royal Society.

4. Kelly, K.L., et al., *The optical properties of metal nanoparticles: the influence of size, shape, and dielectric environment.* The Journal of Physical Chemistry B, 2003. **107**(3): p. 668-677.

5. Jin, R., et al., *Photoinduced conversion of silver nanospheres to nanoprisms.* Science, 2001. **294**(5548): p. 1901-1903.

APPENDIX B

CALCULATION OF THE ACTIVE SURFACE AREA ON CHAPTER 1

Extinction coefficient will be equal to the slope which is $1.1170*10^4$. Then we find the adsorbed concentration of 4NTP; by subtracting the initial absorbance from final and dividing it by extinction coefficient of 4NTP.

Next step was to find the number of particles inside the 3ml solution. From the plasmon peak absorbance inside the 3ml solution and extinction coefficient we found the concentration of particles. Then by using Avogadro's number we convert it to the number of particles in 3ml.

We plotted the Langmuir isotherm plot between the equilibrium concentrations of 4NTP divided by adsorbed concentration of 4NTP per particle versus the equilibrium concentrations of 4NTP. The slope of isotherm plot will give us reciprocal of the number of moles of 4NTP on the surface of each particle so the active surface area will be equal to:

Surface area = $1/(\text{slope}) \times (N_A) \times (0.187)\ nm^2$

Where the number $0.187nm^2$ is the average surface area which each 4NTP molecule occupies and N_A is Avogadro's number. By using equation above Active surface area for Au nanospheres, Au hollowspheres and Au nanocages were calculated.

VITA

BATYR GARLYYEV

Batyr was born in Turkmenistan (former USSR), in 1990. He attended university in Istanbul, Turkey, received a B.Sc. in Chemistry from Fatih University, in 2011, before coming to Georgia Tech to pursue a doctorate in Chemistry. He will be continuing his career as a postdoc in Germany at Technical University of Munich. When he is not working on his research, Batyr enjoys football related activities.